

REPORT DOCUMENTATION PAGE		READ INSTRUCTIONS BEFORE COMPLETING FORM
1. REPORT NUMBER	2. GOVT ACCESSION NO.	3. RECIPIENT'S CATALOG NUMBER
4. TITLE (and Subtitle) PARAMETER SPACE TECHNIQUES FOR ROBUST CONTROL SYSTEM DESIGN		5. TYPE OF REPORT & PERIOD COVERED Technical Report
7. AUTHOR(s) Juergen Ackermann, S. Norman Franklin, Christine B. Chato, and Douglas P. Looze		6. PERFORMING ORG. REPORT NUMBER R-890 (DC-39) UILU:ENG 2222
9. PERFORMING ORGANIZATION NAME AND ADDRESS Coordinated Science Laboratory University of Illinois at Urbana-Champaign Urbana, Illinois 61801		8. CONTRACT OR GRANT NUMBER(s) JSEP-N00014-79-C-0424 AFOSR-78-3633
11. CONTROLLING OFFICE NAME AND ADDRESS Office for Naval Research		10. PROGRAM ELEMENT, PROJECT, TASK AREA & WORK UNIT NUMBERS
14. MONITORING AGENCY NAME & ADDRESS (if different from Controlling Office)		12. REPORT DATE July, 1980
		13. NUMBER OF PAGES 187
		15. SECURITY CLASS. (of this report) UNCLASSIFIED
		15a. DECLASSIFICATION/DOWNGRADING SCHEDULE
16. DISTRIBUTION STATEMENT (of this Report) Approved for public release; distribution unlimited		
17. DISTRIBUTION STATEMENT (of the abstract entered in Block 20, if different from Report)		
18. SUPPLEMENTARY NOTES		
19. KEY WORDS (Continue on reverse side if necessary and identify by block number) Robust control systems Sensitivity Multivariable control system design Perturbation methods, Aircraft control		
20. ABSTRACT (Continue on reverse side if necessary and identify by block number) The importance of designing control systems which are robust or insensitive to variations in the plant parameters has long been appreciated. However, the rapid advances in design techniques for multivariable systems has heightened interest in the study and design of robust systems. The purpose of this report is to provide an up to date survey of the work in this field and summarize the results of research in this area conducted at the Coordinated Science		

20. ABSTRACT (continued)

Laboratory.

The report begins in Chapter 2 with a description and examples of the robust control problem. Chapter 3 provides a survey of research in the field of robust control. It is apparent from this survey that the work can be divided into two areas. The first assumes unstructured perturbations and analyzes worst case effects. The second considers large, structured perturbations. The parameter space design method presented in Chapter 4 is directed at the second area. The tools of Chapter 4 are applied to a fighter aircraft example in Chapter 5. Chapter 6 presents an optimization approach to the same problem. Finally, Chapter 7 summarizes the report and presents several directions for future research.

UILLU-ENG-80-2222

PARAMETER SPACE TECHNIQUES FOR ROBUST CONTROL
SYSTEM DESIGN

by

Juergen Ackermann, S. Norman Franklin, Christine B. Chato,
and Douglas P. Looze

This work was supported in part by the Joint Services Electronics
Program (U.S. Army, U.S. Navy, and U.S. Air Force) under Contract N00014-79-
C-0424, and in part by the U.S. Air Force under Grant AFOSR-78-3633

Reproduction in whole or in part is permitted for any purpose of
the United States Government.

Approved for public release. Distribution unlimited.

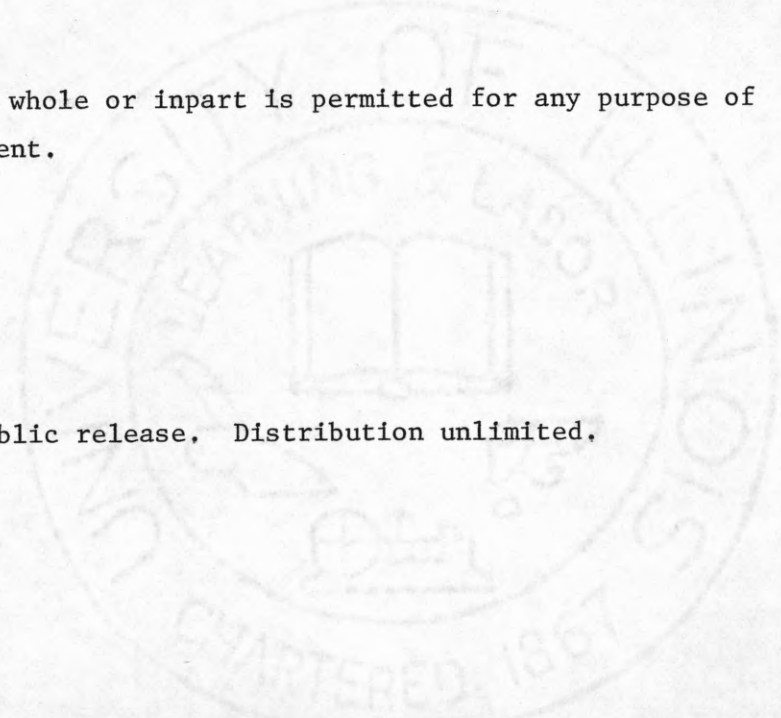


TABLE OF CONTENTS

	Page
1. INTRODUCTION.....	1
2. THE ROBUST CONTROL PROBLEM.....	2
2.1. Description of the Robust Control Problem.....	2
2.2. Controller Structure and Other Design Considerations.....	6
3. A SURVEY OF ROBUST CONTROL RESULTS.....	12
3.1. Introduction.....	12
3.2. Sensitivity and Unstructured Perturbations.....	13
3.2.1. Frequency Domain Methods.....	13
3.2.2. State Space Methods.....	17
3.3. Robustness with Respect to Large Perturbation in Known Directions.....	21
3.3.1. Parameter Methods.....	21
3.3.2. Integrity: Robustness with Respect to Sensor and Actuator Failures.....	23
4. PARAMETER SPACE DESIGN OF ROBUST CONTROL SYSTEMS.....	28
4.1. Introduction.....	28
4.2. Single Input Pole Placement - A Linear Mapping.....	37
4.2.1. State Feedback.....	37
4.2.2. Partial Pole and Gain Assignment, Output Feedback.....	41
4.2.3. Sensitivities, Incremental Stabilization.....	45
4.3. Mapping of Boundaries.....	48
4.3.1. Mapping from λ place to \mathcal{K} space.....	48
4.3.2. Mapping to a Subspace of \mathcal{K}	57
4.4. Robustness with Respect to Large Parameter Variations.....	63
4.5. Robustness with Respect to Sensor Failures.....	66
4.6. Other Features of \mathcal{K} -Space Design.....	69
4.6.1. Input Constraints.....	69
4.6.2. Short Wordlength Control Law Implementation.....	70
4.7. Multi-Input Problems.....	72
4.7.1. Characteristic Parameter Assignment.....	72
4.7.2. Robustness of Multivariable Systems.....	82
4.8. Conclusions.....	85

	Page
5. APPLICATION TO THE LONGITUDINAL CONTROL OF A FIGHTER-AIRCRAFT.....	89
5.1. Introduction.....	89
5.2. System Description and Design Objectives.....	89
5.2.1. Model Formulation.....	89
5.2.2. Design Objectives and Design Specifications.....	94
5.3. Design Using Static Output Feedback.....	97
5.3.1. Robustness with Respect to Changing Flight Conditions...	97
5.3.2. Selection of a Gain in the Permissible Region.....	100
5.3.3. Robustness with Respect to Sensor Failure.....	110
5.4. Design Using Dynamic Output Feedback.....	112
5.4.1. Search for Filters.....	112
5.4.2. Dynamic Feedback of Pitch Rate.....	118
5.4.3. Dynamic Feedback of Normal Acceleration.....	122
5.4.4. Dynamic Feedback of Both Outputs.....	123
5.4.5. Dynamic Feedback Summary.....	125
5.5. Summary and Conclusions.....	131
6. AN OPTIMIZATION TECHNIQUE FOR ROBUST CONTROL SYSTEM DESIGN.....	136
6.1. Introduction.....	136
6.2. The Problem and Its Reformulation.....	137
6.3. Nonlinear Programming Solution Procedure.....	139
6.4. Cost and Constraint Gradient Calculations.....	145
6.5. Second Order Example.....	148
6.6. F-4E Example.....	156
6.7. Results and Discussion for Airplane Example.....	160
6.8. Conclusion and Summary.....	172
7. SUMMARY AND FUTURE RESEARCH.....	174
APPENDIX I: AERODYNAMIC DATA.....	176
APPENDIX II: A TYPICAL CONSTRAINT MAPPING.....	178
REFERENCES.....	183

LIST OF FIGURES

	Page
Figure 2.1.	Nominal plant N with perturbations P 4
Figure 3.1.	Feedback system, return difference for loops broken at a 13
Figure 3.2.	Perturbation by $L(s)$ 16
Figure 3.3.	Response to a step command: F-4 (Phantom) aircraft at 5 extremal flight conditions..... 24
Figure 3.4.	Illustration of failure robustness and emergency boundaries..... 26
Figure 4.1.	Circular boundaries in z -plane..... 33
Figure 4.2.	Hyperbolic boundaries in s -plane..... 34
Figure 4.3.	Stability triangle ABC in k_1 - k_2 -plane for a second order discrete-time system..... 53
Figure 4.4.	Stability region $ABCD$ in k_1 - k_2 - k_3 -space for a third order discrete time system..... 55
Figure 4.5.	Disconnected stability region in k_1 - k_3 -subspace..... 59
Figure 4.6.	Nice stability region for crane with $k_1=500$, $k_4=0$,..... 62
Figure 4.7.	Robustness with respect to sensor failures..... 68
Figure 4.8.	Design boundaries for Example 4.9..... 71
Figure 4.9.	Image of the circle Γ_r 86
Figure 5.1.	Flight envelope and operating points [57]..... 90
Figure 5.2.	Aircraft nomenclature..... 92
Figure 5.3.	Allowable short period eigenvalue locations..... 96
Figure 5.4.	Constraint region for non-short period eigenvalues.... 98
Figure 5.5.	Emergency eigenvalue constraint region..... 98
Figure 5.6.	C_N^* response envelope..... 99
Figure 5.7.	Structure with static output feedback..... 99

	Page
Figure 5.8a.	The region R_{nom2} 101
Figure 5.8b.	Region in s-plane and description of K-space boundary.... 102
Figure 5.9.	The region R_{nom} 103
Figure 5.10.	Constant damping, single real root, and natural frequency curves for flight condition 2..... 105
Figure 5.11.	The regions R_{nom} and $R_{nom}^{(1)}$ 106
Figure 5.12.	δ_e, C_N^* responses for flight condition 1 showing the effect of $\ k\ $ on control..... 107
Figure 5.13a.	C_N^* and δ_e responses for trial gains Q_1 108
Figure 5.13b.	N_z and q responses for trial gains Q_1 109
Figure 5.14.	The regions R_{nom}, R_{em} 111
Figure 5.15.	Output feedback with $m=2$ 113
Figure 5.16.	The regions R and R_{em} 113
Figure 5.17.	Possible observer structure..... 114
Figure 5.18.	Structure of the inverse filter..... 115
Figure 5.19.	Acceleration feedback only..... 117
Figure 5.20.	Structure of controller using dynamic output feedback.... 119
Figure 5.21.	The regions R_{emq} and R_{nomq} 120
Figure 5.22.	The regions R_{21} and R_{32} 121
Figure 5.23.	The region R_{emNz} 122
Figure 5.24.	The regions $R, R_{nom},$ and R_{emq} 124
Figure 5.25.	C_N^* responses for flight condition 2..... 126
Figure 5.26.	Final controller configuration..... 126
Figure 5.27a.	C_N^* and δ_e responses for trial gains Q_2 127
Figure 5.27b.	N_z and q responses for trial gains Q_2 128

	Page
Figure 5.28a.	C_N^* responses for the unfailed and open loop systems..... 132
Figure 5.28b.	C_N^* responses after failure of one sensor..... 133
Figure 5.28c.	C_N^* responses after failure of two sensors..... 134
Figure 6.1.	Second order example: constraint region in the complex plane..... 150
Figure 6.2.	Second order example: constraint region in the k-plane... 151
Figure 6.3.	Aircraft example: constraint region in the complex plane under normal operating conditions..... 157
Figure 6.4.	Constraint region in the complex plane: emergency conditions..... 159
Figure 6.5.	Region of possible gains which satisfy the constraints under normal operating conditions for all four flight conditions..... 163
Figure 6.6.	C_N^* response envelope..... 165
Figure 6.7.	C_N^* responses of two designs..... 166
Figure 6.8.	Control inputs for two designs..... 167
Figure II.1.	Eigenvalue constraint region (not drawn to scale)..... 178
Figure II.2a.	Boundaries in K-space..... 179
Figure II.2b.	Boundaries in K-space (enlargement of Fig. II.2a)..... 180
Figure II.3.	Partitions of k_3, k_2 plane..... 181

CHAPTER 1

INTRODUCTION

The importance of designing control systems which are robust or insensitive to variations in the plant parameters has long been appreciated. However, the rapid advances in design techniques for multivariable systems has heightened interest in the study and design of robust systems. The purpose of this report is to provide an up to date survey of the work in this field and summarize the results of research in this area conducted at the Coordinated Science Laboratory.

The report begins in Chapter 2 with a description and examples of the robust control problem. Chapter 3 provides a survey of research in the field of robust control. It is apparent from this survey that the work can be divided into two areas. The first assumes unstructured perturbations and analyzes worst case effects. The second considers large, structured perturbations. The parameter space design method presented in Chapter 4 is directed at the second area. The tools of Chapter 4 are applied to a fighter aircraft example in Chapter 5. Chapter 6 presents an optimization approach to the same problem. Finally, Chapter 7 summarizes the report and presents several directions for future research.

CHAPTER 2

THE ROBUST CONTROL PROBLEM

2.1. Description of the Robust Control Problem

The objective of a basic control system design problem is to satisfy a set of performance specifications for a given dynamical system. The robust control system design problem adds to the basic control problem by requiring the performance criteria to be satisfied under a specified class of perturbations to the dynamical system. Typical examples of performance criteria for which the overall closed loop system must be robust are:

- 1) Stability or nice stability (e.g. defined by constraints on eigenvalue locations).
- 2) Limited deterioration of a performance index.
- 3) Limited deviation from an ideal behavior, e.g. constraints on step responses or frequency responses or on the return difference.
- 4) Limited deviation from a reference behavior, e.g. deviation from a nominal trajectory or a reference model response.
- 5) Tracking, i.e. zero asymptotic error for a class of reference and disturbance inputs.
- 6) Limited demand on control $|u|$ and control rate $|\dot{u}|$.

The classes of perturbations which are considered can be grouped in two categories: structural perturbations and system parameter perturbations. Some examples of structural perturbations are:

- 1) Sensor failures.
- 2) Actuator failures.
- 3) Switching from automatic to manual control.
- 4) Change in system order due to a failure. Example: An aggregate description for several power generators or a traffic flow or economic variables must be dissolved into a more detailed description of transients between individual components in failure situations.

Parametric perturbations are due to uncertainties in the plant model and in the controller implementation. Examples are:

- 5) Analytically known dependence of a plant model on uncertain physical parameters. Example: The linearized equations of a crane with physical parameters m_c = crab mass, m_L = load mass, l = rope length, g = gravitational constant, and state variables x_1 = crab position, x_2 = crab velocity, x_3 = rope angle and x_4 = rope angular velocity are

$$\dot{\underline{x}} = \begin{bmatrix} 0 & 1 & 0 & 0 \\ 0 & 0 & m_L g / m_c & 0 \\ 0 & 0 & 0 & 1 \\ 0 & 0 & -\omega^2 & 0 \end{bmatrix} \underline{x} + \frac{1}{m_c} \begin{bmatrix} 0 \\ 1 \\ 0 \\ -1/l \end{bmatrix} u \quad (1)$$

with $\omega^2 = (m_c + m_L)g/m_c l$. Input u is the force accelerating the crab. The crane may operate with an unknown load mass m_L between the empty hook and the maximum mass, for which the crane is designed. It may also operate with an unknown constant rope length between zero and the height of the crane.

- 6) Numerically known dependence of a plant model on an unknown physical parameter vector $\underline{\theta}$. Example: linearized equations of longitudinal motion of an aircraft depending on altitude and speed

$$\dot{\underline{x}} = \underline{A}(\underline{\theta}) + \underline{B}(\underline{\theta})u \quad (2)$$

\underline{A} and \underline{B} may be given for J typical flight conditions in the flight envelope. $\underline{A}_j = \underline{A}(\underline{\theta}_j)$, $\underline{B}_j = \underline{B}(\underline{\theta}_j)$, $j = 1, 2, \dots, J$.

- 7) Known dynamics, which have disappeared in a simplified design model by linearization, truncation of structural modes, model reduction, neglecting of actuator and sensor dynamics. In some cases it may be possible to pull out all uncertainties as illustrated by Fig. 2.1, where for $P=0$ the nominal plant N is obtained.

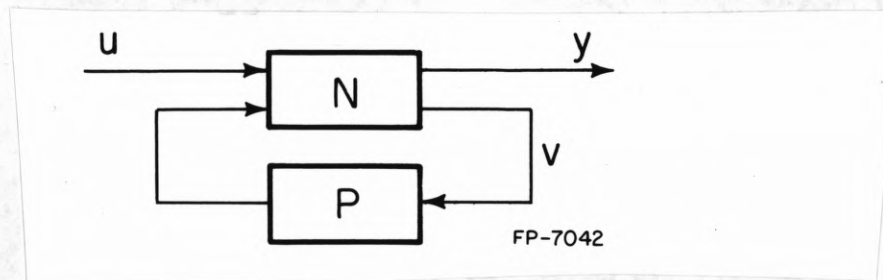


Figure 2.1. Nominal plant N with perturbations P .

In simple cases the perturbations P can be expressed as a diagonal matrix of linear or nonlinear operators.

- 8) Unknown dynamics, which cannot be modeled. In this case only vague assumptions about perturbations δA , δB , δC of the system matrices A , B , C ($\dot{\underline{x}} = A\underline{x} + Bu$, $y = C\underline{x}$) or perturbations $\delta G(s)$ of the transfer function matrix $G(s)$ can be made.

- 9) Quantization effects and time delays in controller implementation.
- 10) Variance of components in mass produced control systems and circuits.

These examples of system properties and perturbations show that many special combinations can be specified. Therefore many different definitions of "robust control" can be found in the literature.

The design problem for a robust control system may be formulated in one of the following three forms:

1. Given a system property, determine the class of perturbations with respect to which the system property is robust. Design the controller such that the class of admissible perturbations is extended in the direction of the really expected perturbations.
2. Given a class of perturbations, determine the maximum deviation from a desired system behavior which occurs under the worst perturbation in the given class. Design the controller such that the maximum deviation is minimized.
3. Given a system property and a class of perturbations, determine if there exists a set of controllers for which the system property is robust under the class of perturbations. If yes, select one on other criteria than robustness. If not, relax specifications.

2.2. Controller Structure and Other Design Considerations

Design problems for control systems are usually parameterized by the assumption of a controller structure which defines a vector of design parameters. Two typical assumptions for the controller structure are adaptive controllers or fixed gain controllers. One extreme is the attempt to obtain as much information about the perturbations as possible by on-line identification and failure detection. Then ideally the structure and parameters of the controller are adapted in order to achieve the best possible performance of the control system given the momentarily available information. An intrinsic difficulty of this approach is that plant inputs, which admit a fast and accurate identification, are not good to achieve the best performance and vice versa. Also a tradeoff between a fast failure detection, identification and adaptation and a reliable one, which avoids false alarms and noise sensitivity of the adaptation, must be made.

The other extreme is the attempt to find a fixed gain controller which accomodates a specified class of perturbations. In this approach it may be necessary to sacrifice some performance in the nominal case in order to achieve robustness for the perturbed situation. The assumed controller structure may be state feedback, or static or dynamic output feedback. Note that full state feedback is not the most general controller. Information about the unknown parameters is contained in past states, their processing in a dynamic system can therefore improve the performance. In some cases the unknown parameters can be introduced as additional states, which may be estimated and fed back. Most design techniques are restricted to linear systems, thus a linear controller is usually assumed.

Only the case of a fixed gain controller is usually called robust

control. However it should be apparent from the previous discussion that robustness is also a desirable feature for an adaptive control system. The fixed gain solution indicates whether a more complex adaptive system is needed at all, or how far one has to go adaptive. Practical solutions to the robustness problem frequently are in between the two extremes and combine features of both cases. Examples are:

1. Gain scheduling with switching or continuous variation between fixed linear feedbacks dependent on a measurement of an environment condition, which has an influence on the plant parameter values.
2. Variable structures with state dependent switching between fixed linear feedbacks.
3. A fixed gain robust controller may be used for stabilization, with an adaptive controller then used for improvement of performance. (Some techniques for design of adaptive controllers assume an open loop stable system).
4. A fixed gain robust controller may be used as backup for the case of a failure in the adaptive system or in a gain scheduling system. Air data measurements (e.g. dynamic pressure) are not very reliable.
5. Under external noise an adaptive system may not adjust fast enough to a fast change in plant parameters. In such cases, it may be possible to switch to a fixed gain robust system until the identification has followed and adaptation can improve the performance.
6. Adaptive control theory usually does not deal with problems

of structural identification (e.g. failure detection) and structural adaptation after a failure has been detected. However problems are related: Fast structural identification may lead to false alarms, in particular under noisy conditions. Slow and reliable structural identification may leave the system in a failed unstable configuration for a while. The control should be designed to provide robustness of stability with respect to the failure to ensure that nothing very bad happens until the failure is detected reliably.

7. Robust fixed gain control may be combined with some redundancy concepts. Various levels are possible:

- a) Passive redundancy by paralleled components. For example the 50% gain reduction margin of IQ designs offers the possibility of using two paralleled sensors or actuators such that in case of a failure the gain is reduced only by 50%.
- b) Removal of failed components. Even if a component failure can be tolerated, as far as stability is concerned, it may be necessary in the long run to remove a failed component, e.g. to close a leaking gas jet valve or to remove a bias term entering into a control system from a sensor failed at a nonzero constant value.
- c) Analytic redundancy may help, if an adaptive observer provides an estimate for a missing signal.
- d) Hardware redundancy, e.g. majority voting in a multiplexed system can bring the system back to its original performance.

~~... system ideally should not~~

However this part of the system ideally should not be vital for stability (see 6).

With the availability of cheap computers there are few constraints on the complexity of the controller structure. However there are several practical limitations and additional aspects for the design. Some of them are given here.

1. A main constraint on the controller complexity is given by the presently available design methods. Also it is a question with which methods the designer has experience and for which he has design software available. Ideally, control theory should provide the designer with convenient tools, e.g. for the computer-aided design of control systems, instead of demanding that the designer has to put all thinkable tradeoff situations into one scalar performance index or set of inequalities.
2. In many control problems structural limitations are mainly dictated by the cost, availability and reliability of sensors and actuators. Thus output feedback and saturation of control or control rate are important design considerations. For robust control systems with control constraints it is a particularly important rule of thumb to make only physically reasonable requirements. For example, one should not try to make a slow system fast or a fast system slow (i.e., do not use one reference model, but fast and slow reference models for different operating conditions, or demand only invariance of damping or maximum overshoot, not of natural frequency or time of maximum overshoot). Of course such considerations

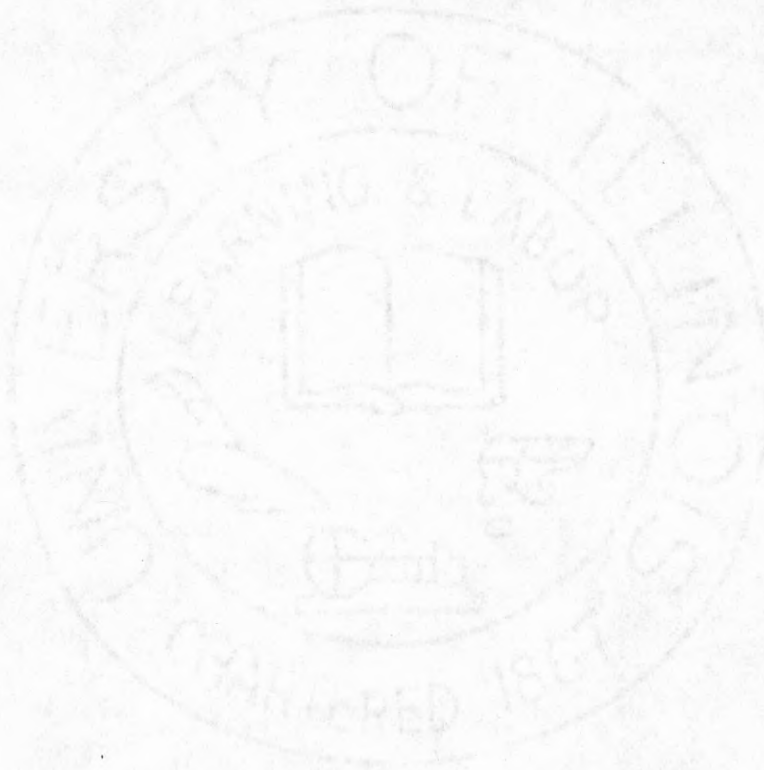
depend on which property of the application must be robust. In the design of an oscillator the frequency must be constant whereas in the design of a crane the frequency is less important. Also it would be not reasonable to require an unchanged performance in cases of sensor or actuator failures. Thus emergency specifications should be given for these cases.

3. Some special consideration must be given to the case for which there is a man (operator, pilot) in the outer loop. A pilot does not want to be a passenger. He may want to identify the controlled aircraft by "playing" with the input signals. Control schemes which give him the same feeling for a wide range of parameter variations may be dangerous if the dynamics suddenly become bad beyond an assumed range of parameter variation. The pilot needs a warning before the "cliff". This is another reason why the dynamics should change with changing parameters.

A plant operator may want to switch one or more loops from automatic to manual control. It is desirable that he always sees a stable system or better one, which he can easily control. A man can control an unstable plant provided the eigenvalues in the right half plane are close to the origin. He has more problems if he has to control fast modes, even if they are slightly damped. In other words, the imaginary axis is not necessarily the best emergency boundary for sensor failures.

The problems of actuator and sensor failures look similar if we interpret them as a row or a column of the feedback matrix being switched to

zero. For the human operator these cases are quite different, since for many variables he has sensors, which he can use as backup. This is rarely the case for actuators.



CHAPTER 3

A SURVEY OF ROBUST CONTROL RESULTS

3.1. Introduction

The discussion of the preceding chapter has demonstrated that robustness is an important issue in areas of control system design ranging from fixed gain controllers to completely adaptive control systems. The intent of this report is to concentrate on fixed gain, linear time invariant control systems. Hereafter in this report, references to robust control system design will assume this structure.

There are two basic philosophies to the analysis and design of robust control systems. The first assumes that the perturbations are largely unstructured. The objective is to design the controller for the worst perturbation and evaluate or bound the size of the permitted perturbations.

The second approach assumes that the structure of the disturbances and their size are known a priori. The design objectives are to minimize the sensitivity of the closed loop systems in the known perturbations directions.

Each of the two approaches have advantages and disadvantages. The first is more likely to provide robustness with respect to unmodeled errors, and hence requires less accurate models. The results are often very conservative. The second requires accurate models of the perturbations which one likely to occur. However, the control effort is directed where it is needed most.

The purpose of this chapter is to review the work which has been done on the robust control problem. The survey is divided into two sections corresponding to the approaches outlined above.

3.2. Sensitivity and Unstructured Perturbations

3.2.1. Frequency Domain Methods

The main reasons for the use of feedback are stabilization and the preservation of desirable system properties in spite of noise inputs and perturbations of system parameters. The reduction of nonlinear distortions was an essential reason for the use of feedback amplifiers, (see Black [1]). The reduction of nonlinearity by high gain feedback has been further investigated by Cruz [2] and Desoer and Wang [3].

In frequency design methods the concept to compensate the loop, such that high gains are possible without instability, is the classic rule of thumb for the reduction of noise and uncertainty. Bode [4] expressed it in terms of gain and phase margins and a sensitivity function, which was generalized to the multivariable case by Cruz and Perkins [5]. A sensitivity matrix $S(s)$ relates the output errors $E_c(s)$ due to perturbations in a feedback system to the output errors $E_o(s)$ due to the same perturbations in a corresponding open loop system by $E_c(s) = S(s)E_o(s)$. The sensitivity matrix $S(s)$ is the inverse of the return difference matrix, for the loop of Fig. 3.1.

$$S(s) = [I + G(s)K(s)H(s)]^{-1} \quad (3)$$

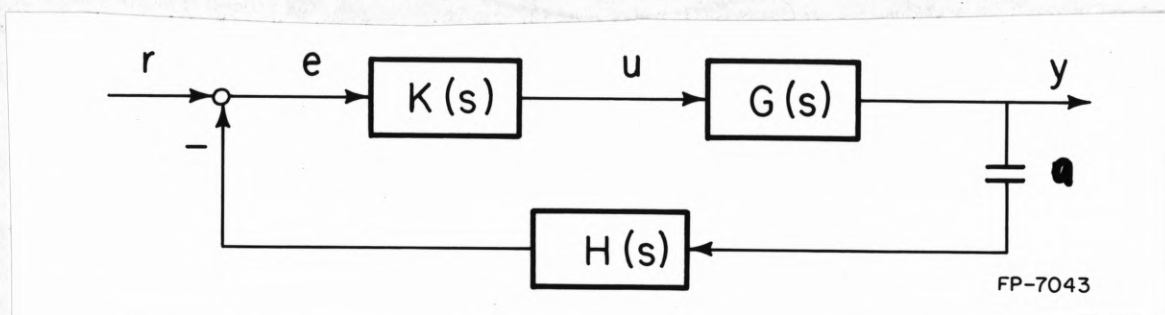


Figure 3.1. Feedback system, return difference for loops broken at a.

Note that $G(s)$ is the actual plant, which may be expressed by the nominal design model $G_N(s)$ and a perturbation $\delta G(s)$, i.e. $G(s) = G_N(s) + \delta G(s)$. If the known $G_N(s)$ is used in eq. (3) instead of the unknown $G(s)$, then all results are local, i.e. restricted to small $\delta G(s)$. For a reduction of sensitivity it is sufficient that

$$S^T(-j\omega)S(j\omega) - I \leq 0 \quad (\text{neg. semidefinite}) \quad (4)$$

over the frequency band of interest, or in terms of the return difference $F(s) = I + G(s)K(s)H(s)$

$$F^T(-j\omega)F(j\omega) - I \geq 0. \quad (5)$$

Hsu and Chen [6] proved the relationship

$$\det F(s) = \frac{\text{closed loop characteristic polynomial}}{\text{open loop characteristic polynomial}}. \quad (6)$$

Thus, if no cancellations occur, closed loop stability can be analyzed using $\det F(s)$. MacFarlane [7] studied the eigenvalues $\rho_j(s)$, $j = 1, 2, \dots, m$ of $F(s)$ and showed that the closed loop is stable, if all characteristic frequency loci $\rho_j(j\omega)$, $j = 1, 2, \dots, m$ satisfy the Nyquist criterion. He also proved a necessary condition for the system to be optimal in the sense of a quadratic criterion $\int_0^{\infty} (y^T Q y + u^T R u) dt$:

$$|\rho_j(j\omega)| \geq 1 \quad \text{for } 0 \leq \omega \leq \infty \quad j = 1, 2, \dots, m \quad (7)$$

or

$$|\det F(j\omega)| \geq 1 \quad \text{for all } \omega. \quad (8)$$

These results have the graphical interpretation that the complex plane plots

of $|\det F(j\omega)|$ or $|\rho_j(j\omega)|$ must not penetrate the interior of the unit disc. It follows from this that the characteristic frequency loci of an optimal proportional feedback controller have infinite gain margin and at least 60° phase margin.

Robustness of stability with respect to gain and phase changes may also be achieved in design by Rosenbrock's inverse Nyquist array [8]. Here $I + G_o^{-1}(j\omega)$ with $G_o(s) = G(s)K(s)H(s)$ (see Fig. 2) is analyzed graphically and modified in the design. A standard technique in multivariable control system design is to use compensation or feedback to decouple or approximately decouple a multivariable system into several single input systems, which may be designed by single-loop techniques. Rosenbrock [8] uses the criterion of diagonal dominance for approximate decoupling.

Doyle showed by counterexamples [9] that these methods can lead to highly optimistic margins for individual loop gains, even if only very small margins exist for simultaneous change of several loop gains. Already in the single-input case, gain and phase margins are insufficient to characterize what happens for simultaneous gain and phase perturbations. Another difficulty is that by compensation or feedback for diagonal dominance the actual location of the uncertainty is obscured.

Doyle [9] examines the properties of the return difference using the concepts of singular values, singular vectors and the spectral norm of a matrix. The singular value σ_i of a matrix A are the non-negative square roots of the eigenvalues of A^*A , where A^* is the conjugate transpose of A . Since A^*A is Hermitian, its eigenvalues are real. The singular values give a measure of how close A is to being singular. The ratio of the smallest singular value $\underline{\sigma}$ and the largest one, $\bar{\sigma}$, is the condition number $\underline{\sigma}/\bar{\sigma}$. One may also

interpret the singular values as generalizing to matrices the notion of gain. This characterization is of great practical value, since good software to compute a singular values is widely accessible [10]. Using this singular value concept Doyle proved the following robustness theorem.

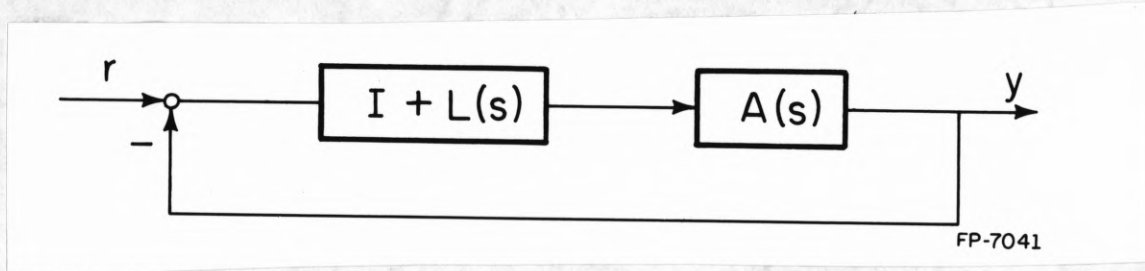


Figure 3.2. Perturbation by $L(s)$.

In the system of Fig. 3.2, let $G(s)$ be rational, square, invertible and such that the nominal closed loop with $L(s) = 0$ is stable, i.e. $G(I+G)^{-1} = I+G^{-1}$ is stable. If the system is perturbed by $L(s)$, which by itself is stable, then the perturbed system is stable if

$$\underline{\sigma}(I+G^{-1}(j\omega)) > \overline{\sigma}(L(j\omega)) \quad \text{for all } \omega. \quad (9)$$

For this theorem Sandell [11] gave a different proof, in which $G(s)$ need not be rational. $\underline{\sigma}(I+G^{-1}(j\omega))$ is a frequency dependent measure of robustness in terms of gain margins. For the eigenvalues λ of A (here $= I+G^{-1}(j\omega)$) generally the relation

$$\underline{\sigma}(A) \leq |\lambda(A)| \leq \overline{\sigma}(A) \quad (10)$$

holds. It is possible that the smallest eigenvalue is much larger than $\underline{\sigma}(A)$. Thus the minimum singular value $\underline{\sigma}$ gives a more reliable measure of robustness than the smallest eigenvalue. In fact Doyle constructed an example, where the diagonal dominance approach as well as the characteristic loci approach

generates a Nyquist or Inverse Nyquist plot, which shows $\pm \infty$ db gain margin and 90° phase margin. However the system is only marginally stable.

The problem of uncertainties due to a reduced order design model is interrelated with the question of which modes of the system must be influenced by the control and which others should ideally not be influenced at all. In vehicle control it may for example be desirable to control the rigid body dynamics fast and accurately, i.e. with a reasonably high bandwidth, without interfering with structural vibrations. In frequency domain design techniques, this is achieved by a 40 db/decade roll off beyond the design bandwidth. This aspect is frequently ignored in state space design techniques. In all design techniques it is important to study carefully the behavior in a frequency range above the bandwidth, where modes are still sufficiently controllable and observable, such that the control may move them into the right half s plane.

Stein and Doyle [12] give a design example for a CH-47 helicopter with two control inputs. They apply singular value analysis and the robustness condition (9). Rotor dynamics and rate limits are translated into $\bar{\sigma}(L(j\omega))$ using a result of Safonov [13]. The two singular values were made approximately equal and the bandwidth in both loops was increased as much as $\bar{\sigma}(L(j\omega))$ admitted. A low pass helped to meet the "roll-off" requirement. The example also showed that these methods may lead to very conservative results in cases of large variations of parameters in specific directions, here the flight condition variation.

3.2.2. State Space Methods

Single-input linear quadratic state feedback regulators have a return difference greater than unity at all frequencies, as was shown by Kalman

[14]. Anderson and Moore [15] showed that this fact implies a $\pm 60^\circ$ phase margin, infinite gain margin and 50 percent gain reduction tolerance. Safonov and Athans [16] generalized this result to the multiinput case:

$$\begin{aligned}\dot{x} &= Ax + Bu \\ u &= -Kx \\ \text{with } m \text{ inputs } u_i.\end{aligned}\tag{11}$$

The feedback matrix K is determined by solving a Riccati equation minimizing

$$J = \int_0^{\infty} (x^T Q x + u^T R u) dt\tag{12}$$

with Q positive definite and $R = \text{diag}[r_1, \dots, r_m]$, $r_i > 0$.

The individual inputs u_i are perturbed to $\eta_i u_i$ without interaction between them, i.e.

$$\dot{x} = Ax + B\eta u \quad \text{with } \eta u = \begin{bmatrix} \eta_1 u_1 \\ \vdots \\ \eta_m u_m \end{bmatrix}.\tag{13}$$

Let each perturbation η_i be linear time invariant with proper rational stable transfer function $P_i(s)$. Its frequency response is $P_i(j\omega) = a_i(\omega) \cdot e^{j\phi_i(\omega)}$. Then the closed loop remains stable under a phase perturbation $\phi_i(\omega)$, with $|\phi_i(\omega)| \leq 60^\circ$ for all ω . It also remains stable under a gain perturbation $a_i(\omega) \geq 0.5$ for all ω .

Note that this emphasizes the importance of the bandwidth of the control system. The 60° phase margin without bandwidth limitations is not sufficient to accommodate neglected error dynamics since physical actuators have at least 90° phase lag at high frequencies. For this reason Otto Smith [17] used the "complex gain margin", i.e. the minimum distance of $G(j\omega)$ to

the critical point, scaled by the local frequency increment along $G(j\omega)$. This approximates the negative real part of a dominant pair of eigenvalues. A multivariable measure for the distance of $G(j\omega)$ from the critical point has been discussed already in form of the singular values of the return difference.

Doyle [18] showed by counterexample that the margins may be arbitrary small if the state is replaced by a state estimate from an observer or a Kalman filter. In his example, the gain margins were arbitrarily small in both the positive and negative db direction. To improve the margin in this situation, Doyle and Stein [19] developed a "design adjustment procedure", which introduces fictitious noise at the control input to the plant. In this procedure the observer eigenvalues tend to the finite transmission zeros and to infinity. Thus the procedure works only for minimum-phase plants. The procedure is essentially the dual of Kwakernaak's sensitivity recovery method [20]. This however drives the plant poles instead of the observer poles to the transmission zeros, which may lead to large control inputs u .

Gain and phase margins may be much smaller in discrete time linear quadratic state feedback systems. Jacques Willems and van de Voorde [21] give bounds for the single-input case, which show that the system may be very sensitive to feedback gain variations. This is not surprising, since the hold element may be approximated by a phase shift of one half sampling interval.

Safonov and Athans [16] also generalize a single-input result by Anderson and Moore [15], which is useful for actuator nonlinearities. If the perturbation operator \mathcal{N} in eq. (13) describes a time varying, memoryless nonlinearity $\mathcal{N}_i u_i = f_i(u, t)$, then it is a sufficient condition for the closed loop stability, that

$$\frac{1}{2} < \frac{1}{u} f(u, t) \leq M \quad \text{for some } M < \infty \text{ and for all } t. \quad (14)$$

For example, for an actuator saturation, stability is guaranteed if the inputs do not exceed twice the saturation level.

Comparisons of numerous optimization techniques for insensitive control systems were made by Harvey and Pope [22,23] for wing load alleviation for the C-5A aircraft and by Vinkler and Wood [24] for a lateral autopilot for a rudderless remotely piloted vehicle. A minimax technique by Salmon [25] and an uncertainty weighting technique by Porter [22] were judged superior to six other techniques in the first report; both however failed in the comparison [27]. Here an expected cost technique by Ly and Cannon [26] and a multistep guaranteed cost technique by Vinkler and Wood [27] came out better than four other techniques. In [23] an information matrix approach by Kleimann and Rao [28] compared favorably with other techniques.

In problems with insignificant constraints on the control inputs, the weighting matrix R in a quadratic criterion may be small. This leads to high gain solutions as they were discussed in the previous section. A comparison of various high gain feedback systems is made by Young, Kokotovic and Utkin [29]. This comparison also includes variable structure systems, which in their sliding mode are insensitive to parameter variations and disturbances, similar to the high-gain system [30]. Young [31] applied this concept to the design of an adaptive model following control system and compared the results for the longitudinal motion of a Convair C-131B aircraft with other model following techniques.

A special case of a high gain control system is useful, if the reference or disturbance input signals can be exactly modeled and asymptotic

tracking or disturbance rejection is required. The use of integrators in the loop for zero stationary errors in step and ramp responses is a classical recipe. Also for other inputs an internal model of the input can be used, e.g. a tuned oscillator (notch filter) for disturbance rejection of helicopter rotor vibrations, whose frequency is regulated. Such a high gain at particular frequencies makes asymptotic tracking robust to plant parameter variations as long as the loop remains stable. This robustness problem was studied by Davison [32] and others. In sampled-data systems the internal model is to be implemented in continuous time, if the tracking property is required also between the sampling instants [33].

Some common problems in all high gain concepts are

- Measurement noise goes highly amplified to the actuator inputs.
- High values for $|u|$ and $|\dot{u}|$ may occur.
- Non-cooperative efforts of the actuators may occur.

The LQG design method offers a systematic way to avoid these difficulties by increase in the R matrix and by the use of a Kalman filter.

3.3. Robustness with Respect to Large Perturbations in Known Directions

3.3.1. Parameter Methods

In the methods of Section 3 relatively little knowledge about the parametric perturbation is assumed. The results are therefore primarily valid for small perturbations. In some cases information is obtained about how big the perturbation is allowed to be in order to maintain stability.

In situations where large perturbations in known directions occur, the previous methods generally lead to very conservative results. In this section some tools are discussed by which such perturbations can be accommodated in the design. The next chapter and [34] also describe a parameter space

method which is applicable to this problem.

In typical design examples not only the mathematical model of the plant is uncertain, but also the formulation and relative weight of many design criteria. Some of these criteria are in form of inequality constraints; others are to be minimized. It is artificial to put all of them together into one scalar performance index, which is then minimized over the parameters in an assumed controller structure. For the designer an interactive computer-aided design procedure is more useful, where he can make higher level decisions of how to change requirements after each computer solution or failure to find a solution. The computer may have to solve a nonlinear programming problem in each design step. Various aerospace problems have been formulated and solved this way. Schy [37,38] deals with a lateral stability augmentation system for a fighter airplane, Hauser [39] with an autopilot for a flexible space vehicle. Further design examples are given by Karmarkar [40] and Kanarachos [41]. It is convenient to formulate all design criteria for each operating point as components of a performance vector \underline{g} . It may, for example, contain

- bounds on the individual feedback gains $|k_{ij}|$.

and for each flight condition specifications on

- eigenvalue location.
- deviation from nominal response for typical reference and disturbance inputs.
- bounds on the control rate $|\dot{u}|$ for typical reference and disturbance inputs.

Kreisselmeier and Steinhauser [42] use in an example with five flight conditions of a F4-C aircraft a 40 dimensional vector \underline{g} . A vector constraints $\underline{g} < \underline{c}$ (i.e. componentwise $g_i \leq c_i$) is given and the feedback gains K are the solution of

the problem

$$\text{Min}_K \{ \text{Max}_i g_i(K)/c_i \}. \quad (17)$$

Using an algorithm described in [43] Kreisselmeier and Steinhauser obtain a Pareto-optimal solution. Figure 3.3 shows some reference step responses of this design for an F4-C. It is stable in the five flight conditions. The open loop responses on the left side show that the aircraft is slow in flight condition 1 (landing approach). Here a slower reference response was given than for the high speed condition 2 and 4. The desired reference response was specified as $g_i(t) = g_M(\alpha_i t)$ where for each flight condition $i = 1, 2, \dots, 5$ an appropriate time scale α_i was chosen. This resulted in the insensitive closed loop responses on the right side of Fig. 3.3, which required only a relatively small control rate $|\dot{u}|$. The same feedback resulted in similarly good disturbance responses.

Also the results of Shy [38] showed that an amazingly large variation of parameters can be accommodated by a fixed gain controller, if the requirements were in good agreement with the physical limitations. These designs result in low gain solutions, and the dynamics change in an acceptable or desirable way as the physical parameters vary.

3.3.2. Integrity: Robustness with Respect to Sensor and Actuator Failures

If an actuator or sensor is connected to a high gain, then its failure is a larger perturbation than in a low gain situation. Thus requirements for robustness with respect to actuator and sensor failures tend to result in low gain solutions. Even more important is the aspect of avoiding non-cooperative efforts of actuators. If, for example, one input alone places some eigenvalues in the right half plane and another is needed to bring them back

uncontrolled

insensitive control

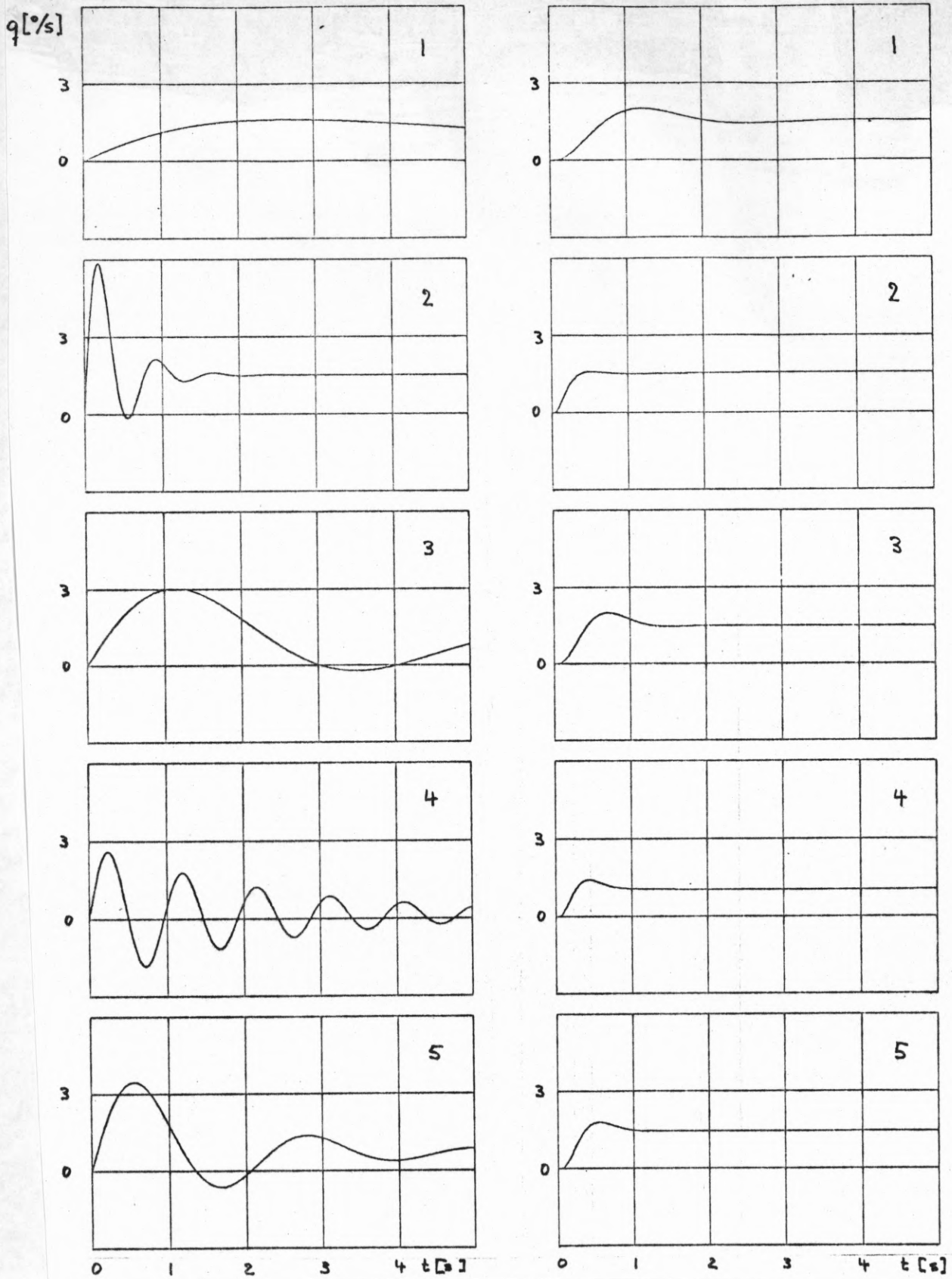


Figure 3.3. Response to a step command: F-4 (Phantom) aircraft at 5 extremal flight conditions (altitude 0 ... 40 000 ft, Mach number .2 ... 2.2).

into the left half plane, then apparently no robustness of stability with respect to actuator failures can be achieved.

One approach to achieve robustness of stability with respect to certain failures is to try to extend gain reduction margins to include gain zero. Belletrutti and MacFarlane [44] use the term "high integrity" for robustness with respect to certain failures. They check the stability conditions for gains reduced to a small ϵ using Nyquist stability criteria for characteristic loci of principal submatrices of the return ratio. In this analysis the loop must be broken at the point where the actual failure may occur and thus the gain reduction margin is needed. Owens [45] derived necessary and sufficient conditions for integrity of systems with multivariable proportional-integral controllers.

Solheim [46] formulated the integrity problem in the context of quadratic optimal control. In examples an increased integrity is obtained with an increased weight R on the control in the quadratic criterion, another indication that the solution will tend to a low gain solution. Wong, Stein and Athans [47] show the following gain reduction result for LQ regulators:

The matrix $A_c(\Lambda) = A + B\Lambda K$ with $\Lambda = \text{diag}[\alpha_1 \dots \alpha_m]$, where K minimizes

$\int_0^{\infty} x'Qx + u'Rxdt$ for $\Lambda = I$, is stable for all

$$\Lambda > \frac{1}{2}[I - (R^{1/2}K'Q^{-1}KR^{1/2})^{-1}]. \quad (18)$$

This generalizes the bound $\alpha_i > 0.5$ from [16]. The recommendation is, from a purely robustness standpoint, to choose Q and R such as to maximize

$$\lambda_0 = \lambda_{\min} \{(R^{1/2}K'Q^{-1}KR^{1/2})^{-1}\}. \quad (19)$$

Kreisselmeier [48] proposes to modify the quadratic criterion, where for each

considered failure situation, a quadratic criterion is formulated and the overall criterion is a weighted sum of these terms.

In failure situations it may be desirable to specify other emergency boundaries in the eigenvalue plane than only the imaginary axis. This problem is treated by parameter space methods in [34] and in Chapter 4. The concept is illustrated for the case of sensor failures in Fig. 3.4. A nominal region for the eigenvalue location and a larger emergency region are mapped into the space of

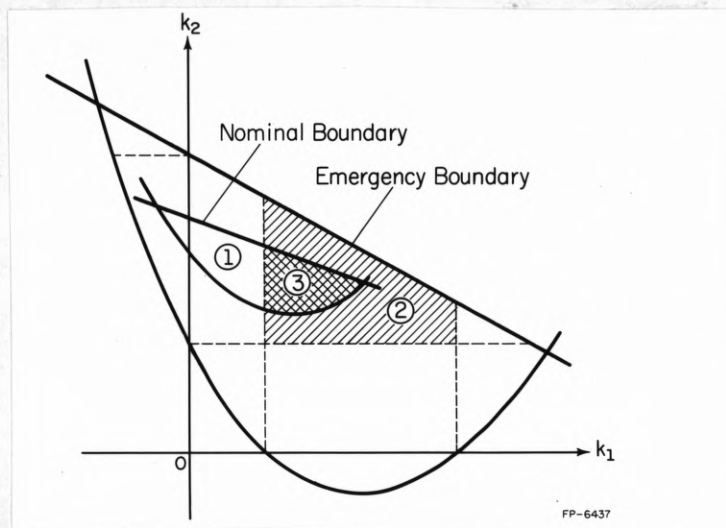


Figure 3.4. Illustration of failure robustness and emergency boundaries.

feedback gains. It is assumed that the system is represented in "sensor coordinates", then a failure of a sensor for state variable x_i corresponds to switching k_i to zero. The projection of point 1 on the k_1 axis is outside the emergency boundary, i.e. the emergency specification is not robust with respect to a sensor failure $k_2 = 0$. It is, however, robust with respect to $k_1 = 0$. For all points in the shaded area the emergency specifications are robust with respect to either sensor failure. An alternative to this robust

solution would be in this example to omit sensor 1 and to use multiplexed sensors for x_2 and failure detection.

In the multiinput case a sensor failure is equivalent to changing a column of the K matrix to zero and an actuator failure is equivalent to changing a row of K to zero. In [34] an actuator failure example is studied, where the problem is formulated such that the eigenvalues are placed in a nominal position with two actuators and move as little as possible towards the stability boundary for failures of either one of two actuators.

Apparently a necessary condition for robustness with respect to failures is that the insufficiently damped eigenvalues (outside the specified region) remain controllable and observable after the failure. In the crane example, the sensor for the crab position x_1 is essential, because x_1 is not observable by other states. In such situations it is apparently misleading to use high gain feedback and to show gain reduction to only a few percent of the high gain. For failures of essential actuators and sensors only redundant components can help.

CHAPTER 4

PARAMETER SPACE DESIGN OF ROBUST CONTROL SYSTEMS

4.1. Introduction

In this chapter a new tool for the design of robust control systems is proposed. First the type of robustness problem for which the tool can be applied is described.

Robustness of a control system is defined in terms of system properties which are invariant under a specified class of perturbations. The system property considered in this paper is "nice stability" as specified by a region Γ in the eigenvalue plane, in which all eigenvalues must remain in spite of perturbations. The perturbations may be large changes of physical parameters of the plant or failures of actuators and sensors or inaccurate implementation of the control law.

The following assumptions are made.

1. Only 1. Only linear plants

$$\underline{x}(k+1) = \underline{A} \underline{x}(k) + \underline{B} \underline{u}(k) \text{ or}$$

$$\dot{\underline{x}}(t) = \underline{A} \underline{x}(t) + \underline{B} \underline{u}(t) \quad (20)$$

$$\underline{x}' = [x_1 \dots x_n], \quad \underline{u}' = [u_1 \dots u_p]$$

are considered. It is assumed that eq. (20) is written in "sensor coordinates", i.e. all measured variables are state variables x_i . It may be part of the design task to decide which states are to be measured.

2. \underline{A} and \underline{B} may depend on a physical parameter vector $\underline{\theta}$. Only some typical values

$$\underline{A}_j = \underline{A}(\underline{\theta}_j), \quad \underline{B}_j = \underline{B}(\underline{\theta}_j) \quad j = 1, 2, \dots, J \quad (21)$$

may be given. Also the required system property Γ_j may depend on the operating point $\underline{\theta}_j$.

3. The simplest assumed controller structure is state feedback

$$\underline{u} = -\underline{K} \underline{x}. \quad (22)$$

It may not be possible to make all plant models \underline{A}_j , \underline{B}_j nicely stable with the same fixed \underline{K} , i.e. to have all roots of

$$\prod_{j=1}^J \det(\lambda \underline{I} - \underline{A}_j + \underline{B}_j \underline{K}) = 0 \quad (23)$$

in the specified region Γ in the λ -plane. In this situation the designer may decide

- a) To relax the eigenvalue region specification such that a solution exists.
- b) To use several feedback gains, each of which nicely stabilizes a group of pairs $\underline{A}_j, \underline{B}_j$. The gains can then be scheduled depending on a measurement, which admits a distinction between the groups.
- c) To use linear dynamic feedback of order m with controller state vector \underline{x}_c , i.e. try to find a state feedback

$$\begin{bmatrix} \underline{u} \\ \underline{u}_c \end{bmatrix} = - \begin{bmatrix} \underline{K} & \underline{L} \\ \underline{M} & \underline{N} \end{bmatrix} \begin{bmatrix} \underline{x} \\ \underline{x}_c \end{bmatrix} \quad (24)$$

which nicely stabilizes the augmented system

$$\begin{bmatrix} \dot{\underline{x}} \\ \dot{\underline{x}}_c \end{bmatrix} = \begin{bmatrix} \underline{A} & \underline{0} \\ \underline{0} & \underline{0} \end{bmatrix} \begin{bmatrix} \underline{x} \\ \underline{x}_c \end{bmatrix} + \begin{bmatrix} \underline{B} & \underline{0} \\ \underline{0} & \underline{I} \end{bmatrix} \begin{bmatrix} \underline{u} \\ \underline{u}_c \end{bmatrix}. \quad (25)$$

The controller $\underline{M}, \underline{N}, \underline{L}$ with n inputs and p outputs may be written in a canonical basis, such that the feedback matrix in eq. (24) contains $pn+mn+mp$ design parameters. ($(p+m) \times (n+m)$ coefficients in eq. (24) of which m^2 are normalized by the choice of an $m \times m$ transformation matrix).

- d) To use nonlinear feedback, e.g. an adaptive system estimating the physical parameter vector $\underline{\theta}$ in eq. (21).

The tool proposed in this paper is useful for problems of the types a), b), and c).

If some states are not available for feedback, then the corresponding columns of \underline{K} in eq. (22) or of \underline{K} and \underline{M} in eq. (24) are zero.

4. A sensor failure is equivalent to switching all elements of the corresponding column of \underline{K} (or \underline{K} and \underline{M}) to zero. An actuator failure is equivalent to switching all elements of the corresponding row of \underline{K} (or \underline{K} and \underline{L}) to zero. Assume that M such failures or failure combinations have to be considered, which lead to M crippled feedback matrices \underline{K}_m , $m = 1, 2, \dots, M$.

The design goal is to find \underline{K} such that all roots of $\prod_{m=1}^M \prod_{j=1}^J (\lambda \underline{I} - \underline{A}_j + \underline{B}_j \underline{K}_m)$ are inside an "emergency region" in λ -plane. Apparently it is a necessary condition for nice stability to be robust under such failures, that the plant modes outside the specified region Γ in the eigenvalue plane remain controllable and observable after the failure. This fact may be used

in the decision for which sensors and actuators redundancy is necessary. Components which are needed to make the insufficiently damped modes observable and controllable are "essential".

Example 4.1: (Essential sensor) Consider a crane with the physical parameters m_c = crab mass, m_L = load mass, l = rope length, g = gravitational constant. Its state variables are x_1 = crab position, x_2 = crab velocity, x_3 = rope angle, and x_4 = rope angular velocity. For small rope angles the linearized state equations are

$$\dot{\underline{x}} = \begin{bmatrix} 0 & 1 & 0 & 0 \\ 0 & 0 & m_L g/m_c & 0 \\ 0 & 0 & 0 & 1 \\ 0 & 0 & -\omega_p^2 & 0 \end{bmatrix} \underline{x} + \frac{1}{m_c} \begin{bmatrix} 0 \\ 1 \\ 0 \\ -1/l \end{bmatrix} u \quad (26)$$

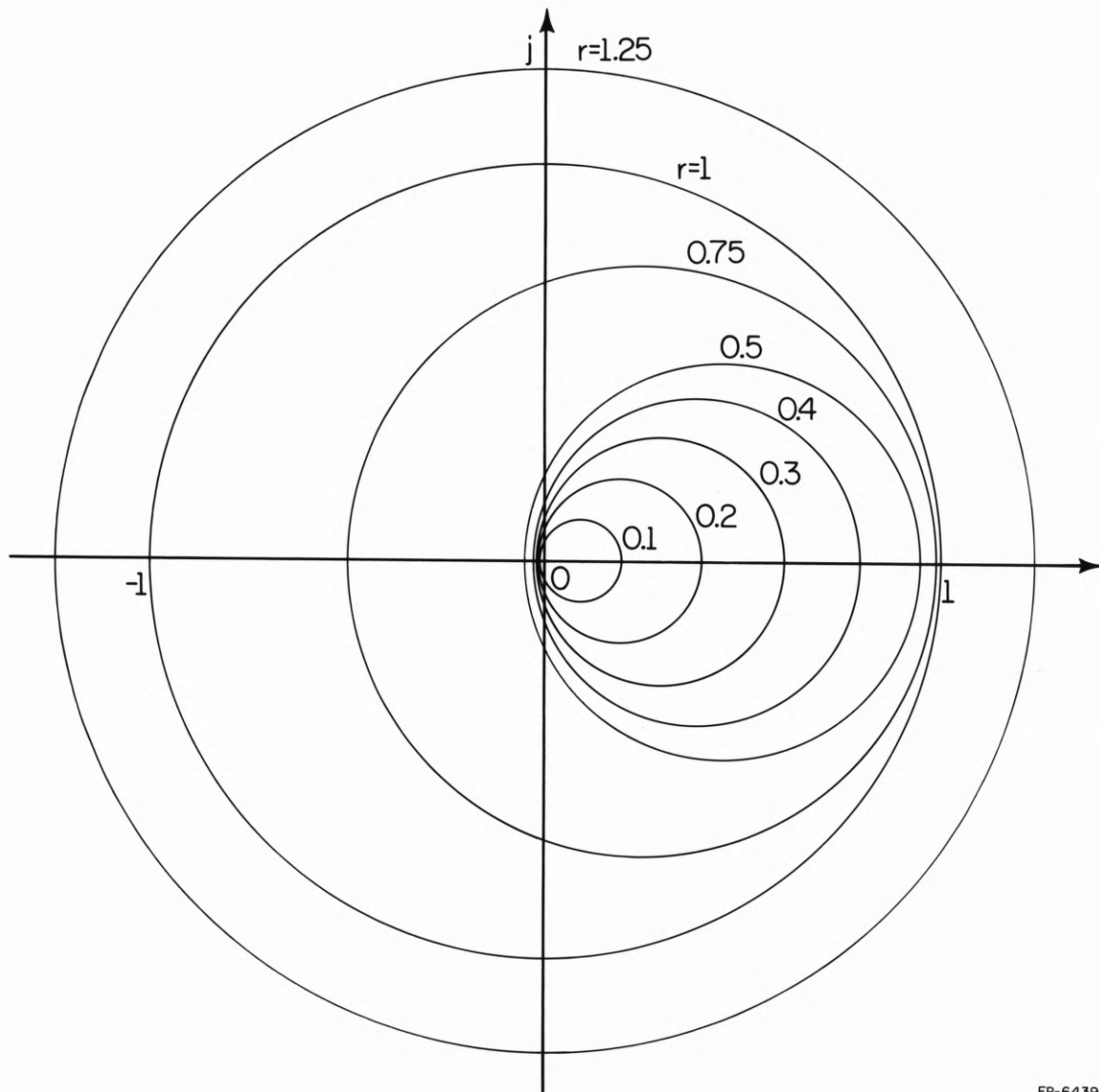
with $\omega_p^2 = (m_c + m_L)g/m_c l$. Input u is the force accelerating the crab. Eigenvalues are $[0, 0, j\omega_p, -j\omega_p]$. The observability analysis shows that x_1 is not observable by x_2 , x_3 , or x_4 . Since one of the zero eigenvalues is unobservable, the crab position sensor is essential for stabilization.

5. It is assumed that desirable features of the dynamic behavior of the control system can be specified by a region Γ in the eigenvalue plane. Examples are
 - a) the stability region, i.e. the left half s plane or the interior of the unit circle in the z plane,
 - b) military specifications for damping and natural frequency of modes of an aircraft,
 - c) in some problem formulations it is convenient to define a

family of regions Γ_r with a parameter r . In the z -plane this may be a family of nonintersecting circles (see Fig. 4.1). For $r=0$ it is a deadbeat solution, and r in the range 0.3 to 0.5 corresponds to well damped transients. (The right shift of this circle excludes heavily oscillatory solutions, the circles approximate the usual logarithmic spirals for constant damping augmented by a constraint on $|z|$). For $r=1$ the stability boundary is obtained. Similarly in the left half s -plane, a family of hyperbolas (guaranteeing a minimum damping and a minimum negative real part of the eigenvalues) may be introduced, augmented by parallels to the imaginary axis in the right half plane (see Fig. 4.2). The equations for these families of boundaries will be given later.

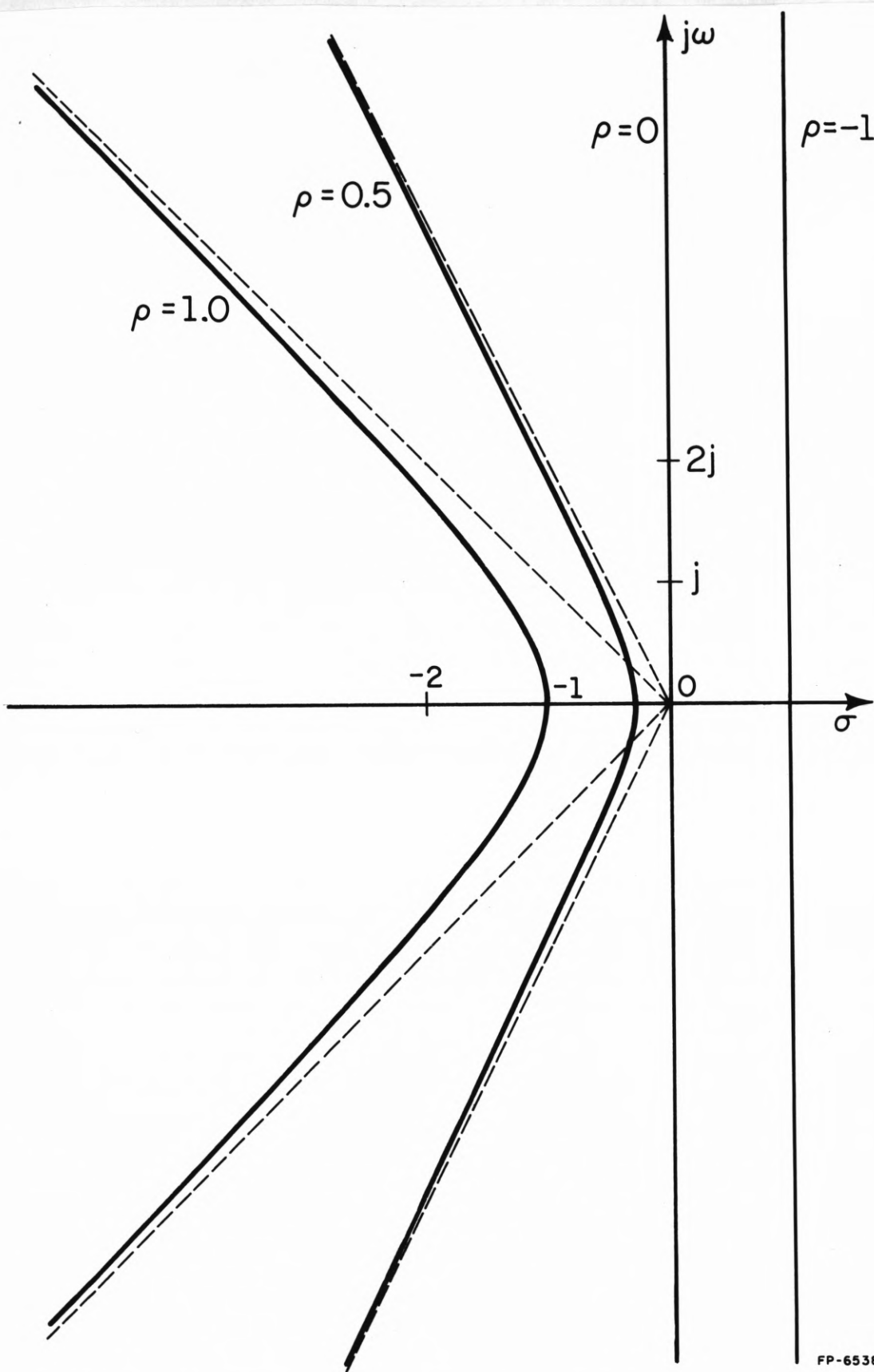
Three types of design problems for robust control system may be distinguished.

1. Given a system property and a controller initially designed for nominal parameter values, under what perturbations of the parameters is the property robust? Modify the controller such as to extend the admissible class of perturbations. Example: Try to extend the gain and phase variations under which stability is robust. It is difficult in this approach to accommodate large perturbation in known directions, e.g. large variations of the physical parameter vector $\underline{\theta}$ in eq. 21. Typically very conservative results are obtained.
2. Given a class of perturbations and a system property with a parameter r , e.g. the family of boundaries Γ_r , for a given controller which is the best value of r such that Γ_r is robust



FP-6439

Figure 4.1. Circular boundaries in z -plane



FP-6538

Figure 4.2. Hyperbolic boundaries in s-plane.

under all perturbations in the given class? Modify the controller to improve r . The system property may be formulated such as to include several design aspects and an optimization can be performed.

3. Given a system property and a class of perturbations, does there exist a state feedback solution such that the property is robust? If not, does there exist a linear dynamic feedback controller of order m , eqs. (24) and (25), such that the property is robust? Find the set of admissible controllers and select one based on criteria, other than robustness, e.g. based on simulations with a nonsimplified nonlinear plant model.

It is primarily this third problem formulation for which the proposed design tool can be applied. The concepts however, are useful also in the second problem. The design tool basically consists in mapping boundaries from the λ plane into boundaries in the parameter space \mathcal{X} , whose coordinates are the elements of the state feedback matrix. Then all tradeoffs between dynamic requirements, robustness requirements, and bounds on the feedback gains can be made in \mathcal{X} space.

The details and most of the examples are worked out for single input plants with state feedback

$$u = -\underline{k}'\underline{x} = -[k_1 \ k_2 \ \dots \ k_n]\underline{x} \quad (27)$$

or state output feedback, i.e. some $k_i = 0$. For multi-input plants the basic result is formulated.

Parameter space methods have a long tradition, mainly in Russia

and Yugoslavia. Siljak [49] gives a historical review of the work by Vishnegradsky, Neimark, Mitrovic, and others. Siljak generalized these parameter mapping methods significantly. A typical procedure for a continuous time system is to assume a controller structure with two free parameters α and β . Determine the closed-loop characteristic polynomial

$$P(s) = \sum_{i=0}^n p_i(\alpha, \beta) s^i = 0. \quad (28)$$

Substitute $s = \sigma + j\omega$ and separate eq. (28) into its real and imaginary parts: $\text{Re}(\sigma, \omega, \alpha, \beta) = 0$, $\text{Im}(\sigma, \omega, \alpha, \beta) = 0$. Assume these nonlinear equations have a solution

$$\alpha = \alpha(\sigma, \omega), \quad \beta = \beta(\sigma, \omega). \quad (29)$$

Equation (29) allows mapping σ, ω pairs on the boundary into the α - β -plane. The image boundaries divide the α - β -plane into regions characterized by the number of eigenvalues inside and outside the s -plane region.

In the present paper the control system structure is restricted to partial state feedback. This permits simplifying the determination of eq. (29) by pole placement methods. Consider for example a second order single-input system with $k_1 = \alpha$, $k_2 = \beta$ in eq. (27). In classical parameter plane methods $P(s) = \det(s\mathbf{1} - \mathbf{A} + \mathbf{b}\mathbf{k}') = p_0(\alpha, \beta) + p_1(\alpha, \beta)s + s^2 = 0$ is determined and with $s = \sigma + j\omega$ solved for α and β . In the method proposed in this paper the p_i are expressed in terms of σ and ω by

$$\begin{aligned} P(s) &= (s - \sigma + j\omega)(s - \sigma - j\omega) = s^2 - 2\sigma s + \sigma^2 + \omega^2 \\ &= p_0(\sigma, \omega) + p_1(\sigma)s + s^2 = 0. \end{aligned} \quad (30)$$

Then by pole placement

$$k_1 = \alpha(p_0, p_1) = \alpha(\sigma, \omega) \quad (31)$$

$$k_2 = \beta(p_0, p_1) = \beta(\sigma, \omega).$$

Thus the mapping equation (29) is obtained in a different way.

More generally for an n th order single input system in both approaches an n dimensional parameter space \mathcal{P} with coordinates p_i is introduced as an intermediate step between the set of eigenvalues $\Lambda = \{\lambda_1 \dots \lambda_n\}$ and the \mathcal{X} -space. The relation between Λ and \mathcal{X} can be expressed in both directions:

- a) From \mathcal{X} to \mathcal{P} by the characteristic equation $P(\lambda) = \det(\lambda \underline{I} - \underline{A} + \underline{b} \underline{k}')$, from \mathcal{P} to Λ by numerical factorization of $P(\lambda)$.
- b) From Λ to \mathcal{P} by multiplication of elementary factors $P(\lambda) = (\lambda - \lambda_1)(\lambda - \lambda_2) \dots (\lambda - \lambda_n)$, from \mathcal{P} to \mathcal{X} by pole placement.

Apparently direction b) is much simpler than direction a). In this paper only direction b) is used.

In the next section pole placement is reformulated as a linear mapping from \mathcal{P} to \mathcal{X} space. This is then used in the third section to map not only a trial point from \mathcal{P} to \mathcal{X} or from Λ to \mathcal{X} , but to map boundaries.

4.2. Single Input Pole Placement--A Linear Mapping

4.2.1. State Feedback

Theorem 1: Given a polynomial $P(\lambda) = p_0 + p_1 \lambda + \dots + p_{n-1} \lambda^{n-1} + \lambda^n$, an $n \times n$ matrix \underline{A} and an $n \times 1$ vector \underline{b} such that $\det \underline{R} \neq 0$, $\underline{R} = [\underline{b}, \underline{A} \underline{b} \dots \underline{A}^{n-1} \underline{b}]$. The unique solution to $\det(\lambda \underline{I} - \underline{A} + \underline{b} \underline{k}') = P(\lambda)$ is

$$\underline{k}' = \underline{p}^* \underline{E} \quad (32)$$

where

$$p^* = [p_0 \ p_1 \ \dots \ p_{n-1} \ 1], \quad E = \begin{bmatrix} \underline{e}' \\ \underline{e}'\underline{A} \\ \vdots \\ \underline{e}'\underline{A}^n \end{bmatrix}$$

and \underline{e}' is the last row of \underline{R}^{-1} .

Proof: Existence and uniqueness of the solution were shown by Rissanen [50] by transformation to control canonical form.

Let $\underline{F} = \underline{A} - \underline{b}\underline{k}'$ and expand powers of F as follows:

$$\underline{F}^0 = \underline{A}^0 = \underline{I} \quad (1)$$

$$\underline{F} = \underline{A} - \underline{b}\underline{k}' \quad (2)$$

$$\underline{F}^2 = \underline{A}^2 - \underline{A}\underline{b}\underline{k}' - \underline{b}\underline{k}'\underline{F} \quad (3)$$

$$\vdots \quad \vdots$$

$$\underline{F}^n = \underline{A}^n - \underline{A}^{n-1}\underline{b}\underline{k}' - \underline{A}^{n-2}\underline{b}\underline{k}'\underline{F} - \dots - \underline{b}\underline{k}'\underline{F}^{n-1}. \quad (n+1)$$

Multiply the first equation by p_0 , the second by p_1 , etc., the $(n+1)$ st row by one and add the equations

$$P(\underline{F}) = P(\underline{A}) - [\underline{b}, \underline{A}\underline{b} \ \dots \ \underline{A}^{n-1}\underline{b}] \begin{bmatrix} \vdots \\ \underline{k}' \end{bmatrix}.$$

By Cayley-Hamilton $P(\underline{F}) = 0$. Then

$$\begin{bmatrix} \vdots \\ \underline{k}' \end{bmatrix} = \underline{R}^{-1}P(\underline{A}), \quad \underline{R} = [\underline{b}, \underline{A}\underline{b} \ \dots \ \underline{A}^{n-1}\underline{b}] \quad (33)$$

\underline{k}' must satisfy the last row, i.e.

$$\underline{k}' = \underline{e}'P(\underline{A}), \quad \underline{e}' = [0 \ \dots \ 0 \ 1]\underline{R}^{-1}. \quad (34)$$

Explicitly

$$\underline{k}' = \underline{e}' [p_0 \underline{I} + p_1 \underline{A} + \dots + p_{n-1} \underline{A}^{n-1} + \underline{A}^n]$$

$$\underline{k}' = [p_0 \ p_1 \ \dots \ p_{n-1} \ 1] \begin{bmatrix} \underline{e}' \\ \underline{e}' \underline{A} \\ \vdots \\ \underline{e}' \underline{A}^n \end{bmatrix} = \underline{P}^* \underline{E}. \quad \text{Q.E.D.}$$

The form (34) of the result was derived in [33]. The $(n+1) \times n$ matrix \underline{E} is a convenient representation of a controllable pair $\underline{A}, \underline{b}$. It maps a vector $\underline{p}' = [p_0 \ p_1 \ \dots \ p_{n-1}]$ in \mathcal{P} space into a vector $\underline{k}' = \underline{P}^* \underline{E} = [\underline{p}' \ 1] \underline{E}$ in \mathcal{X} space. \underline{E} is evaluated only once for a given pair $\underline{A}, \underline{b}$. The mapping of each trial design point in \mathcal{P} space then requires only n^2 multiplications and n^2 additions. This compares favorably with mapping a trial design point from the parameter space of quadratic criteria via the Riccati equation into \mathcal{X} space. This is an advantage for computer-aided design methods, in which many trial design points have to be mapped and displayed graphically.

Example 4.2: (Pole placement, output feedback, gain scheduling). For the crane of Example 4.1

$$\underline{E} = \begin{bmatrix} \ell m_c / g & 0 & \ell^2 m_c / g & 0 \\ 0 & \ell m_c / g & 0 & \ell^2 m_c / g \\ 0 & 0 & -\ell m_c & 0 \\ 0 & 0 & 0 & -\ell m_c \\ 0 & 0 & (m_c + m_L) g & 0 \end{bmatrix} \quad (35)$$

$$k_1 = p_0 \ell m_c / g$$

$$k_2 = p_1 \ell m_c / g$$

$$k_3 = p_0 \ell^2 m_c / g - p_2 \ell m_c + (m_c + m_L) g$$

$$k_4 = \ell m_c (p_1 \ell / g - p_3).$$

This result admits some conclusions about state output feedback and gain scheduling

- i) for stability $p_0 > 0$, i.e. $k_1 > 0$,
- ii) for stability $p_1 > 0$, i.e. $k_2 > 0$,
- iii) $k_3 = 0$ implies the constraint

$$p_2 = p_0 l/g + (m_c + m_L)g/km_c,$$

- iv) $k_4 = 0$ implies the constraint $p_3 = p_1 l/g$,
- v) a gain scheduling for different loads m_L can be implemented as

$$k_3 = k_{30} + m_L g \quad \text{with} \quad k_{30} = p_0 l^2 m_c / g - p_2 km_c + m_c g.$$

The other k_i remain unchanged. With this gain scheduling the closed loop eigenvalues do not depend on the load.

in numerical calculations with large n the accuracy of the vectors $\underline{e}'\underline{A}^i$, $i=1,2,\dots,n$, must be checked. One test is to let $p_0 = p_1 = \dots = p_{n-1} = 0$. Then $\underline{k}' = \underline{e}'\underline{A}^n$. Evaluate $\det(\lambda \underline{I} - \underline{A} + \underline{b} \underline{e}'\underline{A}^n) = \tilde{p}_0 + \tilde{p}_1 \lambda + \dots + \tilde{p}_{n-1} \lambda^{n-1} + \lambda^n$. The \tilde{p}_i should ideally be zero. Their magnitude is a measure for the error in $\underline{e}'\underline{A}^n$. Another convenient test follows from the definition of \underline{e}'

$$\underline{e}'\underline{A}^k \underline{b} = \begin{cases} 0 & k=0,1,\dots,n-2 \\ 1 & k=n-1. \end{cases} \quad (36)$$

This relation also implies that \underline{e}' , $\underline{e}'\underline{A} \dots \underline{e}'\underline{A}^{n-1}$ are invariant under state feedback $(\underline{A}, \underline{b}) \rightarrow (\underline{A} - \underline{b} \underline{k}', \underline{b})$. If the inverse of eq. (32) is needed, the last row of \underline{E} can be brought to the left side

$$\underline{k}' - \underline{e}' \underline{A}^n = \underline{p}' \underline{W}^{-1}, \quad \underline{p}' = [p_0 \ p_1 \ \dots \ p_{n-1}], \quad \underline{W}^{-1} = \begin{bmatrix} \underline{e}' \\ \underline{e}' \underline{A} \\ \vdots \\ \underline{e}' \underline{A}^{n-1} \end{bmatrix}$$

$$\underline{p}' = \underline{W}(\underline{k}' - \underline{e}' \underline{A}^n). \quad (37)$$

It was shown in [33] that the columns of \underline{W} can be evaluated recursively by Leverrier's algorithm, which also gives the coefficients a_i of the characteristic polynomial of \underline{A} , $\det(\lambda \underline{I} - \underline{A}) = a_0 + a_1 \lambda + \dots + a_{n-1} \lambda^{n-1} + \lambda^n$. In this case it is more convenient to express the last row of \underline{E} by the Cayley-Hamilton theorem in terms of the previous ones. Then

$$\begin{aligned} \underline{k}' &= (\underline{p}' - \underline{a}') \underline{W}^{-1}, & \underline{a}' &= [a_0 \ a_1 \ \dots \ a_{n-1}] \\ \underline{p}' &= \underline{W} \underline{k}' + \underline{a}' \end{aligned} \quad (38)$$

4.2.2. Partial Pole and Gain Assignment, Output Feedback

So far the mapping from ϕ to χ has been formulated. This is easily extended to mapping from $\Lambda = \{\lambda_1 \dots \lambda_n\}$ to χ . $P(\lambda)$ may be written as

$$P(\lambda) = (\lambda - \lambda_1)(\lambda - \lambda_2) \dots (\lambda - \lambda_n). \quad (39)$$

Then by eq. (34)

$$\underline{k}' = \underline{e}' (\underline{A} - \lambda_1 \underline{I})(\underline{A} - \lambda_2 \underline{I}) \dots (\underline{A} - \lambda_n \underline{I}). \quad (40)$$

This form of the result admits consecutive assignment of one eigenvalue after the other. $P(\lambda)$ may be factorized in any form

$$\begin{aligned} P(\lambda) &= Q(\lambda)R(\lambda) \\ R(\lambda) &= r_0 + r_1 \lambda + \dots + r_{g-1} \lambda^{g-1} + \lambda^g \\ Q(\lambda) &= q_0 + q_1 \lambda + \dots + q_{n-g-1} \lambda^{n-g-1} + \lambda^{n-g}. \end{aligned} \quad (41)$$

Let for example the $n-g$ roots of $Q(\lambda)$ be fixed, then

$$\underline{k}' = \underline{e}'P(\underline{A}) = \underline{e}'Q(\underline{A})R(\underline{A}) = \underline{e}'_QR(\underline{A})$$

$$\underline{k}' = [r_0 \ \dots \ r_{g-1} \ 1] \begin{bmatrix} \underline{e}'_Q \\ \vdots \\ \underline{e}'_Q \underline{A}^g \end{bmatrix} = \underline{r}'\underline{E}_Q = [\underline{r}' \ 1]\underline{E}_Q. \quad (42)$$

It is also possible to fix g gains $k_i = p^*n_i$, where n_i is the i th column of \underline{E} .

These g linear equations in the p coefficients may be used to eliminate \underline{r}'

[55]. p^* is written as

$$p^* = [p_0 \ \dots \ p_{n-1} \ 1] = [r_0 \ \dots \ r_{g-1} \ 1] \begin{bmatrix} q_0 & q_1 & \dots & q_{n-g-1} & 1 & 0 & \dots & 0 \\ 0 & q_0 & \dots & \dots & q_{n-g-1} & 1 & & 0 \\ & & \ddots & & & & \ddots & \\ 0 & & & q_0 & \dots & & & q_{n-g-1} & 1 \end{bmatrix}$$

$$p^* = [r' \ 1] \begin{bmatrix} \underline{S} \\ \underline{t}' \end{bmatrix}$$

where \underline{S} is a $g \times (n+1)$ matrix and \underline{t}' a $1 \times (n+1)$ vector. Let \underline{k}'_b be the fixed gains, which for convenience, are chosen to be the last g gains in \underline{k}' . Then

$$\underline{k}' = [\underline{k}'_a \ \underline{k}'_b] = p^*[\underline{E}_a \ \underline{E}_b] = [\underline{r}' \ 1] \begin{bmatrix} \underline{S} \\ \underline{t}' \end{bmatrix} [\underline{E}_a \ \underline{E}_b]$$

$$\underline{k}'_b = \underline{r}'\underline{S}\underline{E}_b + \underline{t}'\underline{E}_b$$

which can be solved for

$$\underline{r}' = (\underline{k}'_b - \underline{t}'\underline{E}_b)(\underline{S}\underline{E}_b)^{-1} \quad (43)$$

if the $g \times g$ matrix $\underline{S}\underline{E}_b$ is invertible. Note that this condition does not

depend on the values of \underline{k}'_b . Thus this is the same problem as in output feedback,

$\underline{k}'_b = \underline{0}$, where certain pole locations cannot be achieved [51]. The singularities of $\underline{S}\underline{E}_b$ will require further study. \underline{k}'_a is determined by

$$\underline{k}'_a = \underline{p}^* \underline{E}_a = (\underline{r}'\underline{S} + \underline{t}') \underline{E}_a. \quad (44)$$

Assigning the n -g eigenvalues of $Q(\lambda)$ determines \underline{S} . The remaining eigenvalues can be determined by factoring the residual polynomial $R(\lambda)$ with coefficients given by eq. (43).

Example 4.3: (partial pole placement) For the crane let

$$P(s) = (q_0 + q_1 s + s^2)(r_0 + r_1 s + s^2) \quad (45)$$

where q_0 and q_1 are fixed and r_0 and r_1 remain as free parameters.

$$\begin{aligned} \underline{e}'_Q &= \underline{e}'Q(\underline{A}) = [q_0 \quad q_1 \quad 1] \begin{bmatrix} \underline{e}' \\ \underline{e}'\underline{A} \\ \underline{e}'\underline{A}^2 \end{bmatrix} \\ &= \frac{\underline{c}}{g} [q_0 \quad q_1 \quad \ell q_0 - g \quad \ell q_1] \end{aligned}$$

$$\underline{k}' = \underline{e}'_Q \cdot R(\underline{A})$$

$$\underline{k}' = \frac{\underline{c}}{g} [r_0 \quad r_1 \quad 1] \begin{bmatrix} q_0 & q_1 & \ell q_0 - g & \ell q_1 \\ 0 & q_0 & -q_1 g & \ell q_0 - g \\ 0 & 0 & (\omega_p^2 - q_0)g & -q_1 g \end{bmatrix} \quad (46)$$

Let for example the natural frequency ω_p of the pendulum be unchanged, but introduce a damping d , i.e. $Q(s) = \omega_p^2 + 2d\omega_p s + s^2$, then

$$\underline{k}' = [r_0 \quad r_1 \quad 1] \begin{bmatrix} m_c + m_L & c & m_L \ell & c \ell \\ 0 & m_c + m_L & -c g & m_L \ell \\ 0 & 0 & 0 & -c g \end{bmatrix} \quad (47)$$

with $c = 2d \sqrt{(m_c + m_L)m_c/g\ell}$.

Example 4.4: (fixed feedback gains) For the crane of Example 4.2 let k_1 and k_4 be fixed, i.e. $\underline{k}'_a = [k_2 \ k_3]$, $\underline{k}'_b = [k_1 \ k_4]$

$$\underline{E}_a = \begin{bmatrix} 0 & \ell^2 m_c / g \\ \ell m_c / g & 0 \\ 0 & -\ell m_c \\ 0 & 0 \\ 0 & (m_c + m_L)g \end{bmatrix} \quad \underline{E}_b = \begin{bmatrix} \ell m_c / g & 0 \\ 0 & \ell^2 m_c / g \\ 0 & 0 \\ 0 & -\ell m_c \\ 0 & 0 \end{bmatrix}.$$

Then by eq. (43)

$$\underline{r}' = [\underline{r}_0 \ \underline{r}_1] = [k_1 \ k_4 + q_1 \ell m_c] \cdot \begin{bmatrix} q_0 \ell m_c / g & q_1 \ell^2 m_c / g \\ 0 & \ell m_c (q_0 \ell / g - 1) \end{bmatrix}.$$

The inverse exists if $q_0 \neq g/\ell$ and $q_0 \neq 0$. Then

$$\underline{r}_0 = \frac{k_1 g}{q_0 \ell m_c}, \quad \underline{r}_1 = \frac{q_1 m_c - k_1 q_1 / q_0 + k_4 \ell}{m_c (q_0 \ell / g - 1)} \quad (48)$$

and with eq. (44)

$$k_2 = \frac{q_0 q_1 m_c \ell - k_1 g q_1 / q_0 + k_4 q_0}{q_0 \ell - g} \quad (49)$$

$$k_3 = \ell (k_1 / q_0 - m_c) (q_0 + \frac{q_1^2 g}{q_0 \ell - g}) + g (\frac{k_4 q_1}{q_0 \ell - g} - \frac{k_1}{q_0} + m_c + m_L)$$

k_1 will be fixed by the following consideration: Assume a force limitation $|u(t)| \leq U$ for all t for a typical operation of the crane, i.e. a displacement of a load at rest, $\underline{x}(0) = [L \ 0 \ 0 \ 0]'$, $L > 0$ (e.g. length of a loading bridge) to a final position $\underline{x}(t_E) = [0 \ 0 \ 0 \ 0]'$. Typical responses of sufficiently

stabilized cranes show an initial peak $u(0)$ of the force as the maximum value of $|u(t)|$. A simple approach to avoid saturation is therefore to meet a necessary condition by fixing $|u(0)| = U$ and checking the conditions for $\dot{u}(0)/u(0) \leq 0$. Then $|u(t)|$ for $t > 0$ may be checked in a simulation. Here

$$u(0) = -\underline{k}'\underline{x}(0) = -k_1 L \quad (50)$$

$$\dot{u}(0) = -\underline{k}'(\underline{A} - \underline{b}\underline{k}')\underline{x}(0) = L k_1 (k_2 - k_4/l)/m_c = L k_1 p_3$$

Thus $\dot{u}(0)/u(0) = -1/p_3 \leq 0$ for all stabilizing feedbacks and $|u(0)| = U$ results in $k_1 = U/L$.

It is desirable to avoid the difficult measurement of the rope angular velocity $x_4 = \dot{\varphi}$. Thus $k_4 = 0$ is chosen. Then by eq. (48)

$$r_0 = \frac{Ug}{L k_m c q_0}, \quad r_1 = \frac{q_1 g (1 - U/L m_c q_0)}{k q_0 - g}. \quad (51)$$

r_0 and r_1 are the coefficients of the residual polynomial, which is obtained after q_0 and q_1 have also been fixed. Necessary and sufficient conditions for stability are $q_0 > 0$, $q_1 > 0$, $r_0 > 0$, $r_1 > 0$. With eq. (49)

$$k_2 = \frac{q_0 q_1 m_c l - U g q_1 / L q_0}{q_0 l - g} \quad (52)$$

$$k_3 = -k m_c \left(q_0 + \frac{q_1^2 g}{q_0 l - g} \right) + \frac{U}{L q_0} \left(q_0 l - g + \frac{k q_1^2 g}{q_0 l - g} \right) + (m_c + m_L) g$$

4.2.3. Sensitivities, Incremental Stabilization

The influence of a coefficient p_i of the characteristic polynomial on \underline{k}' , given the other p_j , follows from eq. (32) as

$$\frac{\partial \underline{k}'}{\partial p_i} = \underline{e}' \underline{A}^i. \quad (53)$$

The influence of an eigenvalue λ_i on \underline{k}' , given the other λ_j , is by eq. (40)

$$\frac{\partial \underline{k}'}{\partial \lambda_i} = -\underline{e}' (\underline{A} - \lambda_1 \underline{I}) \dots (\underline{A} - \lambda_{i-1} \underline{I}) (\underline{A} - \lambda_{i+1} \underline{I}) \dots (\underline{A} - \lambda_n \underline{I}). \quad (54)$$

For complex conjugate eigenvalues quadratic factors in $P(\lambda)$ are more convenient.

Let $P(\lambda) = (a+b\lambda+\lambda^2)R(\lambda)$, then

$$\underline{k}' = \underline{e}' (a\underline{I} + b\underline{A} + \underline{A}^2) \cdot R(\underline{A}) \quad (55)$$

$$\frac{\partial \underline{k}'}{\partial a} = \underline{e}' R(\underline{A}) \quad \frac{\partial \underline{k}'}{\partial b} = \underline{e}' \underline{A} R(\underline{A}). \quad (56)$$

Example 4.5: (Incremental stabilization, global robustness) For the crane of eqs. (26) and (35) the open loop characteristic equation is $s^2(s^2 + \omega^2) = 0$.

Find a small stabilizing feedback $\Delta \underline{k}'$ with the least number of required sensors.

$$P(s) = (s^2 + as + b)(s^2 + cs + \omega_p^2 + d) \quad \text{with small } a > 0, b > 0, c > 0, \text{ and small } d$$

$$\underline{k}' \underline{k}' = \underline{e}' (\underline{A}^2 + a\underline{A} + b\underline{I}) [\underline{A}^2 + c\underline{A} + (\omega_p^2 + d)\underline{I}] \quad (57)$$

$$\Delta \underline{k}' = \frac{\partial \underline{k}'}{\partial a} \cdot a + \frac{\partial \underline{k}'}{\partial b} \cdot b + \frac{\partial \underline{k}'}{\partial c} \cdot c + \frac{\partial \underline{k}'}{\partial d} \cdot d \quad (58)$$

$$\left. \frac{\partial \underline{k}'}{\partial a} \right|_{b=c=d=0} = \frac{\partial}{\partial a} \underline{e}' (\underline{A}^2 + a\underline{A}) (\underline{A}^2 + \omega_p^2 \underline{I}) = \underline{e}' (\underline{A}^3 + \omega_p^2 \underline{A})$$

$$\left. \frac{\partial \underline{k}'}{\partial b} \right|_{a=c=d=0} = \frac{\partial}{\partial b} \underline{e}' (\underline{A}^2 + b\underline{I}) (\underline{A}^2 + \omega_p^2 \underline{I}) = \underline{e}' (\underline{A}^2 + \omega_p^2 \underline{I})$$

$$\left. \frac{\partial \underline{k}'}{\partial c} \right|_{a=b=d=0} = \frac{\partial}{\partial c} \underline{e}' \underline{A}^2 (\underline{A}^2 + c\underline{A} + \omega_p^2 \underline{I}) = \underline{e}' \underline{A}^3$$

$$\left. \frac{\partial \underline{k}'}{\partial d} \right|_{a=b=c=0} = \frac{\partial}{\partial d} \underline{e}' \underline{A}^2 [\underline{A}^2 + (\omega_p^2 + d)\underline{I}] = \underline{e}' \underline{A}^2$$

$$\Delta \underline{k}' = \underline{e}' \cdot [(a+c)\underline{A}]^3 + (b+d)\underline{A}^2 + a\omega_p^2 \underline{A} + b\omega_p^2 \underline{I}]$$

$$\Delta k_1 = b\omega_p^2 \ell m_c / g = (m_c + m_L) \cdot b$$

$$\Delta k_2 = a\omega_p^2 \ell m_c / g = (m_c + m_L) \cdot a$$

$$\Delta k_3 = b\omega_p^2 \ell^2 m_c / g - (b+d) \ell m_c = \ell(m_L b - m_c d)$$

$$\Delta k_4 = a\omega_p^2 \ell^2 m_c / g - (a+c) \ell m_c = \ell(m_L a - m_c c)$$

With $a > 0$, $b > 0$, $c > 0$ this is the cone of stabilizing directions at the origin of the four dimensional χ space. It includes the directions $\Delta k_3 = 0$ and $\Delta k_4 = 0$, i.e. no feedback of the rope angle is necessary with

$$d = \frac{m_L}{m_c} b. \quad (59)$$

No feedback of the rope angular velocity is necessary with

$$c = \frac{m_L}{m_c} a. \quad (60)$$

Δk_1 and Δk_2 must be positive for stabilization, i.e. crab position and crab velocity must be available for feedback. Output feedback

$$\Delta \underline{k}' = (m_c + m_L) [b \ a \ 0 \ 0] \quad (61)$$

with small positive a and b then stabilizes the system. For sufficiently small a and b the characteristic polynomial is arbitrarily close to

$$P(s) = (s^2 + as + b) \left(s^2 + \frac{m_L}{m_c} as + \omega_p^2 + \frac{m_L}{m_c} b \right). \quad (62)$$

If the physical parameters of the crane are unknown, and output feedback

$$\Delta \underline{k}' = [\Delta k_1 \ \Delta k_2 \ 0 \ 0] \text{ with small } \Delta k_1 > 0, \quad (63)$$

$$\Delta k_2 > 0$$

is applied, then in eq. (61) $a = k_2/(m_c + m_L)$ and $b = k_1/(m_c + m_L)$ are unknown, but positive, i.e. with the feedback of eq. (63) stability is robust with respect to arbitrary changes of load mass m_L , crab mass m_c , rope length l , and gravitational constant g . Thus in this example global robustness of stability with respect to perturbations in four directions is achieved.

Note that it is possible to destabilize the model \underline{A} and \underline{b} in eq. (26) with feedback (63), if small changes in arbitrary coefficients of \underline{A} and \underline{b} are permitted. The general assumption in this paper is that \underline{A} and \underline{b} do not change arbitrarily but in known directions. Only by this assumption does it become possible to accommodate large parameter variations.

4.3. Mapping of Boundaries

4.3.1. Mapping from λ plane to \mathcal{X} space

In the complex plane of eigenvalues

$$\lambda = v + jw \quad (64)$$

boundaries $w^2 = w^2(v)$ (i.e. symmetric with respect to the real axis) are of interest, which are related to desirable system properties, e.g. stability, damping, bounds on the natural frequency. Examples were given in Figs. 4.1 and 4.2.

Assume, due to a change of the state feedback gains \underline{k}' , a real root crosses the boundary at its intersection with the real axis at $\lambda = v_R$. Then in \mathcal{X} space a boundary

$$P(\lambda) = (\lambda - v_R) \cdot R(\lambda), \quad R(\lambda) = r_0 + r_1 \lambda + \dots + r_{n-2} \lambda^{n-2} + \lambda^{n-1} \quad (65)$$

is crossed, which is linear in its parameters r_0, r_1, \dots, r_{n-2} , i.e. it is an

(n-1) dimensional hyperplane. Due to the linearity of $\underline{k}' = \underline{p}^* \underline{E} = [\underline{p}' \quad \underline{I}] \underline{E}$, this boundary maps into a hyperplane in \mathcal{X} space, which is crossed by the feedback gain vector \underline{k}' .

Assume, due to a change of the state feedback gains \underline{k}' a complex conjugate pair crosses the λ -boundary at $v \pm jw$. Then in \mathcal{O} space a boundary

$$P(\lambda) = (\lambda - v - jw)(\lambda - v + jw) \cdot R(\lambda) = Q(\lambda)R(\lambda) \quad (66)$$

where

$$Q(\lambda) = \lambda^2 - 2v\lambda + v^2 + w^2 \quad (v)$$

and

$$R(\lambda) = r_0 + r_1\lambda + \dots + r_{n-3}\lambda^{n-3} + \lambda^{n-2}$$

is crossed. For a fixed v , i.e. a fixed pair of eigenvalues on the boundary, this is a (n-2) dimensional hyperplane in \mathcal{O} and \mathcal{X} space. However, for different values of v different hyperplanes are obtained. For fixed $R(\lambda)$ the boundary line in \mathcal{O} and \mathcal{X} space is obtained by moving a pair of conjugate eigenvalues along the boundary. In this case the form of the boundary $w^2(v)$ in eq. (66) determines the shape of the boundary line in \mathcal{O} and \mathcal{X} space.

Some boundaries of particular interest are:

- 1) Imaginary axis, stability boundary in s-plane, $v=0$, $Q(\lambda)$

$$Q(\lambda) = \lambda^2 + w^2, \text{ boundary linear in } w^2.$$

- 2) Parallel to imaginary axis

$$v = v_1, \quad Q(\lambda) = \lambda^2 - 2v_1\lambda + v_1^2 + w^2, \text{ linear in } w^2.$$

- 3) Conic section symmetric to the real axis, i.e.

$$w^2 = c_0 + c_1 v + c_2 v^2. \quad (67)$$

Special cases are

$c_2 < 0$ ellipse, of particular interest are circles $c_2 = -1$, e.g.

constant natural frequency curves in s-plane, stability limit and other boundaries in z-plane, see Fig. 1.

$c_2 = 0$ parabola, or if also $c_1 = 0$, $c_0 > 0$ straight line parallel to the real axis. For $c_0 = c_1 = c_2 = 0$ boundary between real and complex eigenvalues.

$c_2 > 0$ hyperbola, in particular 2 straight lines for $w^2 = c_2(v-v_0)^2$, $c_2 > 0$, e.g. constant damping lines in s-plane. This boundary is frequently combined with a parallel to the imaginary axis. Here it is more convenient to use a hyperbola, which guarantees the required damping and minimum negative real part of the eigenvalues, see Fig. 2.

Substituting eq. (67) into $Q(\lambda)$ from eq. (66) gives

$$Q(\lambda) = \lambda^2 - 2v\lambda + (1+c_2)v^2 + c_1v + c_0. \quad (68)$$

The boundary is quadratic in v . It becomes linear only if $c_2 = -1$, i.e. for a circular boundary in λ plane. In other words: If $n-2$ roots in $R(\lambda)$ are fixed and the remaining two roots of $P(\lambda)$ move as a conjugate pair along any circle in the λ -plane with center on the real axis, then the corresponding point in θ and χ space moves along a straight line. This is the reason for the proposal of a family of circles Γ_r in the z-plane in Fig. 4.1. Its equation is

$$\begin{aligned} (v-v_0)^2 + w^2 &= r \\ v_0(v_0-1) &= 0.99r(r-1), \quad v_0 < 0.5 \quad \text{for } r < 1 \\ v_0 &= 0 \quad \text{for } r \geq 1. \end{aligned} \quad (69)$$

For $r=0$ it is the deadbeat solution with all eigenvalues at $z=0$. With increasing r the center v_0 of the circles moves to the right until it reaches 0.45 for $r=0.5$, it then goes back to zero to produce the unit circle for $r=1$. If boundaries in the unstable region are needed, concentric circles with radius r may be used. We may begin with a radius r such that all open loop eigenvalues are enclosed by the circle, and design the feedback such that r is reduced to a radius smaller than 1. In the further reduction of r at tradeoff with the required gains must be made. For continuous-time systems the family of hyperbolas Γ_ρ of Fig. 4.2 in the $s(=\sigma+j\omega)$ -plane may be used. Its equation is

$$\begin{aligned} \omega^2 &= -\rho^2 + \sigma^2 / \rho^2 & \text{for } \sigma < 0 \\ \sigma &= -\rho & \text{for } \sigma > 0. \end{aligned} \tag{70}$$

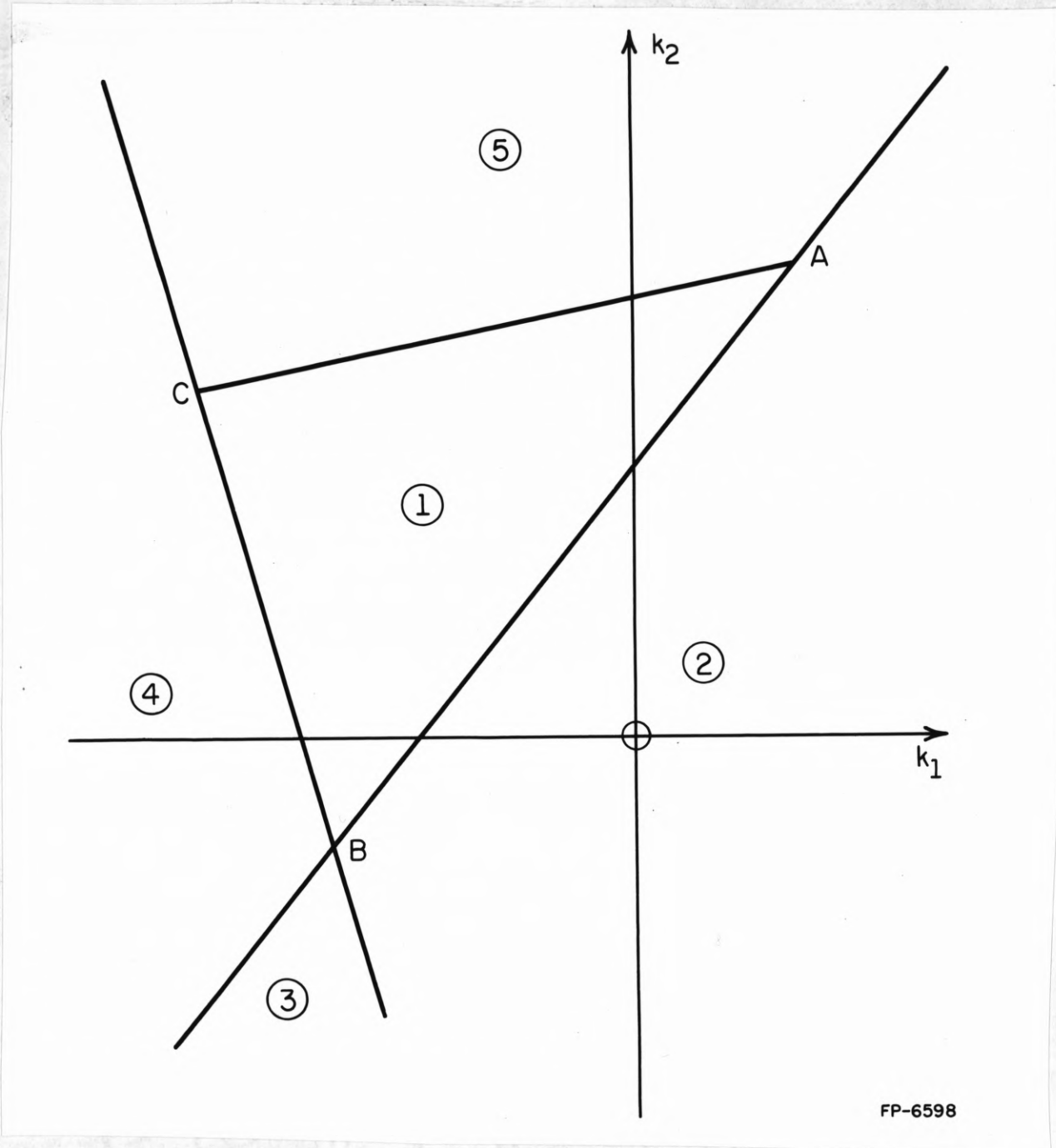
For large ρ an extremely fast solution is obtained, $\rho=1$ gives the $1/\sqrt{2}$ damping line as asymptotes, for $\rho \rightarrow 0$ it goes to the imaginary axis. Negative ρ represent parallels to the imaginary axis in the right half plane. Beginning with a sufficiently negative ρ to have all open loop eigenvalues to the left of the boundary Γ_ρ , ρ may be increased by the feedback to positive values, where again a tradeoff with the required gains must be made.

Besides the real and the complex root boundary there is the third possibility of a root leaving the region through infinity. This can be avoided by closing the contour in the s -plane by an arc of a circle with large radius. Practically this may be a circle corresponding to the design bandwidth. This is of particular importance if we need a 40 db/decade "roll off" bandwidth limitation, e.g. to avoid interaction with unmodeled modes at higher frequencies.

Typical desirable regions for the eigenvalue location in the s - or z -plane are connected and have two intersections with the real axis. In this case there are two real root boundaries and a (possibly piecewise defined) complex root boundary in ϕ and χ space.

Equations (65) and (66) show that the mapped boundaries in ϕ and χ space represent the conditions under which the number of eigenvalues inside and outside a λ -region can change. The boundaries partition the ϕ and χ space into regions, each of them corresponds to a fixed number of eigenvalues inside the λ region, and it must be decided for which ϕ or χ region all eigenvalues are inside the λ region. For closed contours in the λ -plane the χ region is bounded, since by eq. (32) no k_i can go to infinity. If there are several bounded regions, a simple test is to check the eigenvalues for an arbitrary \underline{k}' in the considered χ region. An alternative are Siljak's "shading rules" for the boundaries [49].

For second and third order systems it is possible to visualize regions in χ space graphically. This is done in the following for the unit circle, i.e. the stability region of discrete systems in χ space is determined. Figure 4.3 shows the regions in the k_1 - k_2 -plane for a second order system. The two real root boundaries are two infinite straight lines intersecting at B. Thus B can be obtained by placing one pole at $z = -1$ and one at $z = 1$. The complex root boundary is the straight line AC. A is obtained by placing a double pole at $z = -1$ and C by a double pole at $z = 1$. Thus Fig. 4.3 is completely determined by three pole placements



FP-6598

FIGURE 4

Figure 4.3. Stability triangle ABC in k_1 - k_2 -plane for a second order discrete-time system

$$\begin{aligned}
 \underline{k}'_A &= [1 \quad 2 \quad 1] \underline{E} \\
 \underline{k}'_B &= [-1 \quad 0 \quad 1] \underline{E} \\
 \underline{k}'_C &= [1 \quad -2 \quad 1] \underline{E}.
 \end{aligned}
 \tag{71}$$

The boundaries partition the k_1 - k_2 -plane into five regions with the properties 1) both poles inside the unit circle, 2) one left, one inside, 3) one left, one right, 4) one inside, one right, 5) complex outside or both left or both right (a distinction between these three cases in region five would require a further boundary distinguishing real and complex roots). Usually only the stability region 1 is of interest.

Only the stability region will be determined now for third order systems. It is shown in Fig. 4.4. The two real root boundaries are the two planes in which the triangles ABC and BCD are contained. They intersect along the straight line BC. B is obtained by placing two poles at $z = -1$ and one at $z = 1$, C corresponds to one pole at $z = -1$ and two at $z = 1$. For any fixed real eigenvalue and the two others moving along the unit circle a straight line is obtained. Thus the complex root boundary may be visualized as being generated by a moving straight line from a point on AB to a point on CD. It moves as the real eigenvalue moves from -1 to $+1$. A corresponds to a triple eigenvalue at $z = -1$ and D to a triple eigenvalue at $z = +1$. Thus the vertices of the stability region are obtained as

$$\begin{aligned}
 \underline{k}'_A &= [1 \quad 3 \quad 3 \quad 1] \underline{E} \\
 \underline{k}'_B &= [-1 \quad -1 \quad 1 \quad 1] \underline{E} \\
 \underline{k}'_C &= [1 \quad -1 \quad -1 \quad 1] \underline{E} \\
 \underline{k}'_D &= [-1 \quad 3 \quad -3 \quad 1] \underline{E}.
 \end{aligned}
 \tag{72}$$

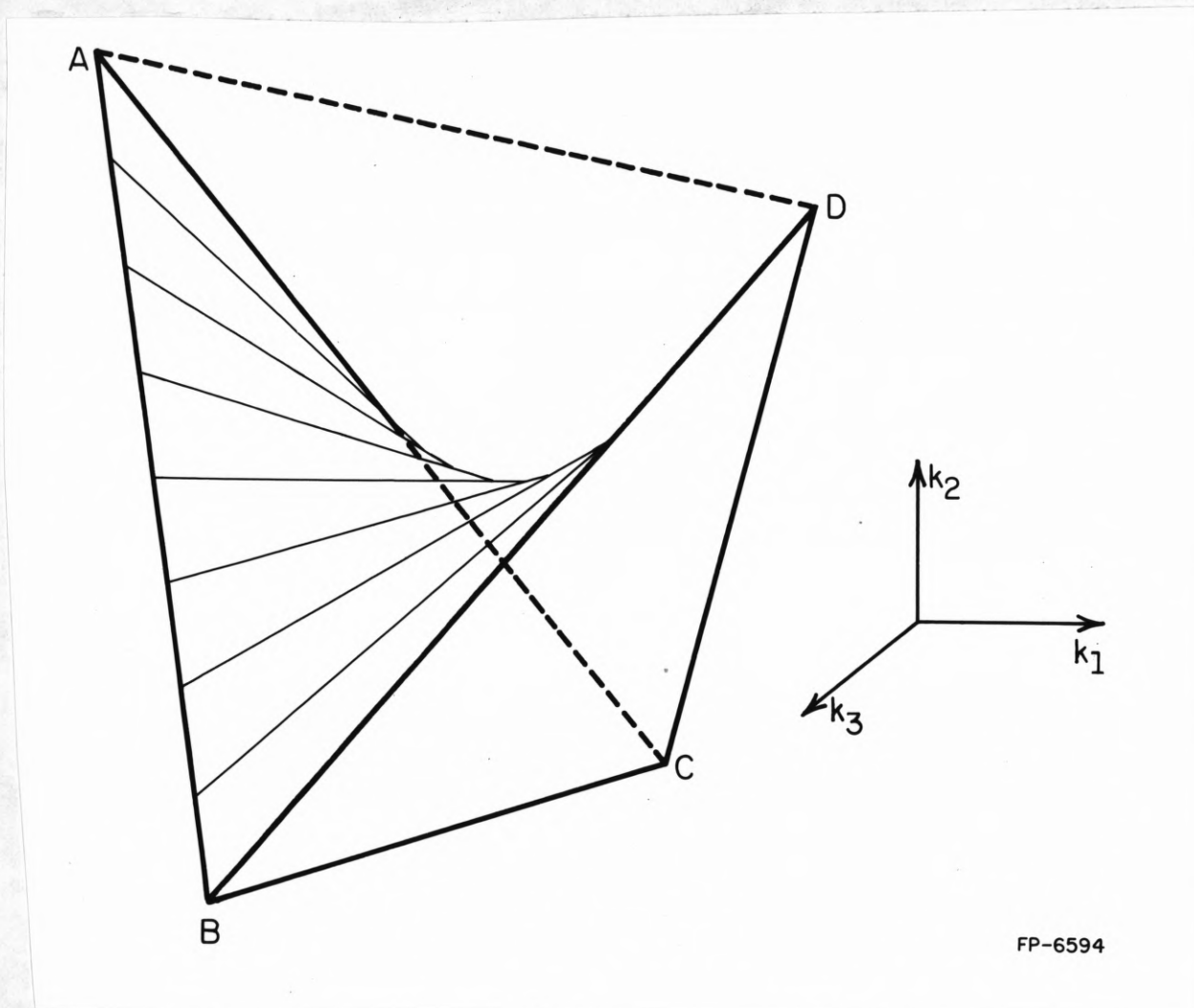


Figure 4.4. Stability region ABCD in k_1 - k_2 - k_3 -space for a third order discrete-time system.

Apparently the tetrahedron ABCD is a convex hull for the stability region. For the \mathcal{P} space Fam and Meditch [38] showed that this property generalizes to arbitrary degree n of the characteristic polynomial.

Theorem 2 (Fam, Meditch): For an n -th order discrete system a convex hull of the stability region in \mathcal{P} space is a polyhedron whose vertices correspond to the $n+1$ polynomials with zeros in the set $\{-1, 1\}$.

Proof: See [38].

Corollary: If the unit circle is replaced by a circle with center v_0 and radius r in the z -plane, which intersects the real axis at $v_1 = v_0 - r$ and $v_2 = v_0 + r$, then the vertices of the convex hull of the corresponding region in \mathcal{P} space correspond to the $n+1$ polynomials with zeros in the set $\{v_1, v_2\}$. This may be shown by reducing this problem to the previous one via $z' = (z - v_0)/r$.

Theorem 3: A necessary condition for all roots of $\det(zI - A + b k')$ (A, b controllable) to be inside a circle with real center and real axis intersections at $z = v_1$ and $z = v_2$ is that k' is in a polyhedron in \mathcal{K} space, whose vertices are obtained by pole placement of the $n+1$ polynomials with zeros in the set $\{v_1, v_2\}$.

Proof: Follows from Theorem 2 and the linearity of the map $k' = p^*E$.

If the circle in z -plane is deformed to a different closed contour with the same real axis intersections at v_1 and v_2 , then the certices of the region in \mathcal{K} space and the two real root boundaries remain unchanged, only the hypersurface for the complex root boundary is deformed. It is an open question, how far the region in λ space can be extended in the λ -plane such that k' remains in the previously described polyhedron. The inverse problem (given a region in \mathcal{K} , which is the corresponding region in the λ -plane?) leads to sufficient conditions on k' to place all eigenvalues in the resulting region.

This problem was studied by Marden [52, Theorem 8.2]. However, these regions in λ -plane are not nicely related to desirable dynamic properties. For the polyhedron discussed above the region in λ -space is the union of two circles with complex conjugate centers and real axis intersections at v_1 and v_2 . Marden showed that this region cannot be reduced. Note that in this direction from the n -dimensional \mathcal{X} -boundary to the two-dimensional λ -boundary no necessary and sufficient conditions can be obtained for an arbitrary defined \mathcal{X} region. This problem is overdetermined. Thus it is advisable to assume a region in λ -plane and to determine the necessary and sufficient conditions on \underline{k}' .

4.3.2. Mapping to a Subspace of \mathcal{X}

Some gains may be fixed to zero, like in output feedback or under sensor failures, or to some other values like in Example 4.4. This means that we are looking for a solution in a subspace of \mathcal{X} . Such a solution may not exist; take for example Fig. 4.3 and fix k_1 to be bigger than $k_1(A)$. Then there does not exist a stabilizing k_2 . The set of admissible solutions may also become disconnected, even if it was connected in \mathcal{X} space; take for example Fig. 4.4 and fix $k_2 = c$ such that the plane $k_2 = c$ intersects the two tips of the stability region.

Example 4.6: (Disconnected stability regions in a subspace of \mathcal{X})

$$\underline{x}(k+1) = \begin{bmatrix} 0 & 1 & 0 \\ 0 & 0 & 1 \\ 0.6 & -2 & 2.1 \end{bmatrix} \underline{x}(k) + \begin{bmatrix} 0 \\ 0 \\ 1 \end{bmatrix} u(k). \quad (73)$$

The system is open loop unstable (eigenvalues $z_1 = 0.5$, $z_{2,3} = 0.8 \pm j\sqrt{0.56}$). Fix $k_2 = 0$ (output feedback) and find the set of stabilizing gains in the k_1 - k_3 -plane. The real root boundaries are the straight lines

$$\text{for } z = 1 \quad k_{3+} = -k_1 - 0.3$$

$$\text{for } z = -1 \quad k_{3-} = -k_1 + 5.7$$

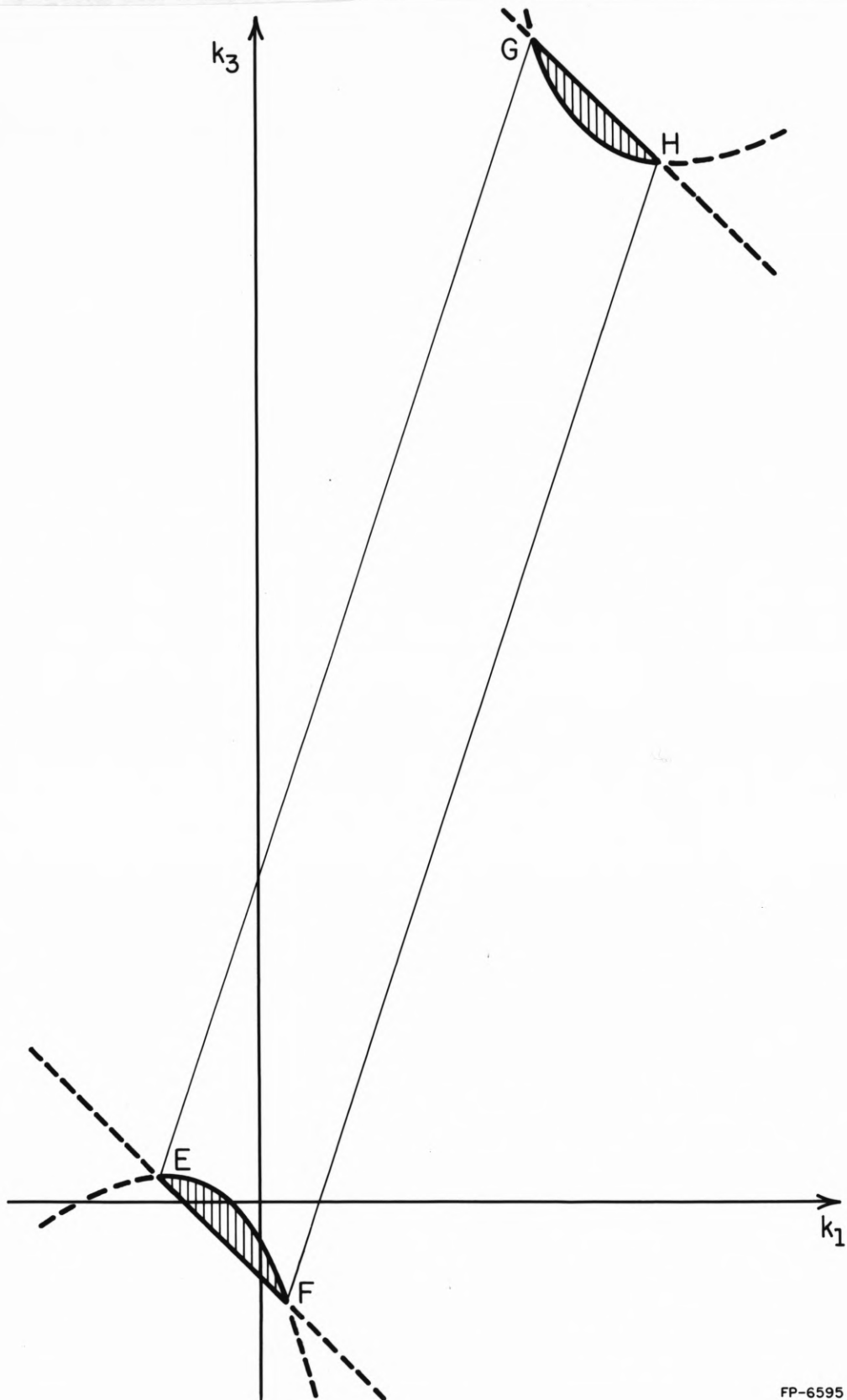
and the complex root boundary is the hyperbola

$$k_{3c} = k_1 + 1.5 + 1/(k_1 - 0.6).$$

Figure 4.5 shows the three boundaries and the two disconnected stabilizing regions. Its vertices are

	k_1	k_3
E	-0.4	0.1
F	0.1	-0.4
G	1.1	4.6
H	1.6	4.1

Nonconvex and disconnected solution sets like in this example lead to difficulties in numerical algorithms. Sirisena and Choi [53] formulate the problem of placing poles in a specified region by output feedback as minimization of a function J , which becomes zero, if a solution is found. Their conclusion from computational experience is: "If however a local (nonzero) minimum of J is reached, the algorithm should be restarted with a different initial value of the feedback matrix. Repeated failure to reduce J to zero would indicate the absence of a solution". If we want to find the set of admissible solutions, a systematic or random search in the appropriate subspace may be necessary. In order to restrict the search to a promising region, necessary conditions, like the one provided in Theorem 3, are very useful. In Example 4.6 this is the quadrangle EFHG, more general the polyhedral cross-section of the subspace with



FP-6595

Figure 4.5. Disconnected stability region in k_1 - k_3 subspace.

the polyhedron in the n dimensional space. If no such cross-section exists, it can be immediately concluded that no solution exists. The example indicates that points near the real root boundaries are promising candidates.

For a fourth order system there exist gains, for which two complex pairs of eigenvalues cross the boundary simultaneously. Here the complex root boundary in \mathcal{X} space intersects itself. If the two crossing points on the boundary approach each other and eventually become a crossing of a double pole, then the bow in the boundary becomes a cusp.

Example 4.7: (Partial gain fixing) For the crane of Example 4 let $m_c = 1000$ kg, $l = 10$ m, $g = 10$ m/sec², $U = 5000$ Newton, $L = 10$ m. The load mass m_L is unknown. Example 2 showed that only $k_3 = k_{30} + m_L g$ depends on the load mass m_L . Without knowledge of m_L only $k_{30} = k_3 - 10m_L$ can be determined. For $k_1 = U/L = 500$ and $k_4 = 0$ find the region in the k_2 - k_{30} -plane, for which all eigenvalues are left of the hyperbola

$$\omega^2 = (2\sigma)^2 - 1/2^2 \quad (74)$$

in the s -plane. Then for the complex root boundary from eq. (66)

$$q_0 = 5\sigma^2 - 0.25, \quad q_1 = -2\sigma. \quad (75)$$

and by eqs. (51) and (52)

$$r_0 = 1/2q_0, \quad r_1 = \frac{q_1(1-1/2q_0)}{q_0-1} \quad (76)$$

$$k_{2c} = \frac{1000q_1}{q_0-1}(q_0-1/2q_0) \quad (77)$$

$$k_{30c} = 10000(1/2q_0 - 1)[q_0-1 + q_1^2/(q_0-1)] \quad (78)$$

$$k_{3c} = k_{30c} + 10 m_L.$$

The nice stability region will be constructed in the k_2 - k_{30} -plane. The complex root boundary $k_2(\sigma)$, $k_{30}(\sigma)$ is obtained by substituting values $\sigma \leq -0.25$ into eq. (75) and q_0 and q_1 into eqs. (77) and (78). The real root boundary at $\sigma_R = -0.25$ follows from eq. (65) with $k_1 = 500$, $k_4 = 0$ as the straight line

$$k_{3R} = k_{30R} + 10 m_L, \quad k_{30R} = 95625 - 42.5 k_2. \quad (79)$$

Both boundaries are shown in Fig. 4.6. For $\sigma = -0.25$ the complex root boundary starts at point A. With increasing σ it goes through point B and for $\sigma \rightarrow -0.5$, (i.e. $q_0 \rightarrow 1$) to infinity. In general this singularity occurs at $q_0 = g/l$. For $\sigma < -0.5$ the complex root boundary returns from the opposite side to intersect the real root boundary at C and itself at B.

Note that the characteristic polynomial is obtained by eqs. (75) and (76) in factorized form. Thus the determination of the eigenvalues is easy. They are given together with the k_2 and k_{30} coordinates in the following table.

	k_2	k_{30}	Eigenvalues
A	4233	-84292	$s_{1,2} = -0.25$, $s_{3,4} = -1.867 \pm j2.125$
B	2367	-35012	$s_{1,2} = -0.275 \pm j0.231$, $s_{3,4} = -0.908 \pm j1.746$
C	2769	-22056	$s_1 = -0.25$, $s_2 = -1.337$, $s_{3,4} = -0.591 \pm j1.071$

At A the real and complex root boundary intersect, i.e. there is a double pole at $s_{1,2} = -0.25$. At B the complex boundary intersects itself, i.e. here we have two complex pairs of eigenvalues crossing the boundary simultaneously. At C a real root at $s = -0.25$ crosses simultaneously with the complex pair $s_{3,4}$. The shaded region with vertices A, B and C corresponds to eigenvalues to the left of the hyperbola in s -plane.

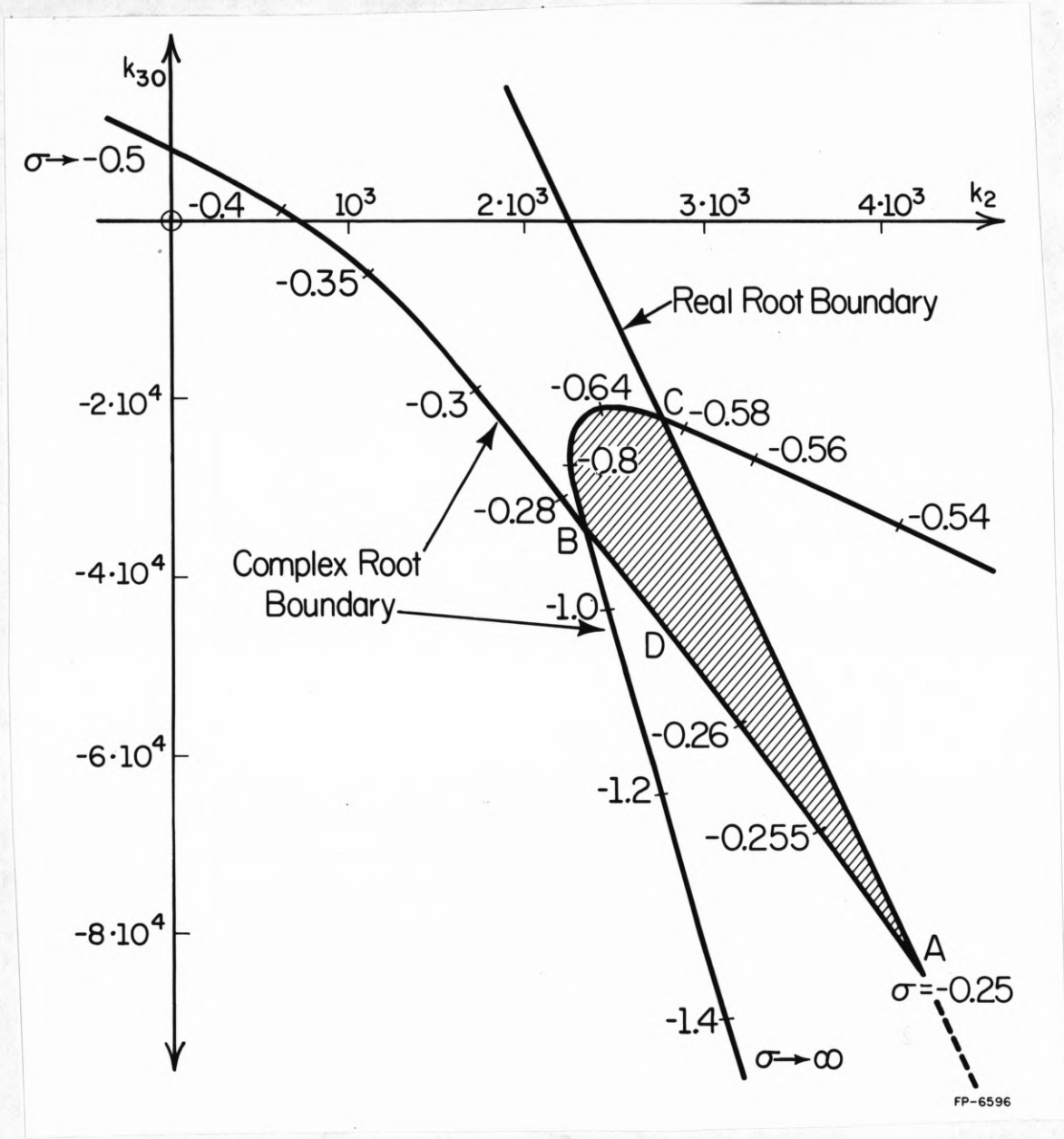


Figure 4.6. Nice stability region for crane with $k_1=500$, $k_4=0$.

4.4. Robustness with Respect to Large Parameter Variations

Most existing methods for the design of parameter insensitive control systems try to achieve robustness of a system property, like stability, with respect to small perturbations of plant parameters in unknown or conveniently analyzable directions, e.g. gain or phase variations. Such methods lead to conservative results when applied to problems with large perturbations in known directions, e.g. for the crane with widely varying load mass or rope length or for an aircraft with widely varying altitudes and speeds. Let the plant model in sensor coordinates

$$\dot{\underline{x}} = \underline{A}(\underline{\theta})\underline{x} + \underline{B}(\underline{\theta})u \quad (80)$$

be given for several typical values of the physical parameter vector $\underline{\theta}$, i.e. $\underline{A}_j = \underline{A}(\underline{\theta}_j)$, $\underline{b}_j = \underline{b}(\underline{\theta}_j)$, $j=1,2,\dots,J$. A fixed state feedback \underline{k}' is sought, such that all eigenvalues of $(\underline{A}_j - \underline{b}_j \underline{k}')$ are located in a specified region Γ in λ -plane.

For each pair $\underline{A}_j, \underline{b}_j$ we obtain a different matrix \underline{E}_j , which maps a desired region from the canonical parameter space \mathcal{P} into the corresponding region R_j in \mathcal{X} -space via $\underline{k}' = \underline{p}^* \underline{E}_j$. The set of solutions to the above problem, if it exists, is the intersection of all regions R_j in \mathcal{X} space. If no intersection for all $j=1,2,\dots,J$ exists, then it can be tested whether at least a group of plant models can be nicely stabilized with one gain, and it may be necessary to switch to a different gain for a different group of plant models.

Example 4.8: (Maximum parameter variation, gain scheduling) Let the mass m_L of the crane load be an unknown constant between the weight of the empty hook and the maximum load for which the crane is designed. Under the constraints of Example 4.7 find the fixed gain controller which accomodates the largest load variation.

The load mass enters only into $k_3 = k_{30} + 10 m_L$. In Fig. 4.6 the origin of the k_3 -axis is identical with $k_{30} = 0$ for $m_L = 0$. With increasing load mass the shape of the region of nice stability is unchanged, but it is moved upwards by $10 m_L$ in the k_2 - k_3 -plane, or equivalently the origin of the k_3 -axis is moved downwards by $10 m_L$ in the k_2 - k_{30} -plane. Thus for load variations of cranes it is not necessary to plot the shifted diagrams in order to find the intersection. The largest load variation can be accommodated at the largest extension of the nice stability region in k_3 direction, this is between C and D. D has the coordinates $k_2 = 2769$, $k_{30} = -45503$ and corresponds to the eigenvalues $s_{1,2} = -0.267 \pm j0.680$ and $s_{3,4} = 1.118 \pm j1.872$. Thus k_2 is chosen as 2769. This results in an admissible load variation $m_L = (-22056 + 45503)/10 = 2344.7 \approx 2345 \text{ kg}$. Assuming the weight of the empty hook is 50 kg, then $k_3 = -21556$ puts the eigenvalues for $m_L = 50 \text{ kg}$ at $s_1 = -0.25$, $s_2 = -1.337$, $s_{3,4} = -0.591 \pm j1.071$, where s_1 and $s_{3,4}$ are on the boundary Γ . For $m_L = 2395 \text{ kg}$ the eigenvalues are at $s_{1,2} = -0.267 \pm j0.680$ and $s_{3,4} = 1.118 \pm j1.872$, where $s_{1,2}$ is on the boundary. In summary: The solution

$$k' = [500 \quad 2769 \quad -21556 \quad 0] \quad (81)$$

gives the following properties of the control system.

- a) Initial peak in the force u limited to $500L$, where L is the required load displacement.
- b) No measurement or estimation of the rope angular velocity $x_4 = \dot{\varphi}$ required.
- c) Under the constraints a) and b) maximum possible load variation. The eigenvalues are left of $\omega^2 = (2\sigma)^2 - 1/2^2$ if and only if $50 \text{ kg} < m_L < 2395 \text{ kg}$.

Now assume that the crane is designed for a maximum load of 3500kg, i.e. a gain scheduling is necessary. The second load range may be chosen as $1155 \text{ kg} < m_L < 3500 \text{ kg}$, i.e. $k_3 = -10506$. Then for $50 \text{ kg} < m_L < 1155 \text{ kg}$, $k_3 = -21556$ must be used and for $2395 \text{ kg} < m_L < 3500 \text{ kg}$, $k_3 = -10506$. For the overlapping range $1155 \text{ kg} < m_L < 2395 \text{ kg}$ either gain is good, such that the crane operator can switch between high and low load based on his very crude load estimate, which may be 135% wrong. This wide overlap provides robustness of the gain scheduling scheme.

If the rope length of the crane is varied, the shape of the nice stability region in Fig. 4.6 changes and an intersection of various regions must be found.

For different values $\underline{\theta}_j$ of a physical parameter vector different regions T_j in the λ -plane may be given and the intersections of the corresponding \mathcal{X} -space regions may be found. This is particularly useful, if the plant is slow for some parameter values and fast for others like in aircraft control. A general recommendation for the design of robust control systems with input constraints is: do not try to make a slow plant fast or a fast plant slow by feedback.

The graphical determination of intersections is limited to two parameters at a time. Intersections of three dimensional regions may be made visible by computer graphic methods. In situations with more free controller parameter the design may proceed iteratively, where in each design step $n-2$ feedback gains are fixed and admissible regions in the plane of the remaining two feedback gains are determined. The results of Section 4.3.1 on mapping circular boundaries give some additional insight, which is useful for a fully computerized search for intersections of regions. First it is important to

note that the nice stability regions are not convex, and thus their intersection may be disconnected. Consider for example the stability region for a third order discrete-time system in Fig. 4.4. Assume that for a different value of the parameter vector the stability region is turned around by 180 degrees such that the two tips of the stability regions intersect. Then the set of solutions is disconnected, even for full state feedback. In this situation a search in \mathcal{X} space may be made. Bounds for the search region are given by the following.

Theorem 4: A necessary condition for all roots of $\prod_{j=1}^J \det(zI - \underline{A}_j + \underline{b}_j \underline{k}') = 0$ to be on or inside a circle with real axis intersections at $z = v_1$ and $z = v_2$ is, that \underline{k}' is on or inside the intersection of J polyhedra. The vertices of the j -th polyhedron are obtained by assigning all $(n+1)$ polynomials $P(z) = \det(zI - \underline{A}_j + \underline{b}_j \underline{k}')$ with zeros in the set $\{v_1, v_2\}$.

Proof: Follows from Theorem 3.

The intersection of polyhedra is a polyhedron itself, its vertices are promising candidates in the search for points which also meet the sufficient conditions. In order to define a rectangular grid for the search it is convenient to put each polyhedron into the smallest box with surfaces parallel to the axes and to restrict the search to the intersection of the boxes.

4.5. Robustness with Respect to Sensor Failures

Sensor failures are assumed to occur in the form that the sensor output is no longer correlated with the measured variable. As far as the characteristic equation is concerned, this is equivalent to having a sensor output zero. There may be a bias or other noise term introduced by the failed sensor. This noise term can be considered as an external input. This

may require that the failure is detected and the failed sensor is removed from the control system. Then also the control law may be changed. However, for this latter decision there should be sufficient time to come to a reliable decision without false alarms. This requires that after the failure the system at least remains stable with some stability margin. In other applications it may suffice to be able to continue the mission after a sensor failure without removal of the failed sensor, e.g. to drive an automobile safely to a service station to get a broken sensor replaced, such that optimal fuel economy, emission control, acceleration, etc. is regained.

The robustness problem is: Consider M failures of a sensor or combinations of sensors leading to the crippled feedback vectors \underline{k}'_m , $m=1,2,\dots,M$, in which the appropriate elements of \underline{k}' are replaced by zero. Find \underline{k}' such that all zeros of

$$\prod_{m=1}^M \prod_{j=1}^J \det(\lambda \underline{I} - \underline{A}_j + \underline{b}_{j-m} \underline{k}'_m) = 0 \quad (82)$$

lie in an "emergency region" Γ_E in λ -plane. The emergency specification is robust with respect to a failure of sensor i if and only if in \mathcal{X} -space the projection of \underline{k}' into the subspace $k_i = 0$ is in the intersection of all J emergency regions.

Figure 4.7 shows an example of the intersection of emergency and nominal regions in the k_1 - k_2 -plane. If we choose \underline{k}' at point 1, then the projection on the k_2 axis is inside the emergency boundary, i.e. Γ_E is robust with respect to a failure of sensor 1. It is, however, not robust with respect to a failure of sensor 2, since the projection on the k_1 axis is outside the emergency region. Points in the shaded region are robust with respect to failure of either sensor. For no \underline{k}' Γ_E is robust with respect to failures of

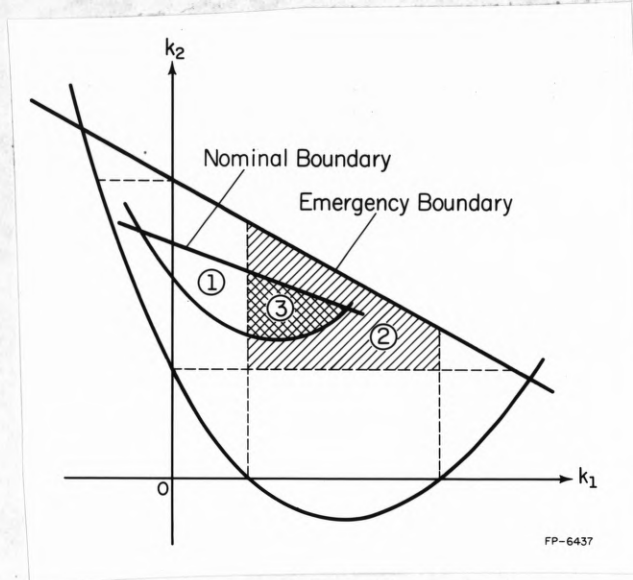


Figure 4.7. Robustness with respect to sensor failures.

sensors 1 and 2, since the origin $k_1 = k_2 = 0$ lies outside the emergency region. Point 3 also meets the nominal specification and is a good candidate for a robust control system. Since the nominal boundary intersects the k_2 axis, an alternative to the robust solution 3 is to eliminate the x_1 sensor and to multiplex the x_2 sensor. This would maintain the nominal specifications under a failure of one of the x_2 sensors. However, it requires failure detection with at least three x_2 sensors. For robustness with respect to sensor failures a dynamic feedback structure like in eqs. (24) and (25) is more advantageous. In Chapter 5 and [54], Franklin designs a flight control system with dynamic feedback such that emergency conditions are robust with respect to an accelerometer or a gyro failure in different flight conditions.

4.6. Other Features of \mathcal{X} -Space Design

4.6.1. Input Constraints

Constraints of the type $|u(t)| \leq U$ for all t or $|\dot{u}(t)| \leq \bar{U}$ for all t can be indirectly treated in \mathcal{X} space. For the regulator problem

$$|u(t)| = |\underline{k}'\underline{x}(t)| \leq \|\underline{x}(t)\| \quad (83)$$

with equality for the worst case of $\underline{x}(t)$ (e.g., $\underline{x} = c\underline{k}$ for some $c \neq 0$). Assuming that all state variables have been normalized to their maximum value, the norm $\|\underline{k}\| = \sqrt{\underline{k}'\underline{k}}$, i.e., the distance from the origin in \mathcal{X} space can be used as a measure for $|u|$. This provides a criterion for the selection of a gain from the admissible set: Choose the point closest to the origin. Similarly $|\dot{u}(t)| = |\underline{k}'\dot{\underline{x}}(t)| = |\underline{k}'(\underline{A} - \underline{b}\underline{k}')\underline{x}(t)|$ and $\|\underline{k}'(\underline{A} - \underline{b}\underline{k}')\|$ can be used as a measure for $|\dot{u}|$.

4.6.2. Short Wordlength Control Law Implementation

The feedback control law may be implemented approximately in a short wordlength microprocessor as

$$\underline{u} + \Delta \underline{u} = (\underline{k}' + \Delta \underline{k}') (\underline{x} + \Delta \underline{x}) \approx \underline{k}' \underline{x} + \Delta \underline{k}' \underline{x} + \underline{k}' \Delta \underline{x}. \quad (84)$$

For small \underline{x} the dominant term in $\Delta \underline{u}$ is $\underline{k}' \Delta \underline{x}$, i.e. the gains should be not too high. For large \underline{x} the dominant term is $\Delta \underline{k}' \underline{x}$. Robustness with respect to $\Delta \underline{k}'$ is achieved by maintaining a distance Δk_i from a boundary in each direction k_i .

Example 4.9:

$$\underline{x}(k+1) = A \underline{x}(k) + b u(k), \quad A = \begin{bmatrix} 0 & -4 \\ 1 & 4 \end{bmatrix}, \quad b = \begin{bmatrix} 6/16 \\ -5/16 \end{bmatrix}$$

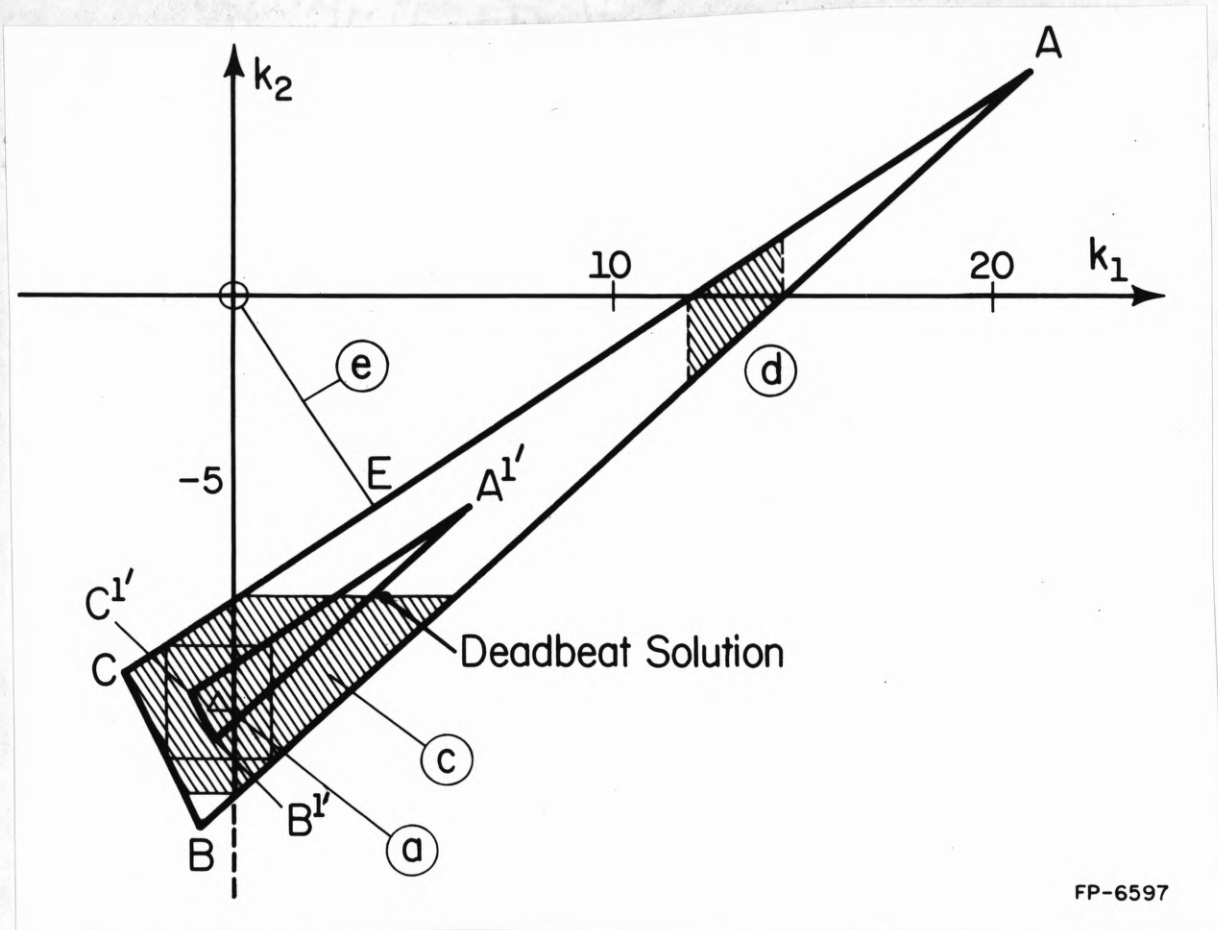
$$u = -[k_1 + \Delta k \quad k_2 \pm \Delta k]$$

Open loop eigenvalues $z_{1,2} = 2$. Find k_1, k_2 such that stability is achieved for the following cases

- maximum admissible Δk ,
- $\Delta k = 1$,
- failure of sensor 1,
- failure of sensor 2,
- $\|k\| = k_1^2 + k_2^2$ minimal.

$$\underline{k}' = \underline{p}^* \underline{E} = [p_0 \quad p_1 \quad 1] \begin{bmatrix} 5 & 6 \\ 6 & 4 \\ 4 & -8 \end{bmatrix}$$

The vertices of the stability triangle ABC in the k_1 - k_2 plane of Fig. 4.8 are determined by the 3 pole placements of eq. (52): $k_A' = [21 \quad 6]$, $k_B' = [-1 \quad -14]$,



FP-6597

Figure 4.8. Design boundaries for example 4.9.

- Fig. 4.8. a) maximally Δk robust
 b) $A'B'C'$ is robust to $\Delta k = 1$
 c) robust to failure of sensor 1
 d) robust to failure of sensor 2
 e) minimum $\|k'\|$ solution

$$k'_C = [-3 \quad -10].$$

- a) This is the center of the largest square inside ABC with sides parallel to the axis. Here $\underline{k}' = [-0.4545 \quad -10.7272]$. It admits $\Delta k = 1.4545$ and places the eigenvalues at $z_1 = 0.132$, $z_2 = 0.686$.
- b) The region for which stability is robust with respect to $\Delta k = 1$, is the triangle A'B'C' with sides parallel to those of ABC, with a distance of the sides of $\sqrt{2}$ under $\pm 45^\circ$. Note that this region does not include the deadbeat solution at $k' = e'A^2 = [4 \quad -8]$. This is a warning that points with the maximum distance from the stability boundary in the λ -plane need not be particularly robust.
- c) The region c is robust with respect to a failure of sensor 1.
- d) The region d is robust with respect to a failure of sensor 2.
- e) Point E with $\underline{k}'_E = [48/13 \quad -72/13]$ has the minimum distance from the origin. This minimum norm solution puts the eigenvalues at $s_{1,2} = 0.442 \pm j0.897$ on the unit circle. For stability k_1 can be increased or k_2 decreased by an arbitrarily small ϵ .

4.7. Multi-Input Problems

4.7.1. Characteristic Parameter Assignment

In the single-input case it was convenient to have the canonical parameter space ϕ as an intermediate step between the λ -plane and \mathcal{X} -space. It allowed studying the shape of stability regions without reference to a particular plant. By the linearity of $\underline{k}' = p^*E$ linear properties in ϕ space

were preserved in the \mathcal{X} space. \mathcal{X} and \mathcal{P} space had the same dimension n and the mapping was one to one. In the case of p inputs the feedback gain matrix \underline{K} has $p \times n$ free parameters. Thus a $p \times n$ dimensional parameter space with the elements of \underline{K} as coordinates is naturally defined. The question here is whether there exists a $p \times n$ dimensional canonical parameter space \mathcal{P}_A , which is linearly related to \mathcal{X} but independent of the particular plant. Another question is: If it exists, is there a simple relationship with the n -dimensional \mathcal{P} space, in which stability or nice stability is defined as before. The answer to both questions is a conditional yes. Some results are available in [56], which will be reformulated and used to design simple systems for robustness with respect to actuator failures. Before the main result can be formulated we have to make some additional assumptions and to introduce some notation.

In the single-input case the implicit assumption was that changes in physical parameters do not cause changes in the order n of the system (which is true for all cranes, aircraft, and other examples). In the generalization to the multivariable case it is assumed here that the controllability structure, as defined by the Kronecker indices, is unchanged by physical parameter variations. For a controllable system

$$\dot{\underline{x}} = \underline{A} \underline{x} + \underline{B} \underline{u}, \quad \underline{B} = [b_1 \ b_2 \ \dots \ b_p] \quad (85)$$

the Kronecker indices μ_i , $i=1,2,\dots,p$, are the smallest integers k such that $r_{i,k} = r_{i-1,k}$, where

$$r_{i,k} = \text{rank} [\underline{B}, \underline{A} \underline{B} \ \dots \ \underline{A}^{k-1} \underline{B}, \underline{A}^k \underline{b}_1 \ \dots \ \underline{A}^k \underline{b}_i] \quad i=1,2,\dots,p \quad (86)$$

$$r_{0,k} = r_{p,k-1}$$

The Kronecker indices satisfy $\mu_1 + \mu_2 + \dots + \mu_p = n$. A vector $\underline{A}^k \underline{b}_i$ is called regular if $r_{i,k} = 1 + r_{i-1,k}$, i.e. the regular vectors

$$\begin{aligned} & \underline{b}_1, \underline{A} \underline{b}_1 \dots \underline{A}^{\mu_1-1} \underline{b}_1 \\ & \underline{b}_2, \underline{A} \underline{b}_2 \dots \underline{A}^{\mu_2-1} \underline{b}_2 \\ & \vdots \\ & \underline{b}_p, \underline{A} \underline{b}_p \dots \underline{A}^{\mu_p-1} \underline{b}_p \end{aligned} \quad (87)$$

are the first n linear independent columns of $[\underline{B}, \underline{A} \underline{B}, \underline{A}^2 \underline{B} \dots]$. By the definition (86) $\underline{A}^{\mu_i} \underline{b}_i$ is not regular and can be uniquely expressed as

$$\underline{A}^{\mu_i} \underline{b}_i = -[\underline{B}, \underline{A} \underline{B} \dots \underline{A}^{\mu_i-1} \underline{B}] \underline{\alpha}_i - [\underline{A}^{\mu_i} \underline{b}_1 \dots \underline{A}^{\mu_i} \underline{b}_{i-1}] \underline{\beta}_i \quad (88)$$

where all elements of $\underline{\alpha}_i$ and $\underline{\beta}_i$ multiplying nonregular vectors are zero, in particular $\underline{\beta}_i = [\beta_{i1} \dots \beta_{ii-1}]$ has $\beta_{ij} = 0$ if $\mu_j \leq \mu_i$. By Popov's theorem on invariants [10] the Kronecker indices μ_i and the β -parameters β_i , $i=1,2,\dots,p$ constitute a complete set of independent invariants for $(\underline{A}, \underline{B})$ under all transformations.

$$\tilde{\underline{u}} = \underline{M}^{-1} \underline{u} \quad (90)$$

In order to avoid the distinction between α - and β -parameters in the definition of a canonical parameter space \underline{A} , first the β -parameters are made zero by an input transformation, i.e. a modified system

$$\dot{\underline{x}} = \underline{A} \underline{x} + \underline{B} \underline{M} \tilde{\underline{u}} = \underline{A} \underline{x} + \tilde{\underline{B}} \tilde{\underline{u}} \quad (91)$$

is considered with the "normalized input"

$$\tilde{\underline{u}} = -\tilde{\underline{K}} \underline{x} + \tilde{\underline{r}} \quad (92)$$

$\tilde{\underline{B}}$ and $\tilde{\underline{K}}$ are related to the original variables by

$$\underline{B}\underline{K} = \tilde{\underline{B}}\tilde{\underline{K}}, \quad \tilde{\underline{B}} = \underline{B}\underline{M}, \quad \tilde{\underline{K}} = \underline{M}^{-1}\underline{K} \quad (93)$$

Now the β -parameters of the pair $(\underline{A}, \underline{B})$ can be made zero by the choice

$$\underline{M} = \begin{bmatrix} 1 & \beta_{21} & \dots & \beta_{p1} \\ 0 & 1 & & \vdots \\ & \ddots & \ddots & \vdots \\ & & 1 & \beta_{pp-1} \\ 0 & 0 & & 1 \end{bmatrix} = \begin{bmatrix} 1 & \boxed{\beta_{-2}} & & \\ 0 & 1 & & \\ & & \boxed{\beta_{-3}} & \\ & & & \ddots \\ & & & & \boxed{\beta_{-p}} \\ 0 & & & & & 1 \end{bmatrix} \quad (94)$$

This can be shown by putting the last term in eq. (88) on the left hand side

$$\underline{A}^{\mu_i} \underline{B} \begin{bmatrix} \beta_i \\ 1 \\ 0 \\ \vdots \\ 0 \end{bmatrix} = -[\underline{B}, \underline{A}\underline{B} \dots \underline{A}^{\mu_i-1} \underline{B}] \alpha_i.$$

Then with $\tilde{\underline{B}} = \underline{B}\underline{M} = [\tilde{b}_1 \dots \tilde{b}_p]$

$$\begin{aligned} \underline{A}^{\mu_i} \tilde{b}_i &= -[\underline{B}, \underline{A}\underline{B} \dots \underline{A}^{\mu_i-1} \underline{B}] \alpha_i \\ \underline{A}^{\mu_i} \tilde{b}_i &= -[\tilde{\underline{B}}\underline{M}^{-1}, \underline{A}\tilde{\underline{B}}\underline{M}^{-1} \dots \underline{A}^{\mu_i-1} \tilde{\underline{B}}\underline{M}^{-1}] \alpha_i \\ \underline{A}^{\mu_i} \tilde{b}_i &= -[\underline{B}, \underline{A}\tilde{\underline{B}} \dots \underline{A}^{\mu_i-1} \tilde{\underline{B}}] \tilde{\alpha}_i. \end{aligned} \quad (95)$$

A comparison with eq. (88) shows that now the β -parameters multiplying $\underline{A}^{\mu_i} \tilde{b}_1 \dots \underline{A}^{\mu_{i-1}} \tilde{b}_{i-1}$ do not appear in eq. (95).

By Popov's theorem the β -parameters remain zero under feedback, i.e. the closed loop system with input $\tilde{\underline{r}} = \underline{M}^{-1} \underline{r}$

$$\dot{\underline{x}} = (\underline{A} - \underline{B}\underline{K})\underline{x} + \underline{B}\underline{r} = (\underline{A} - \tilde{\underline{B}}\tilde{\underline{K}})\underline{x} + \tilde{\underline{B}}\tilde{\underline{r}} = \underline{F}\underline{x} + \tilde{\underline{B}}\tilde{\underline{r}} \quad (96)$$

has no β -parameters and $\underline{F}^{\mu_i} \tilde{\underline{b}}_i$ can be expressed as

$$\underline{F}^{\mu_i} \tilde{\underline{b}}_i = -[\tilde{\underline{B}}, \underline{F}\tilde{\underline{B}} \dots \underline{F}^{\mu_i-1} \tilde{\underline{B}}] \underline{p}_i. \quad (97)$$

The n elements of \underline{p}_i , $i=1,2,\dots,p$, i.e. $n \times p$ parameters will be used in the following as coordinates of a canonical parameter space ϕ_Λ , in which desired closed system properties can be specified without reference to the particular plant, with the only condition that the closed loop must have the same Kronecker indices μ_i as the open loop. In the single-input case $\underline{p}_i = \underline{p}$, i.e. \underline{p}_i consists of the n coefficients of the desired characteristic polynomial, in the multi-input case the $n \times p$ elements of $\underline{p}_1 \dots \underline{p}_p$ will be called characteristic parameters. Note that

$$[\tilde{\underline{B}}, \underline{A}\tilde{\underline{B}} \dots \underline{A}^{k-1}\tilde{\underline{B}}] = [\tilde{\underline{B}}, \underline{F}\tilde{\underline{B}} \dots \underline{F}^{k-1}\tilde{\underline{B}}] \begin{bmatrix} \underline{I} & \underline{K}\underline{B} & \underline{K}\underline{A}\underline{B} & \underline{K}\underline{A}^{k-1}\underline{B} \\ \underline{0} & \underline{I} & \underline{K}\underline{B} & \\ \underline{0} & \underline{0} & \underline{I} & \\ \vdots & & \ddots & \\ \underline{0} & & \underline{0} & \underline{I} \end{bmatrix}. \quad (98)$$

Both sides may be truncated at any column of $\underline{A}^{k-1}\tilde{\underline{B}}$, always the second factor on the right hand side is nonsingular and thus $\underline{F}^{k-1}\tilde{\underline{b}}_i$ is regular if and only if $\underline{A}^{k-1}\tilde{\underline{b}}_i$ is regular. Due to the particular form of \underline{M} in eq. (94) the same relationship exists between $\underline{A}^{k-1}\tilde{\underline{b}}_i$ and $\underline{A}^k \underline{b}_i$.

$$[\tilde{\underline{B}}, \underline{A}\tilde{\underline{B}} \dots \underline{A}^{k-1}\tilde{\underline{B}}] = [\underline{B}, \underline{A}\underline{B} \dots \underline{A}^k \underline{B}] \begin{bmatrix} \underline{M} & \underline{0} & \underline{0} \\ \underline{0} & \underline{M} & \\ \vdots & \ddots & \\ \underline{0} & & \underline{M} \end{bmatrix}. \quad (99)$$

Thus, in eq. (97) the regular vectors are in the same locations as in eq. (96), i.e. the list of regular vectors is the same as in eq. (87) with \underline{A} replaced by $\underline{F} = \underline{A} - \underline{B}\underline{K}$ and \underline{b}_i replaced by $\underline{\tilde{b}}_i$. Then eq. (97) may be rewritten as

$$\underline{F}^{\mu_i} \underline{\tilde{b}}_i = -[\underline{\tilde{b}}_1, \underline{F} \underline{\tilde{b}}_1 \dots \underline{F}^{\mu_i-1} \underline{\tilde{b}}_1 : \underline{\tilde{b}}_2 \dots : \dots : \underline{F}^{\mu_p-1} \underline{\tilde{b}}_p] \begin{bmatrix} p_{i1} \\ p_{i2} \\ \vdots \\ p_{ip} \end{bmatrix} \quad (100)$$

where $p_{ij} = [p_{ijo} \dots p_{ij\mu_j-1}]'$ is a μ_j -vector. Now define the $p \times n$ coefficient matrix

$$\underline{P}_A^* = \begin{bmatrix} p_{11}' & \dots & p_{1p}' \\ \vdots & & \vdots \\ p_{p1}' & \dots & p_{pp}' \end{bmatrix}. \quad (101)$$

It generalizes $p' = [p_0 \dots p_{n-1}]$ to the multi-input case. The generalization of $p^* = [p_0 \dots p_{n-1} \quad 1]$ is the "characteristic matrix"

$$\underline{P}_A^* = \begin{bmatrix} p_{11}' & 1 & p_{12}' & 0 & \dots & p_{1p}' & 0 \\ p_{21}' & 0 & p_{22}' & 1 & & p_{2p}' & 0 \\ \vdots & & \vdots & & & \vdots & \\ p_{p1}' & 0 & p_{p2}' & 0 & & p_{pp}' & 1 \end{bmatrix}. \quad (102)$$

Now eq. (100) for $i=1,2,\dots,p$ may be written

$$[\underline{F}^{\mu_1} \underline{\tilde{b}}_1 \dots \underline{F}^{\mu_p} \underline{\tilde{b}}_p] = -[\underline{\tilde{b}}_1 \dots \underline{F}^{\mu_1-1} \underline{\tilde{b}}_1 : \underline{\tilde{b}}_2 \dots : \dots : \underline{F}^{\mu_p-1} \underline{\tilde{b}}_p] \underline{P}_A^* \quad (103)$$

which also can be expressed as

$$[\tilde{b}_1 \dots \underline{F}^{\mu_1} \tilde{b}_1 \vdots \tilde{b}_2 \dots \vdots \dots \underline{F}^{\mu_p} \tilde{b}_p] \underline{P}_A^* = 0. \quad (104)$$

In the single-input case the characteristic polynomial is obtained from eq. (104) by replacing the vector $\underline{F}^k \tilde{b}_1$ in eq. (104) by λ^k . In the same way in the multi-input case a "characteristic polynomial matrix" is defined as

$$\underline{P}_\lambda = \text{diag}(\underline{Y}_1^i) \cdot \underline{P}_A^*, \quad \underline{Y}_1^i = [1 \quad \lambda \quad \dots \quad \lambda^{\mu_i}]. \quad (105)$$

It is related to the characteristic polynomial of F by

$$P(\lambda) = \det \underline{P}_\lambda \quad (106)$$

as was shown in [56]. The main advantage over a direct calculation of the $\det(\lambda \underline{I} - \underline{A} + \underline{B} \underline{K})$ with general elements k_{ij} is that eq. (106) does not involve \underline{A} and \underline{B} and is done only once for all systems with the same Kronecker indices. The multilinear problem of solving eq. (106) for some characteristic coefficient becomes a linear one if the n coefficients of one row of \underline{P}_λ are expressed in terms of the p_i , $i=1,2,\dots,n$ and the remaining $p \times (n-1)$ free parameters of the other rows of \underline{P}_λ . We are now able to formulate

Theorem 5: $\underline{A} - \underline{B} \underline{K}$ has the characteristic matrix \underline{P}_A^* if

$$\underline{K} = \underline{M} \underline{P}_A^* \underline{E} \quad (107)$$

where \underline{M} is given by eq. (94) and

$$\underline{E} = \begin{bmatrix} \underline{E}_1 \\ \vdots \\ \underline{E}_p \end{bmatrix} \quad \underline{E}_i = \begin{bmatrix} e_i^1 \\ e_i^2 \\ \vdots \\ e_i^{\mu_i} \end{bmatrix} \quad (108)$$

e_i^1 is the last row of the $\mu_i \times n$ matrix \underline{Q}_i in

$$\underline{R}^{-1} = \begin{bmatrix} Q_1 \\ \vdots \\ Q_p \end{bmatrix}, \quad \underline{R} = [\underline{b}_1 \dots \underline{A}^{\mu_1-1} \underline{b}_1 \vdots \underline{b}_2 \dots \vdots \dots \underline{A}^{\mu_p-1} \underline{b}_p]. \quad (109)$$

Proof: Follows from [56].

Example 4.10:

$$\dot{\underline{x}} = \begin{bmatrix} 5 & -1 & 2 \\ -2 & -2 & 6 \\ 4 & -3 & 7 \end{bmatrix} \underline{x} + \begin{bmatrix} 0 & 1 \\ 1 & 5 \\ 1 & 6 \end{bmatrix} \underline{u} = \underline{A} \underline{x} + \underline{B} \underline{u}. \quad (110)$$

Find an output feedback

$$\underline{u} = \begin{bmatrix} k_{11} & 0 & k_{13} \\ k_{21} & 0 & k_{23} \end{bmatrix} \underline{x}$$

if it exists, which places poles at $s_1 = -1$, $s_2 = -2$, $s_3 = -3$ and minimizes the maximum $|k_{ij}|$

$$\det[\underline{b}_1 \quad \underline{b}_2 \quad \underline{A} \underline{b}_1] \neq 0, \quad \text{i.e. } \mu_1 = 2, \mu_2 = 1.$$

For \underline{M} we need the β parameter

$$\underline{A} \underline{b}_2 = -\beta_{21} \underline{A} \underline{b}_1 - \alpha_1 \underline{b}_1 - \alpha_2 \underline{b}_2$$

it is

$$\beta_{21} = -5 \quad \text{and} \quad \underline{M} = \begin{bmatrix} 1 & -5 \\ 0 & 1 \end{bmatrix}.$$

The controllability vectors \underline{e}_1' and \underline{e}_2' are obtained from

$$[b_1 \quad \underline{A} b_1 \quad \vdots \quad b_2]^{-1} = \begin{bmatrix} \cdot \\ e_1' \\ e_2' \end{bmatrix} = \begin{bmatrix} \cdot & \cdot & \cdot \\ 1 & 1 & -1 \\ 0 & -1 & 1 \end{bmatrix}$$

$$\underline{E} = \begin{bmatrix} e_1' \\ e_1' \underline{A} \\ e_1' \underline{A}^2 \\ e_2' \\ e_2' \underline{A} \end{bmatrix} = \begin{bmatrix} 1 & 1 & -1 \\ -1 & 0 & 1 \\ -1 & -2 & 5 \\ 0 & -1 & 1 \\ 6 & -1 & 1 \end{bmatrix} = [\eta_1 \quad \eta_2 \quad \eta_3].$$

The characteristic matrix has the form

$$P_A^* = \begin{bmatrix} P_{110} & P_{111} & 1 & P_{120} & 0 \\ P_{210} & P_{211} & 0 & P_{220} & 1 \end{bmatrix}.$$

It is related to the characteristic polynomial by

$$p(s) = p_0 + p_1 s + p_2 s^2 + s^3 = \det p_\lambda = \det \begin{bmatrix} P_{110} + P_{111} s + s^2 & P_{120} \\ P_{210} + P_{211} s & P_{220} + s \end{bmatrix}.$$

Use the coefficients of the second row as free parameters $\gamma = P_{210}$,

$\delta = -P_{211}$, and $\epsilon = -P_{220}$.

$$p_0 = \gamma P_{120} - \epsilon P_{110}$$

$$p_1 = \delta P_{120} - \epsilon P_{111} + P_{110} \quad (111)$$

$$p_2 = P_{111} - \epsilon.$$

With eq. (107) the output feedback condition results in

$$\begin{bmatrix} k_{12} \\ k_{22} \end{bmatrix} = \underline{M} \underline{P}_A^{-1} \underline{\eta}_2 = \begin{bmatrix} 0 \\ 0 \end{bmatrix}$$

$$P_{110} - P_{120} = 2 \quad (112)$$

$$\epsilon - \gamma = 1.$$

Substitute into eq. (111)

$$P_0 = (\epsilon - 1)P_{120} - \epsilon(2 + P_{120}) = -2\epsilon - P_{120}$$

$$P_1 = \delta P_{120} - \epsilon P_{111} + 2 + P_{120} = 2 - \epsilon P_{111} + (\delta + 1)P_{120}$$

$$P_2 = P_{111} - \epsilon.$$

The particular choice $p_{120} = 0$ leaves δ undetermined and $p_0 = -2\epsilon$, $p_1 = 2 - \epsilon p_{111}$, $p_2 = p_{111} - \epsilon$, and with $P(s) = (s+1)(s+2)(s+3) = 6 + 11s + 6s^2 + s^3$, $\epsilon = -3$, $p_{111} = 3$, $p_{110} = 2$, $\gamma = -4$.

The remaining four feedback gains are

$$\begin{aligned} & \begin{bmatrix} k_{11} & k_{13} \\ k_{21} & k_{23} \end{bmatrix} = \underline{M} \underline{P}_A^{-1} [\eta_1 \quad \eta_3] \\ & = \begin{bmatrix} 1 & -5 \\ 0 & 1 \end{bmatrix} \begin{bmatrix} P_{110} - P_{111} & -1 \\ -\gamma + \delta + 6 & \gamma - \delta - \epsilon + 1 \end{bmatrix} \\ & = \begin{bmatrix} 1 & -5 \\ 0 & 1 \end{bmatrix} \begin{bmatrix} -2 & 6 \\ 10 + \delta & -\delta \end{bmatrix} = \begin{bmatrix} -52 - 5\delta & 6 - 5\delta \\ 10 + \delta & -\delta \end{bmatrix}. \end{aligned}$$

δ is chosen as -5.8 in order to minimize $\max |k_{ij}|$. Then

$$\underline{K} = \begin{bmatrix} -23 & 0 & -23 \\ 4.2 & 0 & 5.8 \end{bmatrix}$$

4.7.2. Robustness of Multivariable Systems

In principle all concepts for the design of robust control systems in \mathcal{X} space carry over from the single-input to the multi-input case. However, the \mathcal{X} space now has dimension $p \times n$, such that graphical methods in several two-dimensional subspaces require many iterations and can become feasible only with a good software for graphical displays and interactive design. General results, which would give a clearer understanding of the multivariable \mathcal{X} space, are presently not available.

Changes of physical parameters can be tackled in the same way as in the single-input case. Sensor failures now result in p coefficients of one column of \underline{K} becoming zero. Actuator failures could not be handled at all with the single-input method. Here some insight into the geometry of the problem and possible problem formulations can be gained from eq. (107), as will be illustrated by

Example 4.11:

$$x(k+1) = \begin{bmatrix} 1 & 1 \\ 0 & 1 \end{bmatrix} x(k) + \begin{bmatrix} 1 & 1 \\ 1 & 2 \end{bmatrix} \begin{bmatrix} u_1(k) \\ u_2(k) \end{bmatrix}. \quad (113)$$

The state feedback $\underline{u} = \underline{K} \underline{x}$ may have three configurations

a) nominal

$$\underline{K} = \begin{bmatrix} k_{11} & k_{12} \\ k_{21} & k_{22} \end{bmatrix}$$

b) failure of actuator 1

$$\underline{K}_2 = \begin{bmatrix} 0 & 0 \\ k_{21} & k_{22} \end{bmatrix}$$

c) failure of actuator 2

$$\underline{K}_1 = \begin{bmatrix} k_{11} & k_{12} \\ 0 & 0 \end{bmatrix}.$$

Find \underline{K} such that it places a double pole at $z=0.4$ and the eigenvalues in the two failed cases are in the smallest possible circle in the family of circles Γ_r of Fig. 4.1.

In eq. (107) $\underline{M} = \underline{I}$ and

$$\begin{aligned} \underline{K} = \frac{\underline{P}^* \underline{E}}{\underline{P} \underline{A} \underline{E}} &= \begin{bmatrix} p_{11} & 1 & p_{12} & 0 \\ p_{21} & 0 & p_{22} & 1 \end{bmatrix} \begin{bmatrix} 2 & -1 \\ 2 & 1 \\ -1 & 1 \\ -1 & 0 \end{bmatrix} \\ &= \begin{bmatrix} 2p_{11} + 2 - p_{12} & -p_{11} + 1 + p_{12} \\ 2p_{21} - p_{22} & -p_{21} + p_{22} \end{bmatrix} \end{aligned}$$

$$P(z) = \det \begin{bmatrix} p_{11} + z & p_{12} \\ p_{21} & p_{22} + z \end{bmatrix} = z^2 + (p_{11} + p_{22})z + (p_{11}p_{22} - p_{12}p_{21}).$$

In case a) $P(a) = (z-0.4)^2 = z^2 - 0.8z + 0.16$. Use $\alpha = -p_{21}$, $\beta = -p_{22}$ as free parameters, then $p_{11} = \beta - 0.8$ and $p_{12} = P(\beta)/\alpha$. Eliminating α and β by k_{21} and k_{22} gives

$$k_{11}(k_{21}, k_{22}) = \frac{(k_{21} + 2k_{22} + 1.4)^2}{k_{21} + k_{22} + 1} 2k_{21} - 4k_{22} - 1.6 \quad (114)$$

$$k_{12}(k_{21}, k_{22}) = -k_{11}(k_{21}, k_{22}) - k_{21} - 2k_{22} - 3.2.$$

These two equations describe a two dimensional surface in the four dimensional χ space. All points on this surface give the desired pole placement.

The failed cases are single-input problems for which a circle in z -plane maps into a triangle in the subspaces of the remaining gains. The problem can then be described geometrically as follows: For a given circle radius the two triangles are obtained. Now we are looking for a point in the surface (112) which has projections into the k_{11} - k_{12} -plane and the k_{21} - k_{22} -plane, which lie in the respective triangles. To check whether such a solution exists we could find the regions in the surface (112), which have such projections, and see whether the two regions overlap. It is more convenient however, to use one of the planes, say the k_{11} - k_{12} -plane, where the triangle is one of the regions and the other is obtained by reflecting the triangle in the k_{21} - k_{22} -plane at the surface (112) into the k_{11} - k_{12} -plane. If there exists an intersection, then the radius of the z -plane circle is reduced until the set of admissible solutions shrinks to a point.

We begin with $r = 0.5$. The two triangles are shown in Fig. 4.9a and b. The vertices D, E, F are now mapped by eq. (111) into D', E', F' in the k_{11} - k_{12} -plane. The sides of the figure $D'E'F'$ are not straight lines, since they have been reflected through a curved surface. However, it is easy to check that there exists a set of admissible solutions between F' and C , thus r may be reduced. Figure 4.9c shows the case $r = 0.4$, where no solution exists.

Going to $r = 0.41$ as shown in Fig. 4.9d then results in the solution

$$K = \begin{bmatrix} 0.278 & 0.522 \\ 0.020 & 0.190 \end{bmatrix}.$$

The following eigenvalue locations are obtained

nominal	$z_{1,2} = 0.4$
failure of actuator 1	$z_{1,2} = 0.8$ on circle $\Gamma_{0.41}$
failure of actuator 2	$z_{1,2} = 0.6 \pm 0.344j$ on $\Gamma_{0.41}$
both failures	$z_{1,2} = 1$ open loop unstable.

4.8. Conclusions

The design of control systems in the parameter space \mathcal{X} of state feedback gains has been studied. Conceptually this offers the following advantages:

1. Robustness with respect to large parameter variations can be achieved. It is possible to design the feedback such as to maximize the admissible variations in known directions.
2. Robustness with respect to sensor and actuator failures can be achieved. The feedback can be designed such that in the considered failure situations at least some emergency specifications are met or such that the deviation from the nominal behavior is minimized.
3. The feedback can be designed such that for the worst case initial conditions the maximal required control input $|u(t)|$ is minimized and thus saturation can be avoided.

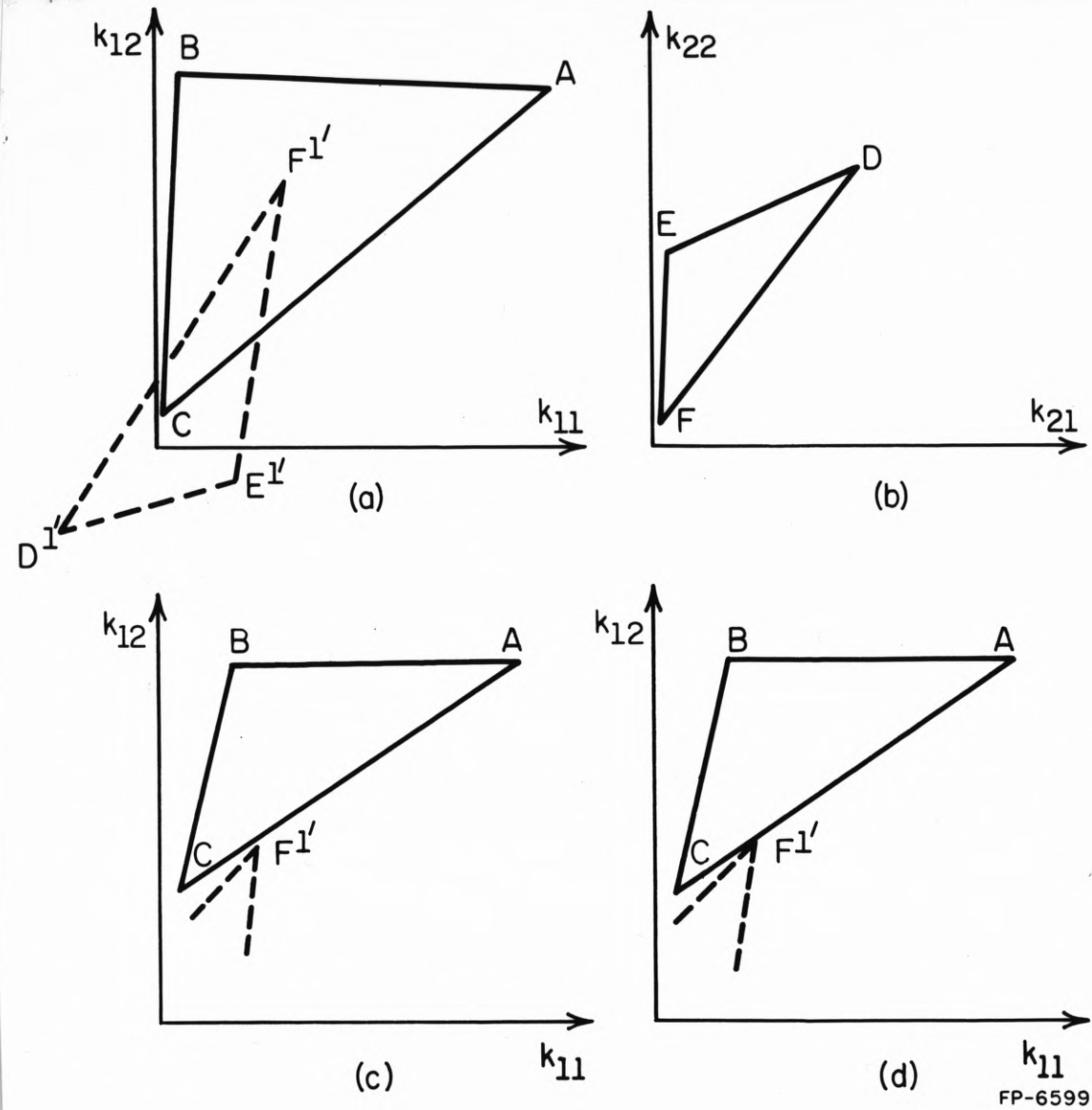


Figure 4.9.1 Image of the circle Γ .

a) and b) for $r = 0.5$ in two subspaces

c) $r = 0.4$

d) $r = 0.41$

4. The feedback system can be designed for robustness with respect to short wordlength implementation or other inaccuracies of the feedback law.
5. Static output feedback or fixing some gains simplifies the analysis since it reduces the number of free parameters. It will of course give less favorable results.
6. Dynamic feedback can be tackled by the same methods. It is particularly desirable in situations with sensor failures.

These conceptual advantages are apparent in situations with only two essential parameters. Here it is general engineering practice to present and analyze results in diagrams, showing boundaries, regions and their overlap, etc. However, in most cases the boundary points have to be calculated point by point in more or less involved computations. In this paper desirable dynamic properties of control systems are specified in terms of regions in the eigenvalue (λ) plane. A particularly simple pole placement algorithm is introduced and used for mapping boundaries from the λ -plane to the \mathcal{X} space. The mapping of boundaries point by point becomes very simple. In fact all examples of this paper were done by pocket calculator. This makes it promising to develop software for computer-aided design with rapidly changing graphical displays of boundaries in various subspaces.

Due to the simplicity of the mapping it was possible to obtain a few general results on the shape of boundaries and stability regions in \mathcal{X} space. For the design of digital control systems a family of circular boundaries in the z -plane can be used to characterize desirable dynamic properties. Circles have particularly nice mapping properties and the convex

hull of their image in the χ space is easily determined. For arbitrary order systems, it is useful as a necessary condition for the existence of various robust solutions. Further research will be necessary to obtain more general results on the shape of boundaries, sufficient conditions, etc. also for other than circular boundaries in λ -plane. The development of good numerical algorithms will depend on such insights into the geometry of the solution sets. It was shown that already in very simple examples this set may be disconnected. A systematic search inside the convex hull of the χ space region may be necessary.

In its present stage the design in χ space is already a useful design tool. It may be used for example in conjunction with the root locus method, which visualizes the influence of one gain on the eigenvalue location. The present method visualizes the influence of two gains on the eigenvalue locations. The use of this tool has been shown in this paper by the example of a crane. In Chapter 5, it will be used to design a dynamic controller for the short period longitudinal mode of an F4-E aircraft with canards, which is unstable in the subsonic flight conditions. A solution using two gyros and one accelerometer was found which meets the nominal specifications for the unfailed system or after a failure of any single sensor, and also meets the emergency specifications after failure of any two sensors, where these properties pertain to four very different flight conditions.

CHAPTER 5

APPLICATION TO THE LONGITUDINAL CONTROL OF A FIGHTER AIRCRAFT

5.1. Introduction

The purpose of this chapter is to apply the parameter or K space design procedure described in Chapter 4 to a realistic design problem. The system to be considered is a third order model of the longitudinal axis of a McDonnell-Douglas F4-E fitted with horizontal canards.

5.2. System Description and Design Objectives5.2.1. Model formulation

Airframe dynamics. The example chosen to illustrate \mathcal{K} -space design is control of the longitudinal axis of a fighter aircraft. The complete equations of motion describing the dynamics of the airplane are nonlinear and too complex to be used in control law development. Standard procedure is to linearize these equations about typical flight conditions, and then use these linear system representations to design the control system. The linearization decouples the dynamical equations into two separate sets of equations called the longitudinal, and lateral-directional. Typically a separate control system is designed for each set of equations. For fighter aircraft two dominant modes describe the longitudinal rigid body motion. One of these modes, called the phugoid mode, is usually very slow. It is easily controlled by the pilot, and therefore is not included in the control law design. The other mode, called the short period mode, is the mode that most effects the handling qualities of the aircraft, and is the only airframe mode considered in this report.

The state description of the short period mode depends on the individual aircraft and flight condition. The aircraft chosen for this paper was a special F4-E fitted with horizontal canards. Figure 5.1 shows the F4-E flight envelope and those flight conditions for which linearized aerodynamic data are available.

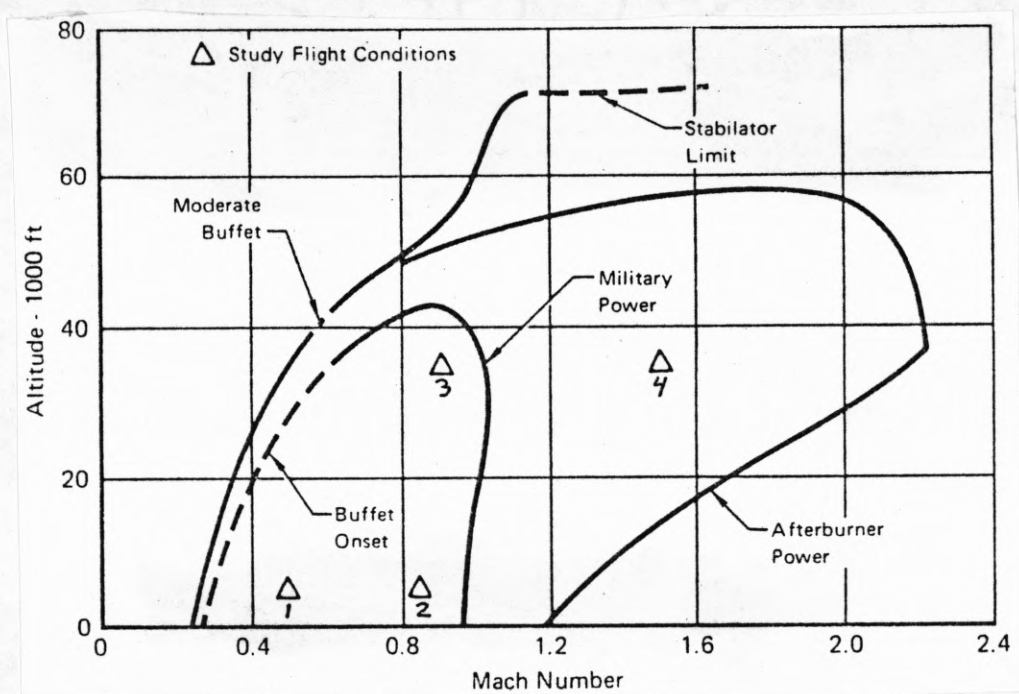


Figure 5.1. Flight envelope and operating points [57].

A complete description of the aircraft including aero data is given in [57]. One notable feature is that the uncontrolled short period mode is unstable for all subsonic flight conditions. Table 5.1a lists the uncontrolled short period eigenvalues for each of the four flight conditions.

Table 5.1a. Open Loop Short Period Eigenvalues

FC	Mach	Altitude	Open Loop Short Period Eigenvalues	
1	.5	5000'	-3.07	1.23
2	.85	5000'	-4.90	1.78
3	.9	35000'	-1.87	.56
4	1.5	35000'	-.87 + j4.3	

Actuators. The two major control surfaces available for control of the short period mode are the elevator position (δ_e) and the canard position (δ_c); these are shown in Figure 5.2. Simplified models for the canard and elevator actuators were used. The actuator state equation used was

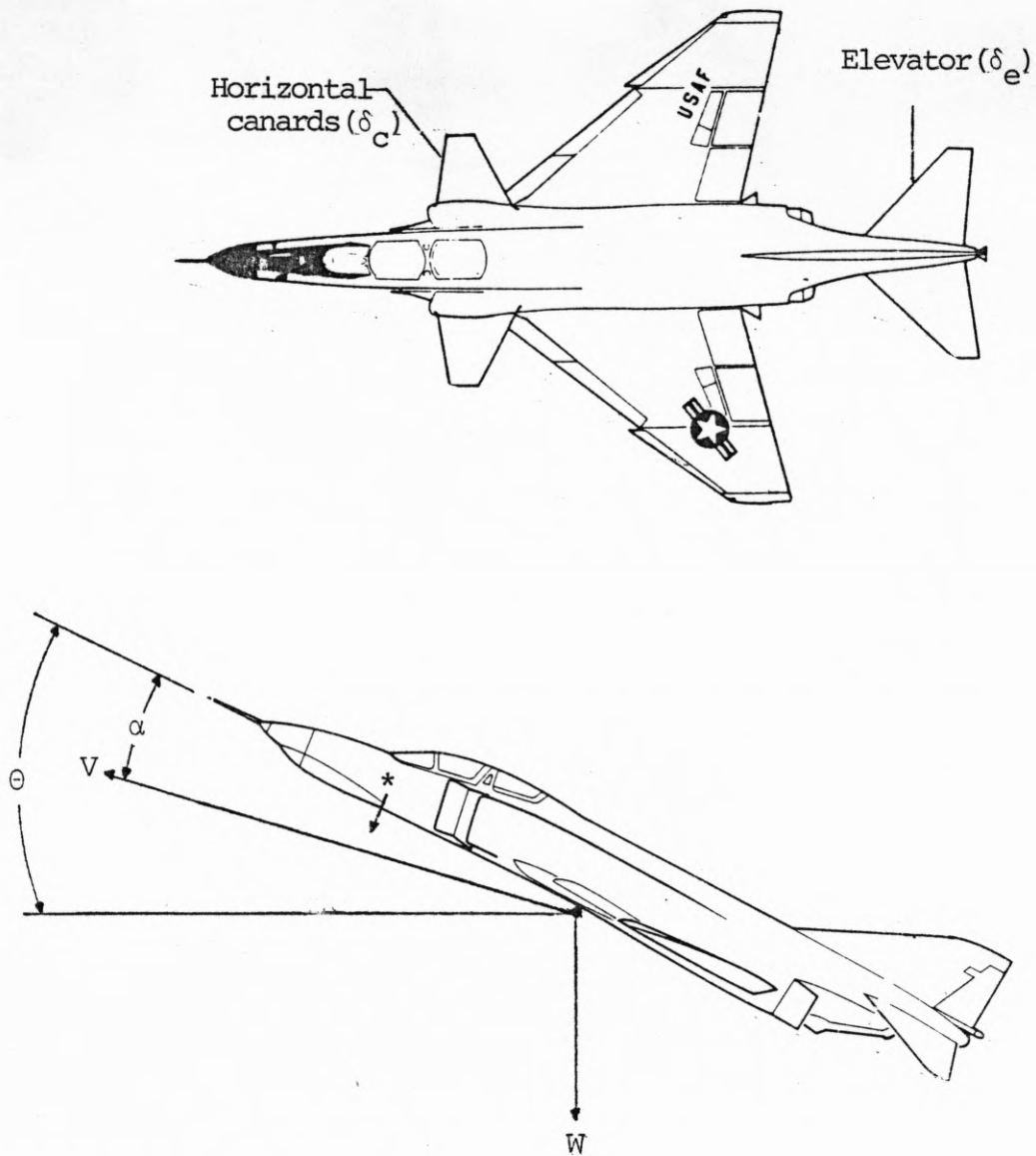
$$\dot{\delta} = -a\delta + a\delta_{com} \quad (115)$$

where δ is the actuator position, a is the actuator eigenvalue (time constant or equivalent bandwidth) and δ_{com} is the commanded actuator position.

Sensors. Typical sensors which are used to control the pitch axis are (for definitions see Figure 5.2):

- 1) Inertial sensors which measure pitch rate (q) and normal acceleration (N_z).
- 2) Air data sensors which measure angle of attack (α) and dynamic pressure.
- 3) Position sensors which measure the elevator and canard positions.

Only the pitch rate and normal acceleration are assumed to be available for feedback. Air data sensors were not used due to their unreliability. Position sensors, although reliable, would not be useful without an estimate



V \equiv velocity vector
 W \equiv weight
 α \equiv angle of attack
 θ \equiv pitch angle
 $\dot{\theta}$ \equiv pitch rate
 N_z \equiv normal acceleration at sensor (*)

Figure 5.2. Aircraft nomenclature.

of the equilibrium (trim) surface position. This estimation was undesirable. A failed sensor will be one which in the output is uncorrelated with the input.

System state description. The aero data and equations of motion given in [57] were transformed to a state space description resulting in the following system representation for the airframe and actuators

$$\frac{d}{dt} \begin{bmatrix} \alpha \\ q \\ \delta_e \\ \delta_c \end{bmatrix} = \begin{bmatrix} a_1 & a_2 & a_3 & a_4 \\ a_5 & a_6 & a_7 & a_8 \\ 0 & 0 & -a_e & 0 \\ 0 & 0 & 0 & -a_c \end{bmatrix} \begin{bmatrix} \alpha \\ q \\ \delta_e \\ \delta_c \end{bmatrix} + \begin{bmatrix} 0 & 0 \\ 0 & 0 \\ a_e & 0 \\ 0 & a_c \end{bmatrix} \begin{bmatrix} \delta_{ecom} \\ \delta_{ccom} \end{bmatrix} \quad (116a)$$

$$\begin{bmatrix} Nz \\ q \end{bmatrix} = \begin{bmatrix} c_1 & c_2 & c_3 & c_4 \\ 0 & 1 & 0 & 0 \end{bmatrix} x \quad (116b)$$

where a_1 - a_8 and c_1 - c_4 depend on the flight condition and are listed in Appendix I.

This two-input representation was reduced to a single input problem by considering the canard command to be proportional to the elevator command. A study was done in [57] to determine this proportionality constant, K_c , for minimum drag flight under a wide range of conditions. That minimum drag value, $K_c = -.7$, was the value used in this paper. There is not much loss of generality in this assumption of dependent inputs since the ratio of control surface effectiveness (essentially a_8/a_7 since a_3 and a_4 are small) between the canard and elevator does not change much as flight conditions change.

To study the effect of sensor failures it is easiest to have the system equations written in sensor coordinates. Equations (116) were

transformed to make the normal acceleration a state variable. Transforming the system, using $K_c = -.7$, and assuming $a_c = a_e$ resulted in the following system description.

$$\frac{d}{dt} \begin{bmatrix} Nz \\ q \\ \delta_e \end{bmatrix} = \begin{bmatrix} a_{11} & a_{12} & a_{13} \\ a_{21} & a_{22} & a_{23} \\ 0 & 0 & -a \end{bmatrix} \begin{bmatrix} Nz \\ q \\ \delta_e \end{bmatrix} + \begin{bmatrix} b_1 \\ 0 \\ a \end{bmatrix} u \quad (117a)$$

with output

$$y = \begin{bmatrix} 1 & 0 & 0 \\ 0 & 1 & 0 \end{bmatrix} \begin{bmatrix} Nz \\ q \\ \delta_e \end{bmatrix} \quad (117b)$$

where δ_e now represents the effective control position of the elevator and canard, and "a" represents the effective bandwidth of both actuators. This effective bandwidth was assumed to be 14 rad/sec. Appendix I gives a tabulation of the a_{ij} , b_1 used.

5.2.2. Design Objectives and Design Specifications

Using normal acceleration and/or pitch rate feedback, the basic design objective is to design a continuous time, fixed gain controller which:

- 1) meets certain nominal performance requirements at all four flight conditions when all sensors are available and
- 2) meets emergency performance requirements after sensor failure. The specific requirements to be met are:

- 1) the controlled short period eigenvalues must be in the range specified by military standards [58],
- 2) the remaining closed loop eigenvalues resulting from actuator and controller dynamics should be in a specified region,

- 3) time responses of the so called C_N^* output to pilot step commands should be acceptable in the sense of [57].

The region of allowable short period eigenvalue location is given in [58] as a requirement on the range of damping and natural frequency for the short period mode. For the short period mode described by

$$s^2 + 2\zeta_{sp} \omega_{sp} s + \omega_{sp}^2 = 0 \quad (118)$$

the restricted range of ζ_{sp} and ω_{sp} under normal operating conditions is

$$.35 \leq \zeta_{sp} \leq 1.3 \quad (119a)$$

$$\omega_a \leq \omega_{sp} \leq \omega_b \quad (119b)$$

and for emergency conditions is

$$.15 \leq \zeta_{sp} \quad (120a)$$

$$\omega_c \leq \omega_{sp} \quad (120b)$$

where ω_a , ω_b , and ω_c depend on flight condition.

Table 5.2 lists the frequency range for each flight condition and Figure 5.3 shows the region defined by equations (119). Since the short period damping can be greater than 1, a single real eigenvalue is permitted outside the circle of radius ω_b or inside the circle of radius ω_a . As discussed next, the single real eigenvalue region $S > \omega_b$ would overlap with the permissible region for non-short period eigenvalues and thus make a distinction between the two types of eigenvalues impossible. To prevent this overlap, the simplified region shown in Figure 5.3 will be used as the short period eigenvalue permissible region. Since all real pairs of eigenvalues inside the simplified region result in a damping less than 1.3, all eigenvalues in the simplified region meet military specifications.

Table 5.2. Short Period Frequency Limits

Mach	Altitude	ω_a (rad/sec)	ω_b (rad/sec)	ω_c (rad/sec)
.5	5000'	2.02	7.23	1.53
.85	5000'	3.50	12.6	2.65
.9	35000'	2.19	7.86	1.65
1.5	35000'	3.29	11.8	2.49

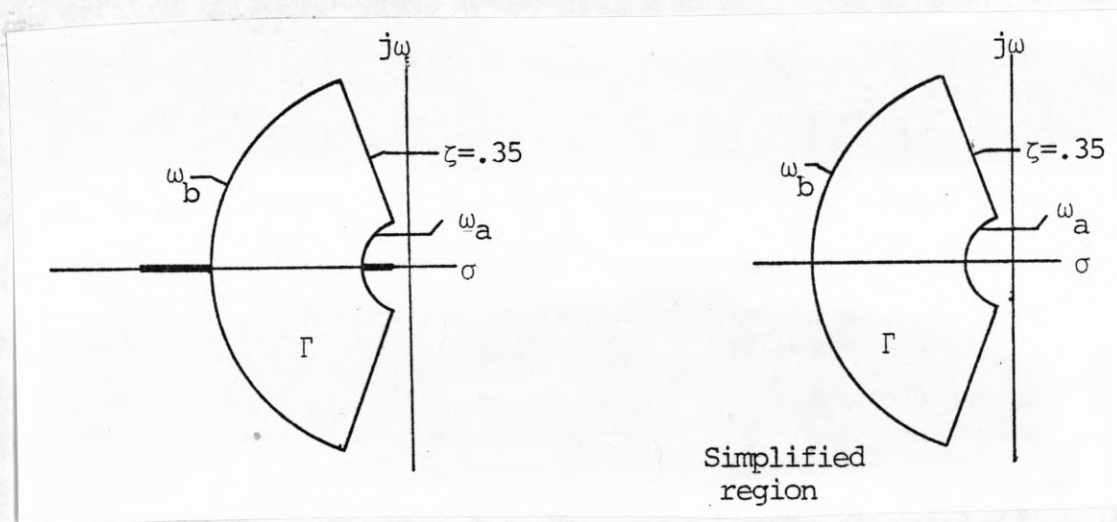


Figure 5.3. Allowable short period eigenvalue locations,

As described in [57] this aircraft has several lightly damped structural modes which were not modeled in this paper. The control bandwidth should be less than the lowest structural frequency, which is 85 rad/sec, so

the upper limit on all eigenvalues was set at 70 rad/sec. This is a high limit, and in the design process an attempt will be made to lower this value. The requirements on the non-short period eigenvalues (requirement 2) will be that they lie in the region defined by

$$\omega_b < \omega < 70 \text{ rad/sec} \quad (121)$$

with a minimum damping of .35 (see Figure 5.4). In the emergency situations no distinction between eigenvalues will be made. Figure 5.5 shows the required region for all eigenvalues under emergency conditions.

Well placed eigenvalues do not guarantee good time responses. Requirement 3 will ensure well behaved transient response. The response of most interest will be the C_N^* response. As discussed in [57], C_N^* is a linear combination of normal acceleration and pitch rate given by

$$C_N^* = (Nz_p + 12.43q)/Kc^* \quad (122)$$

where Nz_p is the normal acceleration at the pilot's location (same as Nz for this plane) and the stationary value, Kc^* , is used for normalization. The C_N^* response to a pilot step command should fall in the region shown in Figure 5.6.

5.3. Design Using Static Output Feedback

5.3.1. Robustness with Respect to Changing Flight Conditions

The first design objective will be to design a controller which meets the nominal requirements at all flight conditions. We initially assume a controller structure using only static, or unfiltered, feedback of the two states; normal acceleration, and pitch rate. Figure 5.7 shows the system

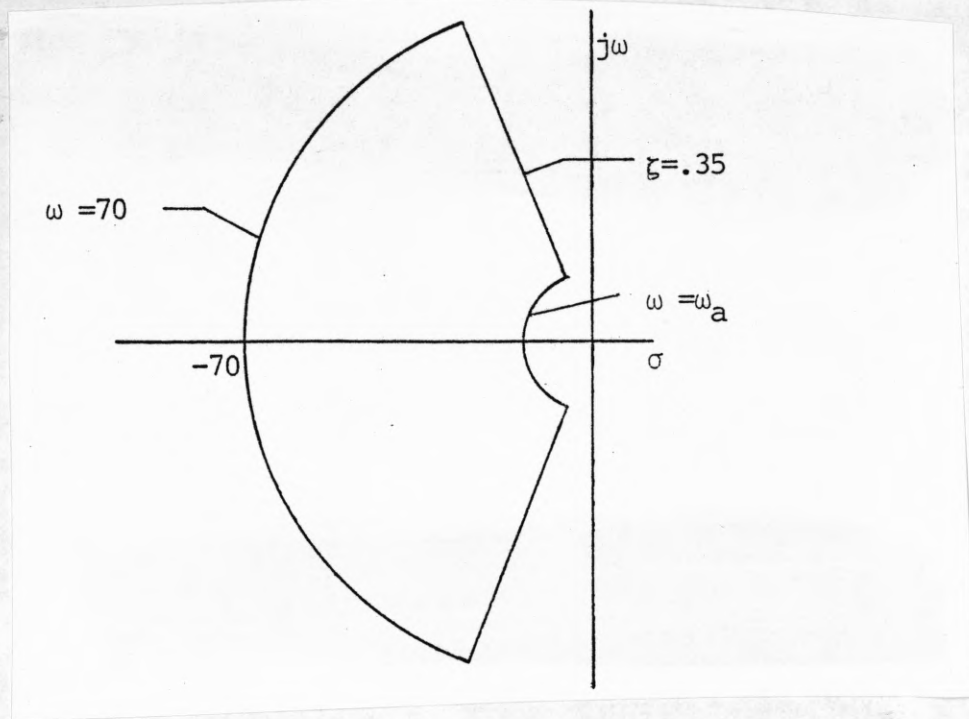


Figure 5.5. Constraint region for non-short period eigenvalues.

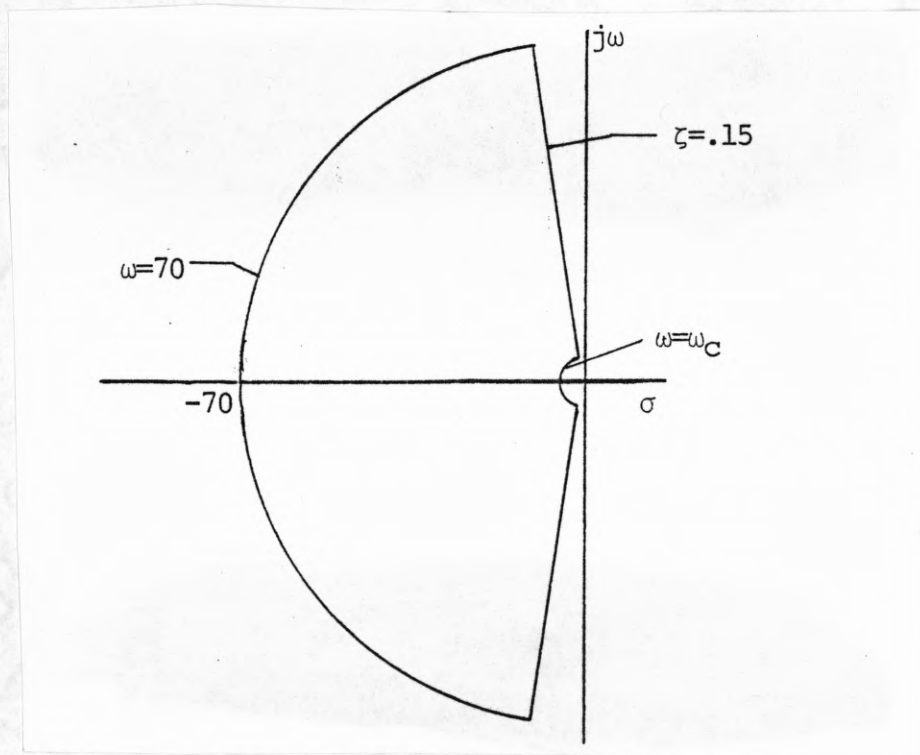


Figure 5.5. Emergency eigenvalue constraint region.

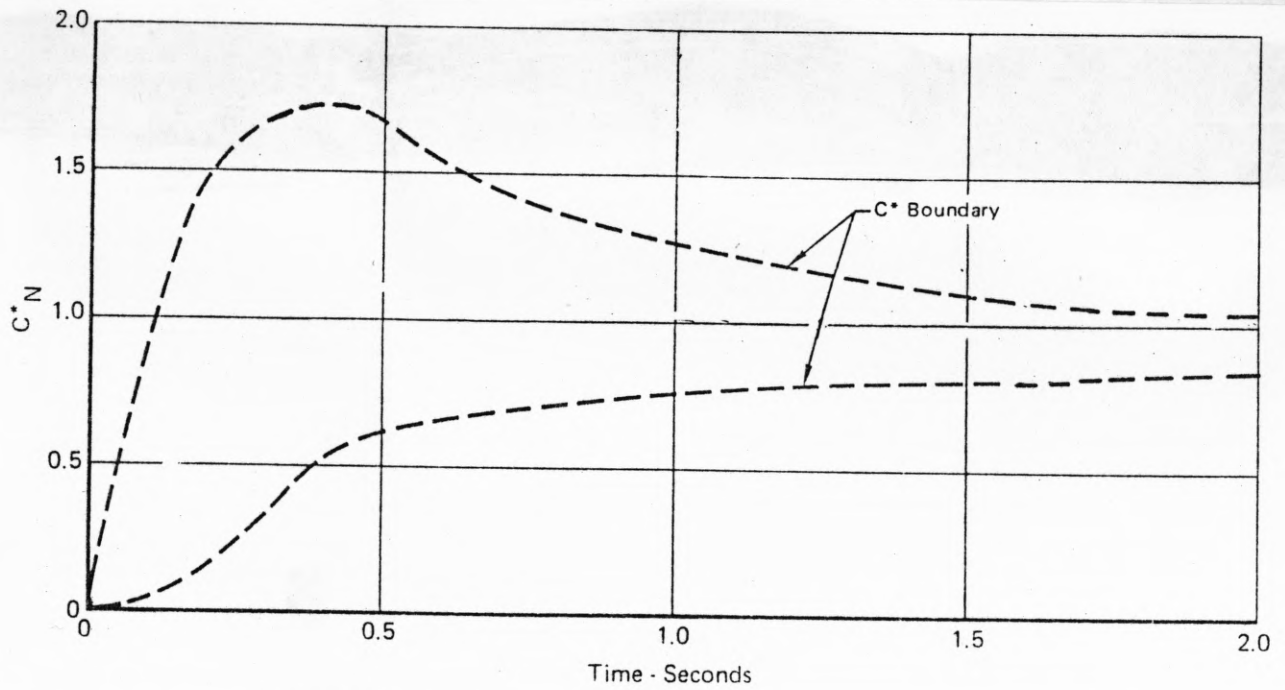


Figure 5.6. C_N^* response envelope.

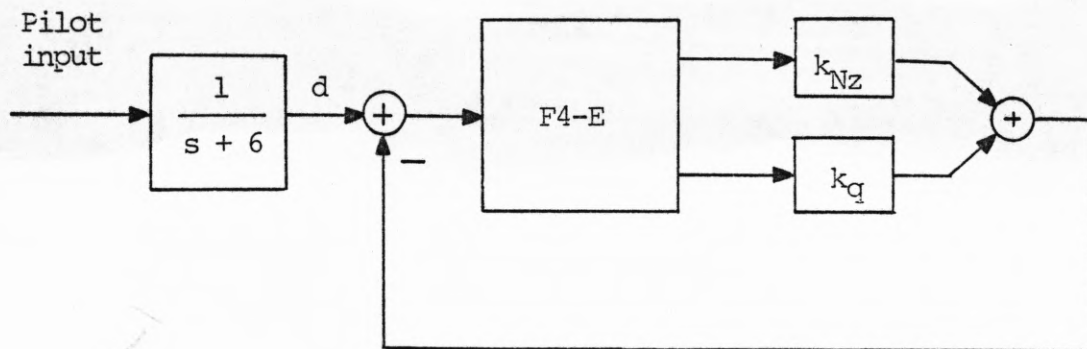


Figure 5.7. Structure with static output feedback.

structure where equations describing the F4-E dynamics were given in Section 5.2, and the pre-filter used to shape the step responses is the same as in [57].

Computer programs using the algorithms of Chapter 4 were developed to perform the mapping of the eigenvalue constraints given in Section 5.2. Boundaries in the k_{Nz} , k_q plane were found for each flight condition. A typical boundary (for flight condition 2), is shown in Figure 5.8a. For gains in the region R_{nom2} the closed loop eigenvalues will all be in the region Γ_{nom2} , which is shown in Figure 5.8b. Each section of the K-space boundary is described in Figure 5.8b.

The regions R_{nom1} - R_{nom4} were found by mapping the eigenvalue constraints for each flight condition (Γ_{nom1} - Γ_{nom4}). The intersection of these regions, R_{nom} , is shown in Figure 5.9. For any gain chosen in R_{nom} the i th flight condition will have closed loop eigenvalues in Γ_i , $i=1,2,3,4$. Therefore, the requirement that the system be robust with respect to changing flight condition can be met by using static output feedback. Since R_{nom} does not intersect either axis, no robustness with respect to either sensor failure can be achieved by static output feedback.

5.3.2. Selection of a Gain in the Permissible Region

Any gain choice from R_{nom} would meet the nominal eigenvalue requirements. Several alternative methods are available to aid in the selection of a specific design point. One method could be analysis of the eigenvalue locations corresponding to different points in K-space as described in [49]. Every point in the k_{Nz} , k_q plane represents a set of closed loop eigenvalues for each flight condition. Using the mapping algorithms of

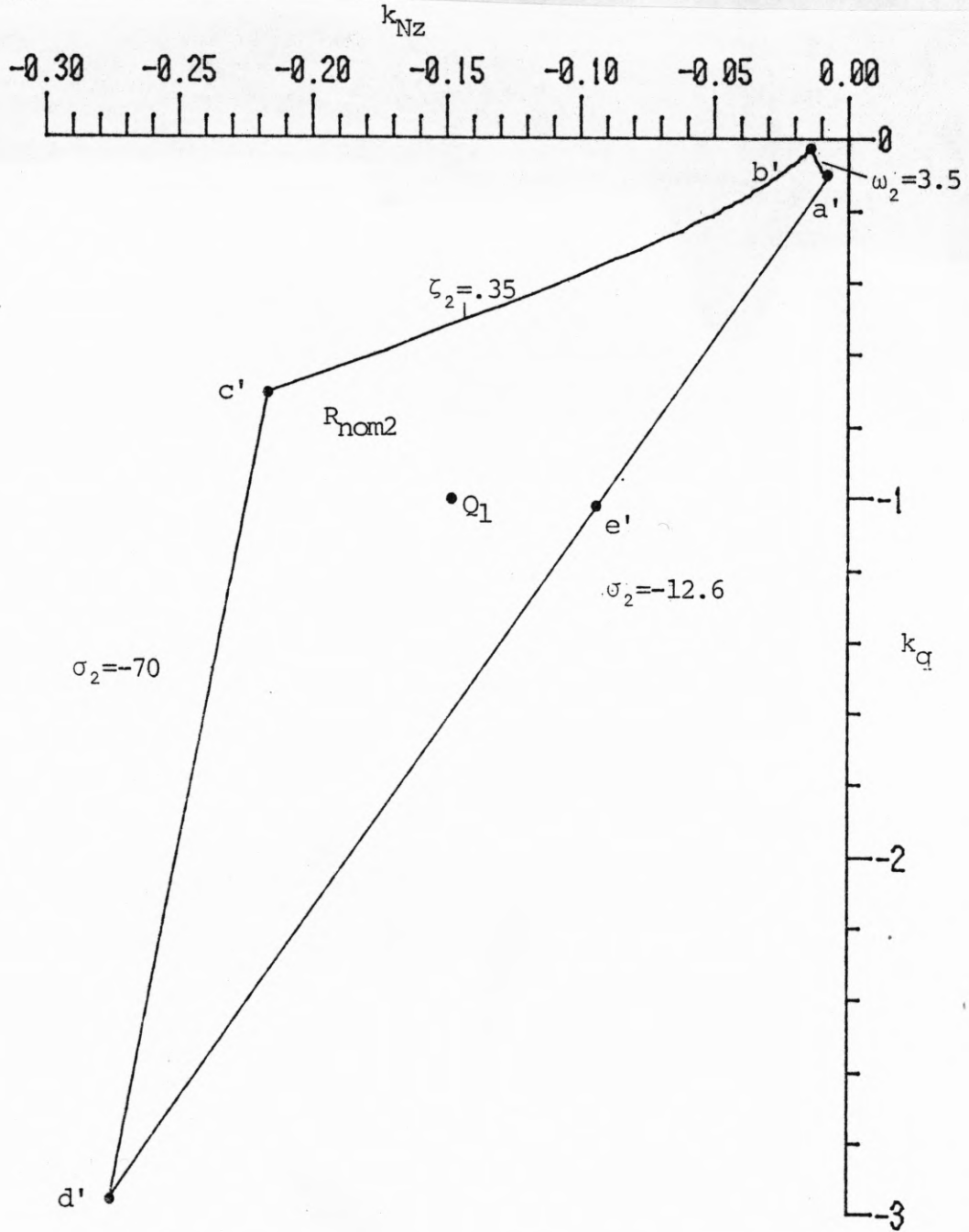
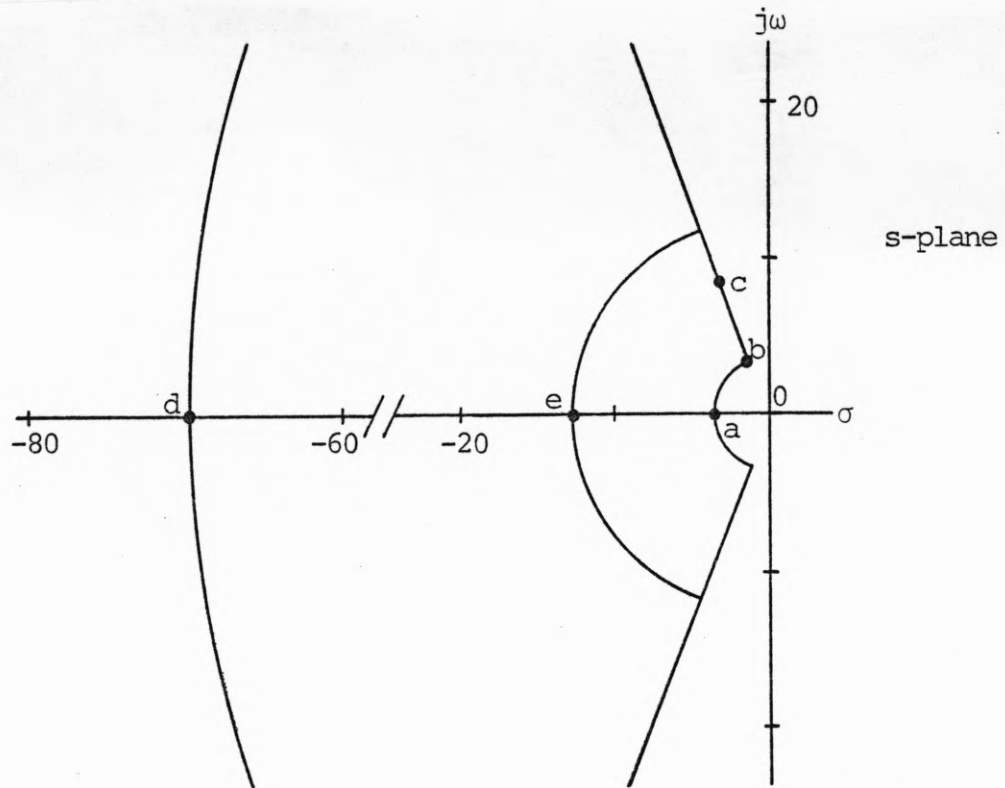


Figure 5.8a. The region R_{nom2} .



For k_{Nz} , k_q on

- | | | |
|-------|---|----------------------|
| a'-b' | the short period eigenvalues are on a-b | ($\omega_2=3.5$) |
| b'-c' | the short period eigenvalues are on b-c | ($\zeta_2=.35$) |
| c'-d' | the actuator eigenvalue is at d | ($\sigma_2=-70$) |
| d'-e' | a short period eigenvalue is at e | ($\sigma_2=-12.6$) |
| e'-a' | the actuator eigenvalue is at e | ($\sigma_2=-12.6$) |

Figure 5.8b. Region in s-plane and description of K-space boundary.

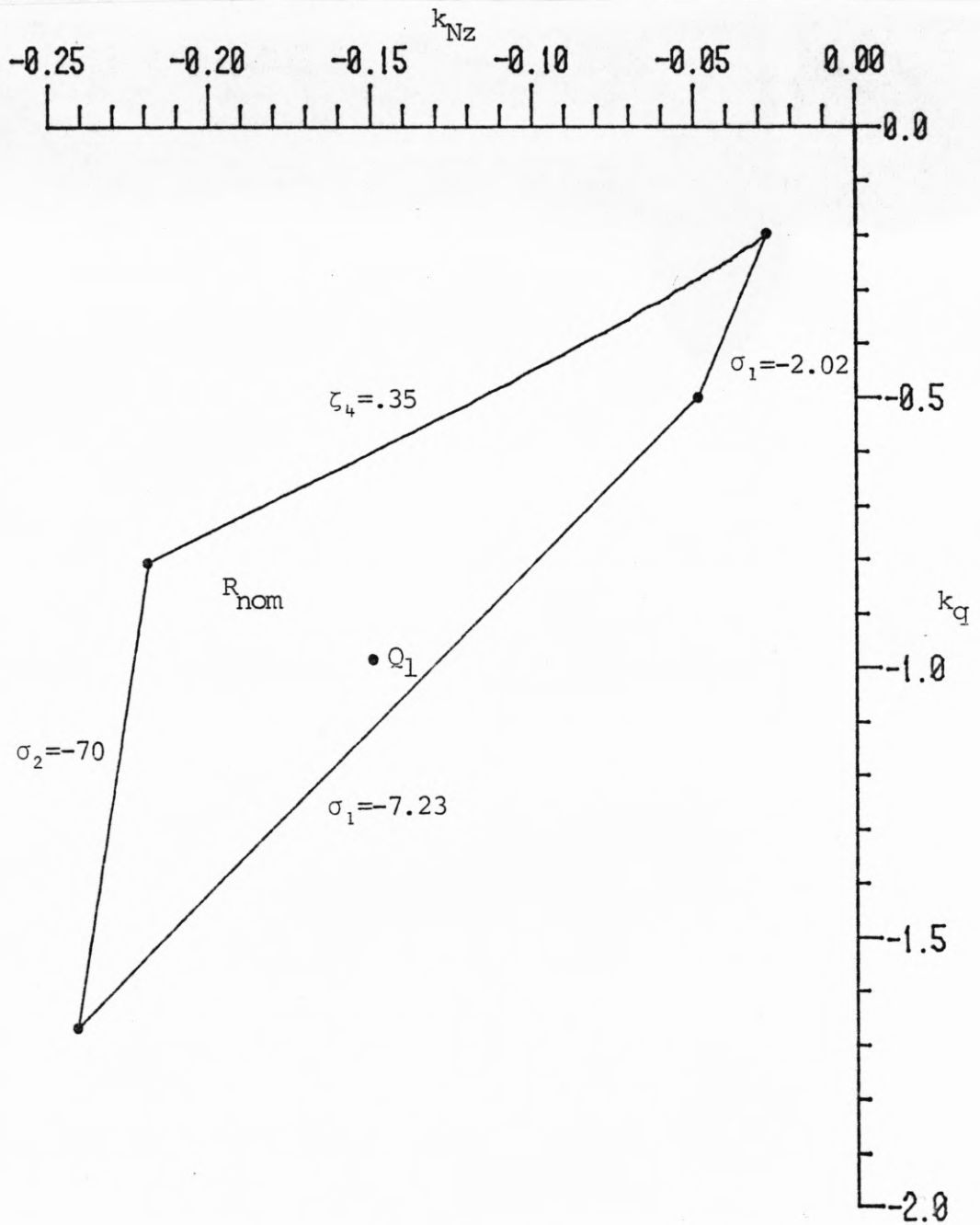


Figure 5.9. The region R_{nom} .

Chapter 4 families of constant damping, constant frequency and single real root curves may be obtained. Figure 5.10 shows such families for flight condition 2.

Another method would be to decrease the allowable eigenvalue regions and thereby decrease the size of R_{nom} . Figure 5.11 shows the region $R_{\text{nom}}^{(1)}$ where the high frequency limit has been lowered from 70 to 50 rad/sec, the minimum damping has been increased to .5, and the minimum short period frequency has been increased by fifty percent for each flight condition. Any gain chosen from $R_{\text{nom}}^{(1)}$ would meet these tighter requirements at all four flight conditions.

A further technique is to use gains which will require smaller control inputs. In [34] Ackermann shows for systems where the state variables have been normalized to their maximum values, the distance from the origin in K-space can be used as a measure of the maximum control needed, Where

$$|u| = |k'x| \leq \|k\| \cdot \|x\|. \quad (123)$$

Even though Nz and q have not been normalized to their maxima, this principle can easily be demonstrated. For gains g_1, g_2, g_3 of Figure 5.11, the δ_e and C_N^* responses to a step command for flight condition 1 are shown in Figure 5.12. As seen from the figure, the control (essentially δ_e) is less for the smaller gains, as is the control rates.

Using the above methods as guides, point Q_1 of Figures 5.8-5.10 was selected as a trial design point. Using these trial gains, the step responses shown in Figures 5.13a,b were obtained. The C_N^* responses are seen to be well within the required boundaries for all flight conditions.

Table 5.3 lists the closed loop eigenvalue locations using the gains of point

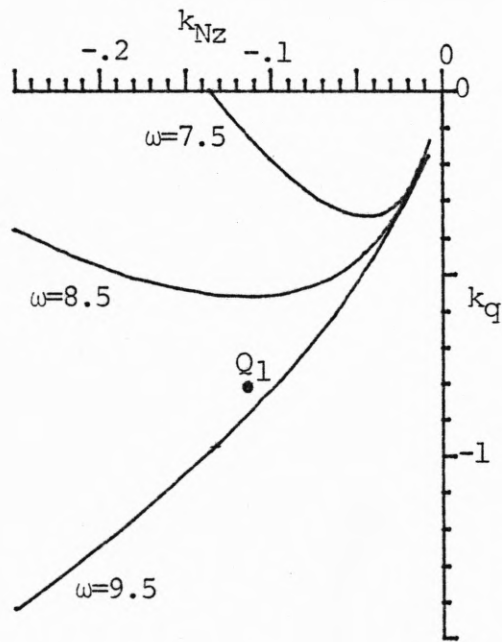
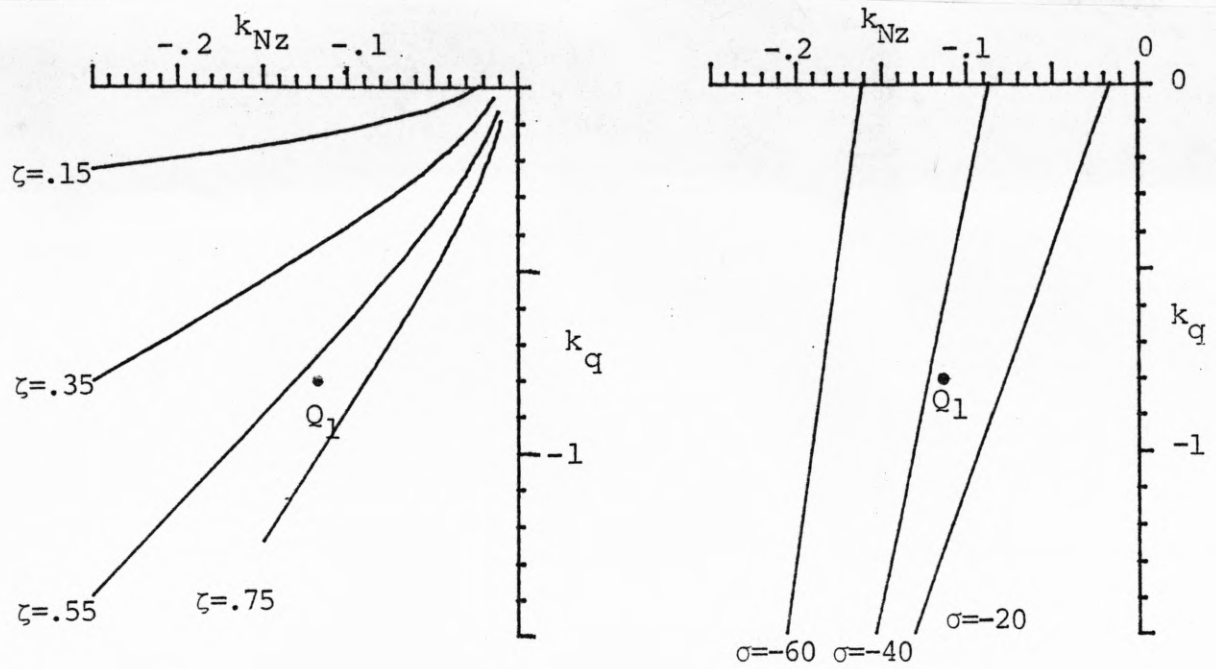


Figure 5.10. Constant damping, single real root, and natural frequency curves for flight condition 2.

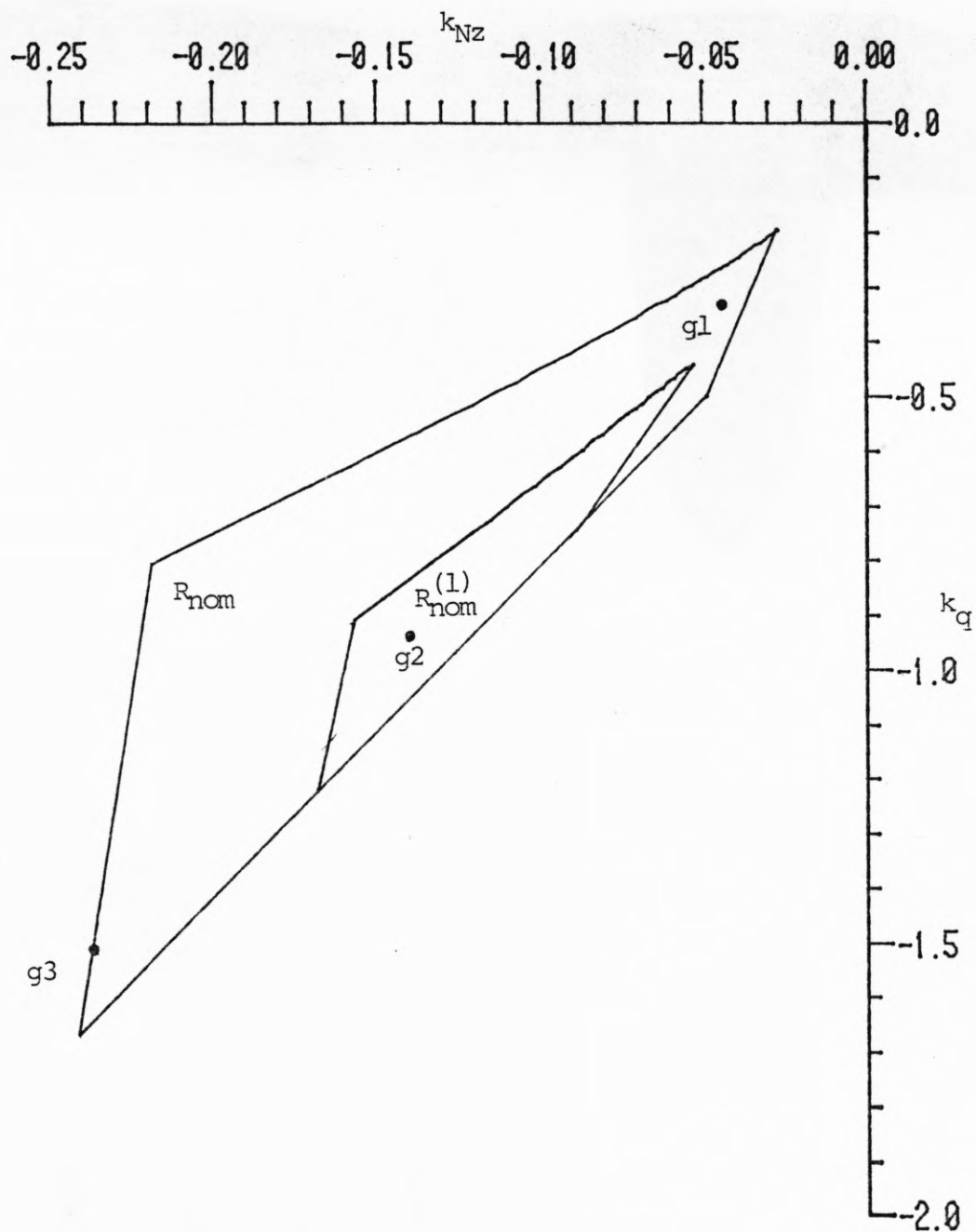


Figure 5.11. The regions R_{nom} and $R_{\text{nom}}^{(1)}$.

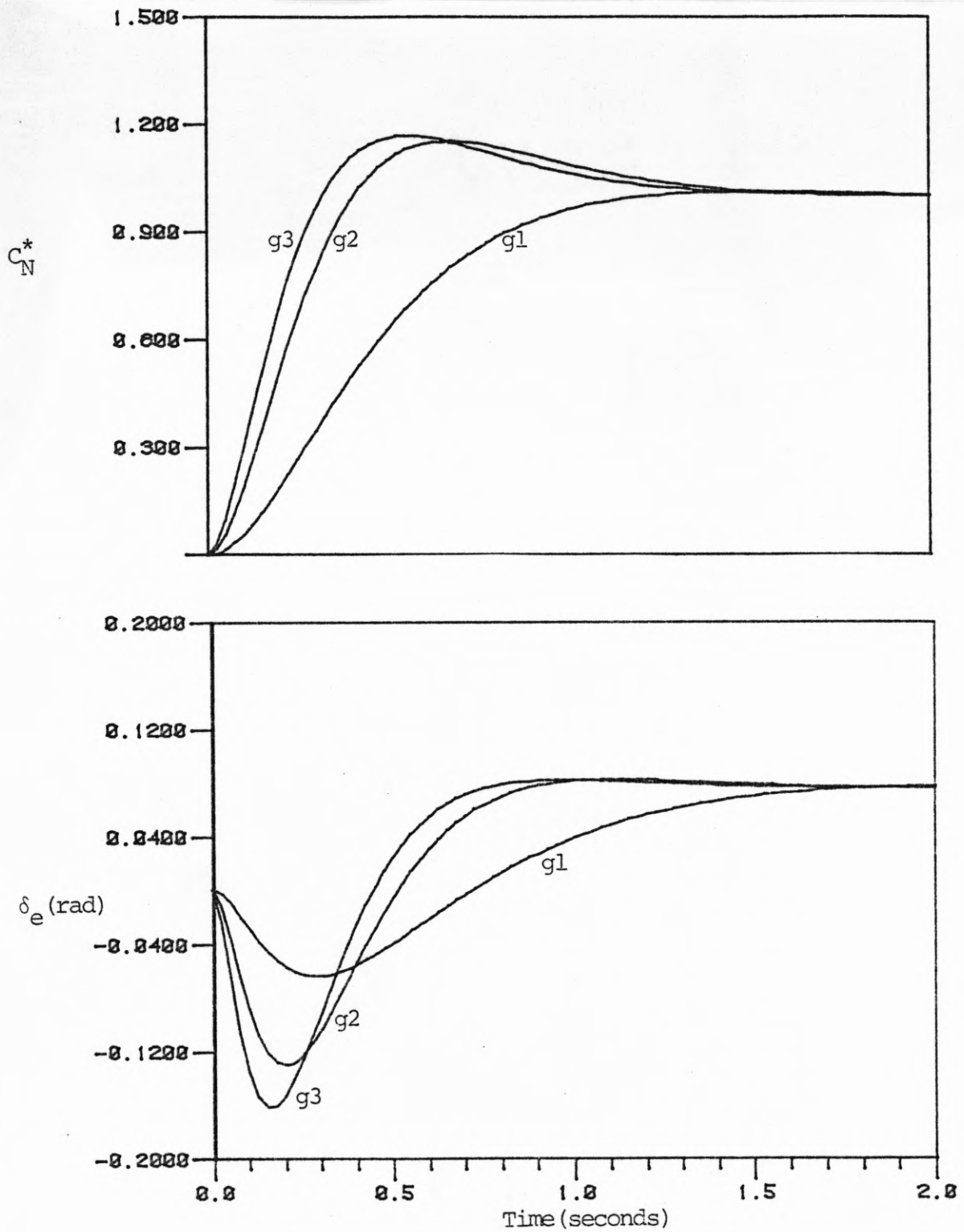


Figure 5.12. δ_E , C_N^* responses for flight condition 1 showing effect of $\|k\|$ on control.

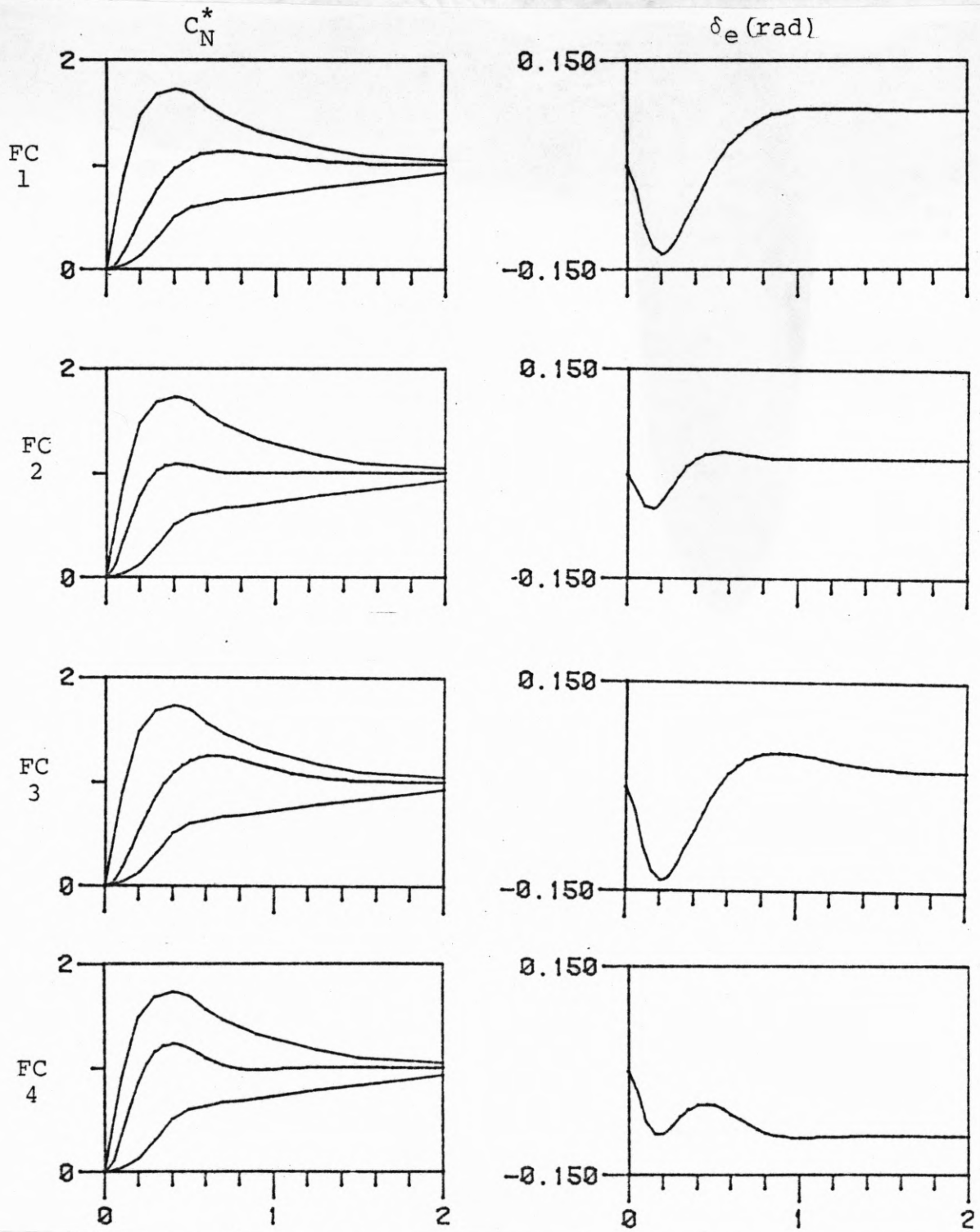


Figure 5.13a. C_N^* and δ_e responses for trial gains Q_1 .

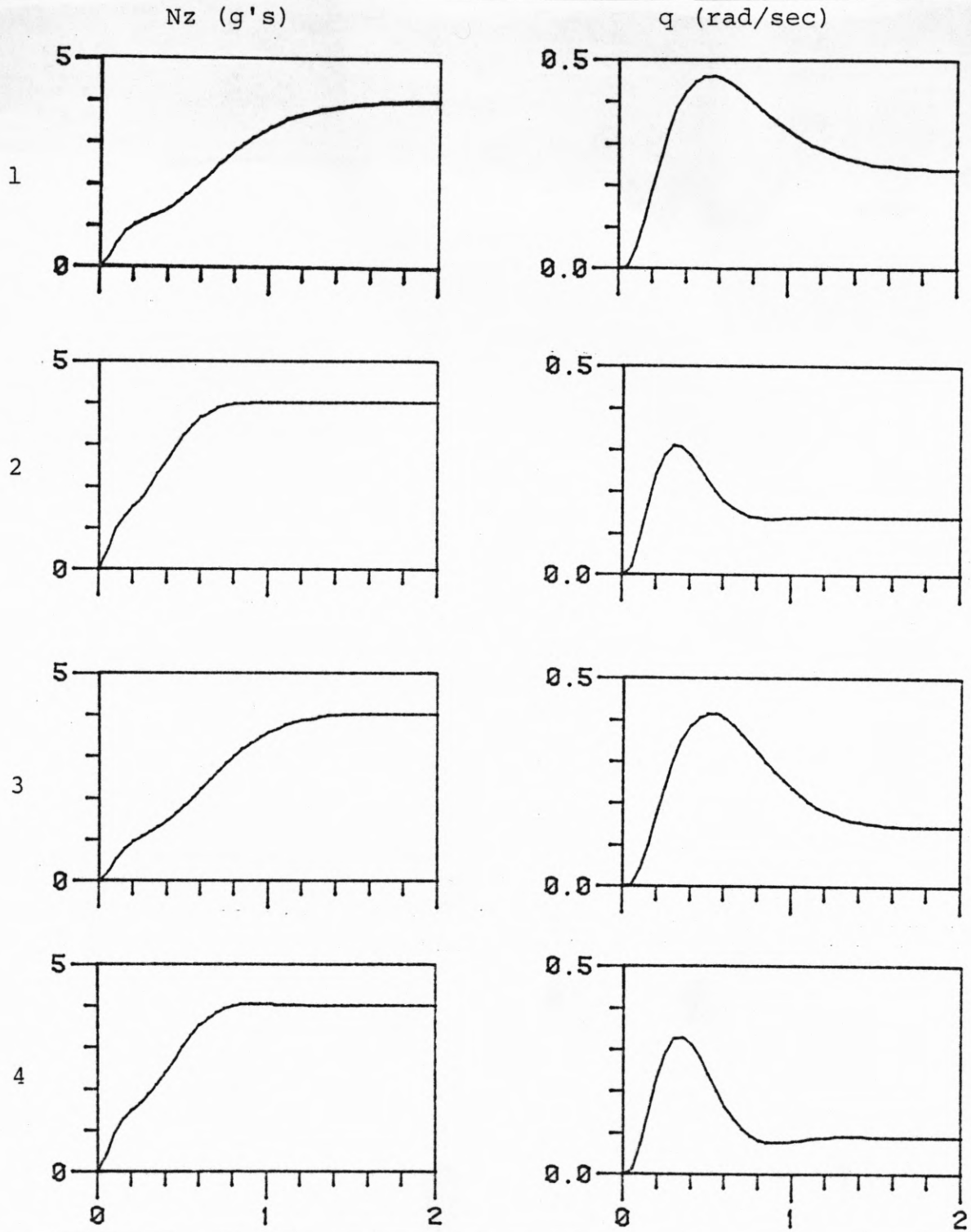


Figure 5.13b. N_z and q responses for trial gains Q_1 .

Q_1 . The notation (ζ, ω_n) refers to the damping and natural frequency of the complex pair of eigenvalues. All eigenvalues are well within the limitations and point Q_1 appears to be a good choice for the controller gains.

Table 5.3. Closed Loop Eigenvalues $k_{Nz} = -.115$ $k_q = -.8$ (point Q_1)

F.C.	Mach	Altitude	Closed Loop Eigenvalues
1	.5	5000'	(.94, 4.68) -19.31
2	.85	5000'	(.61, 9.18) -37.29
3	.9	35000'	(.79, 4.63) -17.78
4	1.5	35000'	(.55, 8.11) -27.04

5.3.3. Robustness with Respect to Sensor Failure

An additional method to help choose a final gain from R_{nom} would be to consider only those gains which will meet the emergency specifications after sensor failure. To determine these gains the emergency eigenvalue regions were mapped into the K_{Nz}, k_q plane for each flight condition. The intersection of these four regions, R_{em} , is shown in Figure 5.14 along with the region R_{nom} redrawn from Figure 5.9.

For the controller structure of Figure 5.7, failure of either sensor results in the corresponding gain going to zero. Since R_{em} does not intersect either axis, there is no gain choice which is robust with respect to failure of either sensor. Additional sensors or dynamic feedback are therefore needed to meet the requirement that the system meet the emergency eigenvalue requirements after sensor failure.

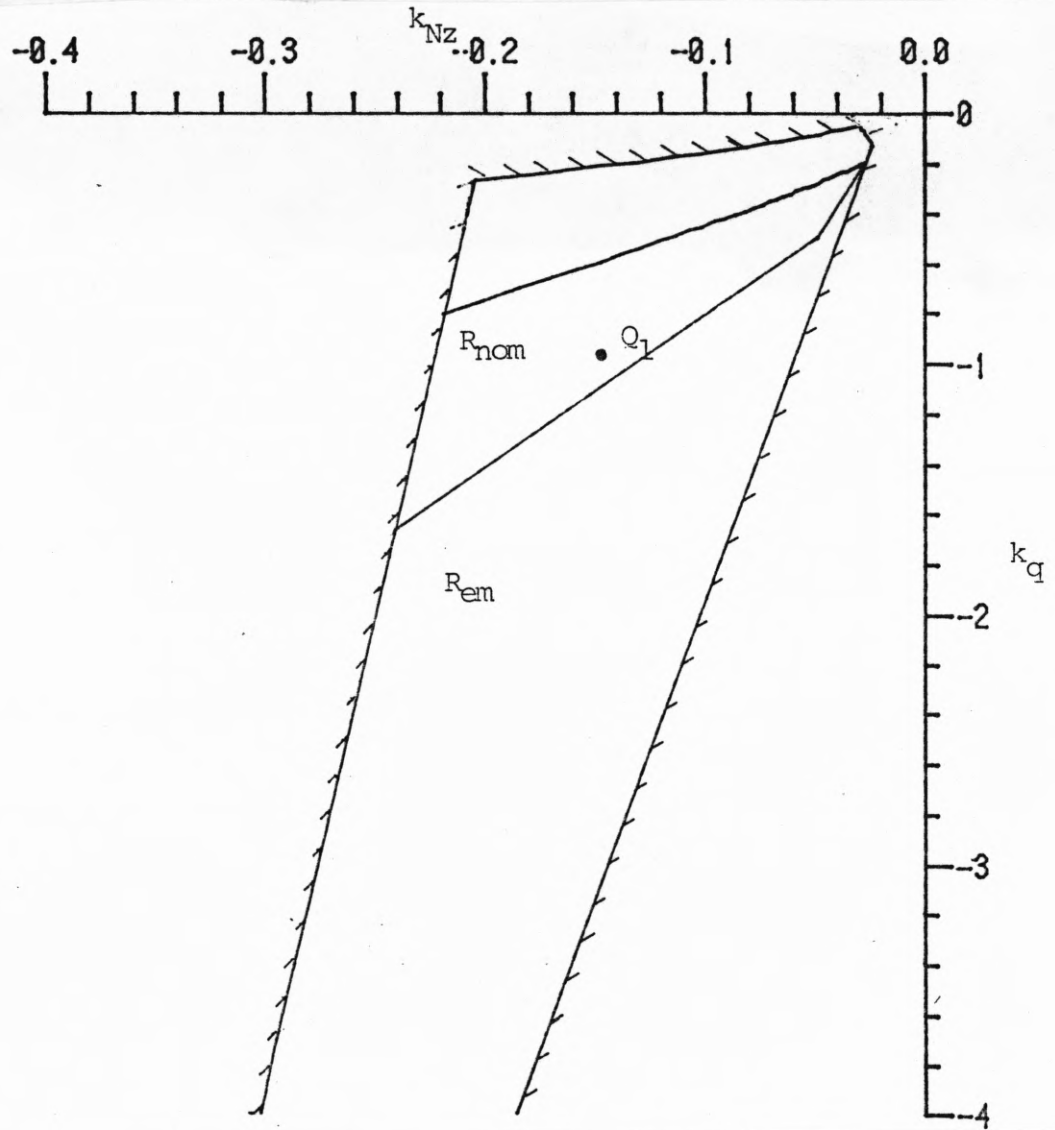


Figure 5.14. The regions R_{nom} , R_{em} .

For a controller with m identical sensors with summed outputs, a sensor failure reduces the total feedback gain by only a fraction $((m-1)/m)$. For the controller structure shown in Figure 5.15 ($m=2$), any k_{Nz}, k_q chosen from the region R of Figure 5.16 will for all flight conditions:

- 1) meet the emergency requirements after failure of any single sensor;
- 2) meet the emergency requirements after the combined failure of an accelerometer and gyro, and
- 3) meet the nominal eigenvalue requirements when no sensor has failed.

After an accelerometer failure the Nz feedback is halved. For design point Q_1 , shown again in Figure 5.16, this failure would result in point A. Similarly a single gyro failure would result in point B. A combined failure of an accelerometer and a gyro would result in point C.

5.4. Design Using Dynamic Output Feedback

5.4.1. Search for Filters

As shown in Section 5.3, a controller using static output feedback requires two sensors to meet the nominal specifications, and four sensors to meet the emergency specifications after failure of any single sensor. The use of dynamic feedback of the outputs may reduce the minimum number of sensors. For example, if an estimate of the normal acceleration was obtained from the gyro signal, the accelerometer may no longer be necessary. A preliminary problem is to find a candidate dynamic feedback structure.

At first it may seem all that need be done is to use a Luenberger observer to construct these estimates. Figure 5.17 shows how an observer might be implemented. Now, when the pitch gyro fails, and the dashed branch

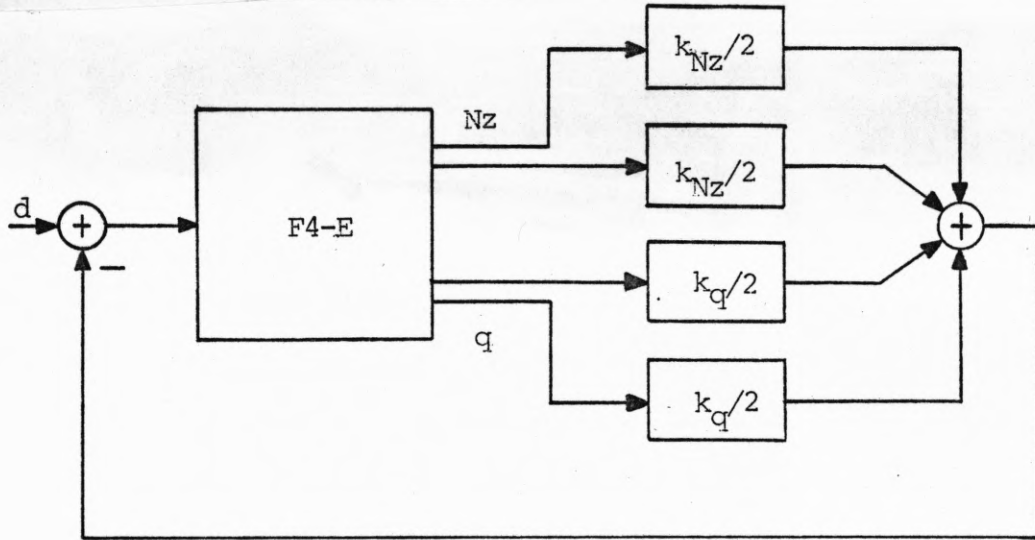


Figure 5.15. Output feedback with $m=2$.

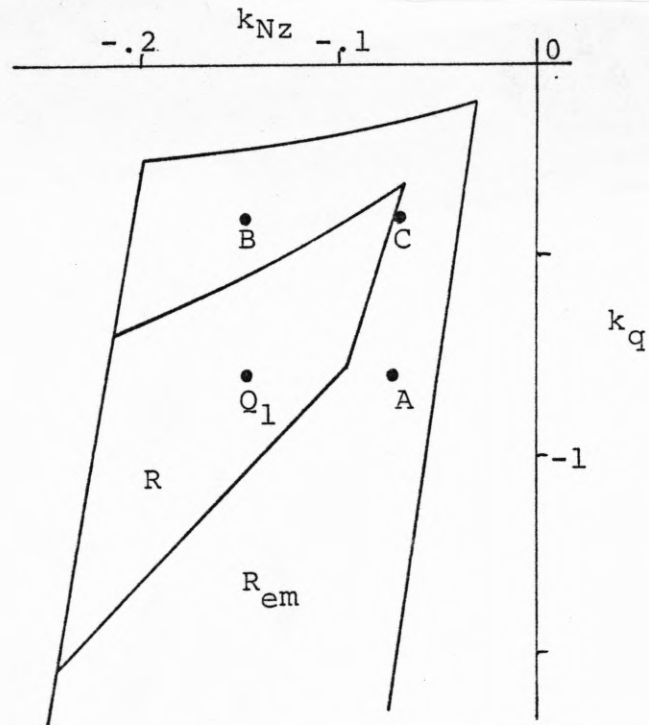


Figure 5.16. The regions R and R_{em} .

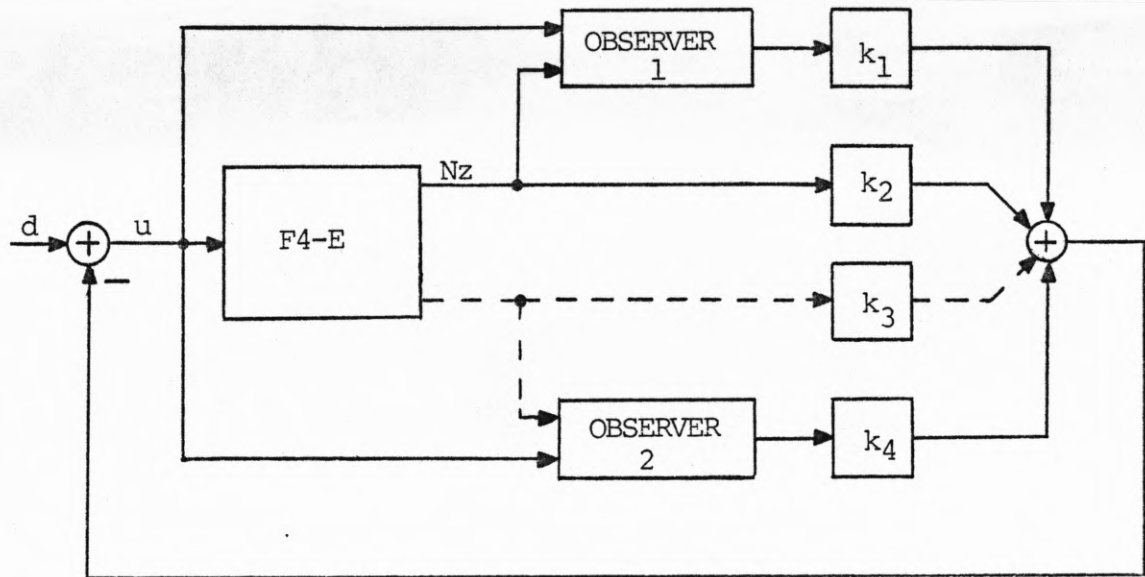


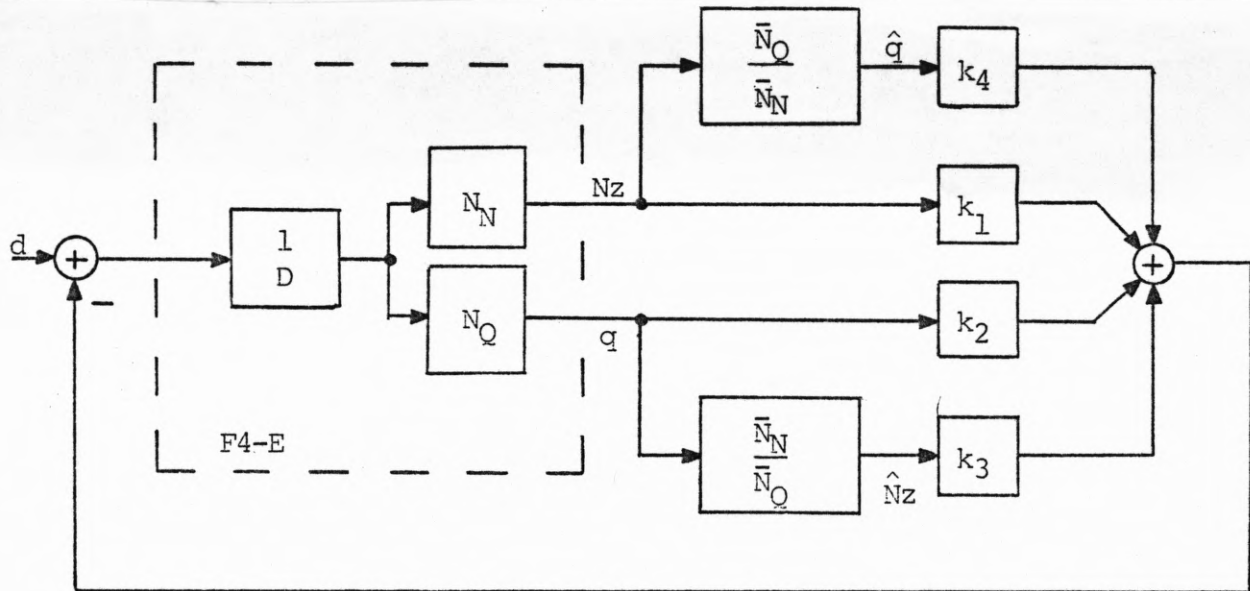
Figure 5.17. Possible observer structure.

is no longer available, the estimate \hat{q} still remains. There are two serious problems with this method. First, the system dynamics change dramatically with flight condition and finding a non-adaptive observer that gives reasonable estimates of q and Nz would be difficult, possibly impossible, to find. As seen from the data in Appendix I the control effectiveness, essentially the open loop gain, changes by a factor of three with changing flight condition, and the open loop eigenvalues vary as shown in Table 5.1.

The second undesirable feature is when one sensor fails, the observer connected to it still is driven by the control u . Therefore the observer still has an effect on the closed loop characteristic equation. Even

for adaptive observers which closely match the system, this effect would complicate the design since the separation principle would no longer hold after sensor failure. For these reasons observer structures were not considered.

In [48] G. Kreisselmeier discusses the use of inverse filters for robust control, which are applicable to minimum phase systems. Figure 5.18 shows the structure of the controller.



$$N_N = K_N(S^2 + z_1S + z_0)$$

$$N_Q = K_Q(S + z_2)$$

$$D = S^2 + a_2S + a_1S + a_0$$

Figure 5.18, Structure of the inverse filter,

If the filter elements \bar{N}_N and \bar{N}_Q are chosen equal to N_N and N_Q , the variables \hat{Nz} , \hat{q} would be estimates of Nz and q . For this case by choosing

$$k_1 = k_3 = k_{Nz}/2 \quad (124)$$

$$k_2 = k_4 = k_q/2 \quad (125)$$

the feedback is the same as that shown in Figure 5.15. Since N_N and N_Q change with flight condition a non-adaptive controller will not generate true estimates of Nz and q , but only signals which hopefully are closely enough related to Nz and q in magnitude and phase to help. If as flight condition changes, K_N/K_Q and the roots of N_N and N_Q remain close, the inverse filter idea may succeed. Table 5.4 lists the critical values,

Table 5.4. Open Loop Zeros and Gain Ratio

Mach	Altitude	q-Zero	Nz-Zeros	K_N/K_Q
.5	5000'	-.884	-.542+j5.33	.527
.85	5000'	-1.57	-.929+j9.12	.536
.9	35000'	-.637	-.392+j5.67	.537
1.5	35000'	-.826	-.481+j8.05	.577
Averaged values		-.98	0.586 j7.04	.543

The averaged values were used to construct two filters

$$\frac{\hat{q}}{Nz} = \frac{1.84(s + .98)}{s^2 + 1.172s + 49.9} \quad \text{Filter 1}$$

$$\frac{\hat{Nz}}{q} = \frac{s^2 + 1.172s + 49.9}{1.84(s + .98)(s + 10)} \quad \text{Filter 2}$$

where the pole at -10 was added to make Filter 2 realizable,

The poles of Filter 1 are only slightly damped, and do not cancel well with the system zeros. When it was tried, highly oscillatory step responses resulted and this filter was discarded. When Filter 2 was implemented, reasonable step responses resulted using typical gains chosen with the aid of the results from subsection 5.3.1. This filter was retained for further investigations. The pole at $-.98$ is weakly controllable since essentially it is cancelled with the pitch rate zero. The system eigenvalue resulting from this pole will be exempt from the eigenvalue requirements given in Section 5.2. The system time responses will give a measure as to the validity of this.

The system of Figure 5.19 was used to study different types of dynamic feedback of Nz . Several filters were tried. One that appeared promising was

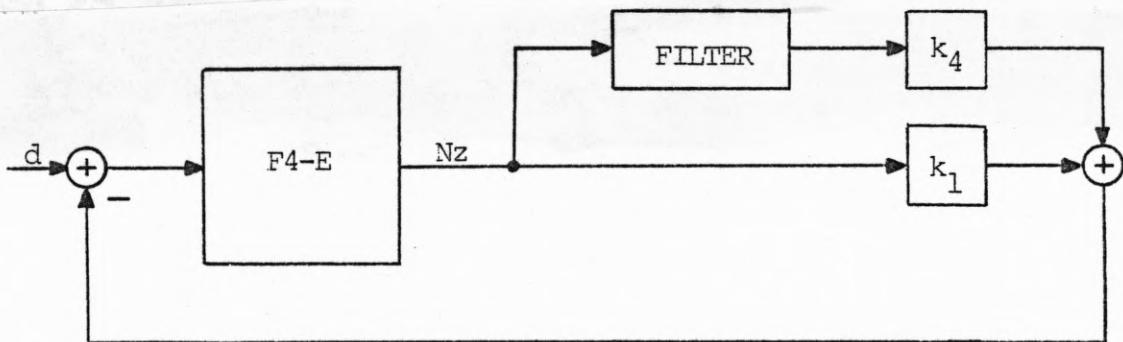


Figure 5.19, Acceleration feedback only,

$$\frac{\hat{q}}{Nz} = \frac{s}{s+15} \quad (126)$$

As discussed in [59] \dot{Nz} is a close approximation to \dot{q} which, if used as a feedback signal, can increase the short period damping. For low frequencies this filter acts as a differentiator.

Figure 5.20 shows the structure of the controller to be investigated, which may be represented in state form as

$$\frac{d}{dt} \begin{bmatrix} Nz \\ q \\ \delta_c \\ W1 \\ W2 \\ W3 \end{bmatrix} = \begin{bmatrix} a_{11} & a_{12} & a_{13} & 0 & 0 & 0 \\ a_{21} & a_{22} & a_{23} & 0 & 0 & 0 \\ 0 & 0 & -14 & 0 & 0 & 0 \\ 0 & 21.79 & 0 & 0 & -9.9 & 0 \\ 0 & -5.331 & 0 & 1 & -10.98 & 0 \\ 1 & 0 & 0 & 0 & 0 & -15 \end{bmatrix} \begin{bmatrix} Nz \\ q \\ \delta_e \\ W1 \\ W2 \\ W3 \end{bmatrix} + \begin{bmatrix} b_1 \\ 0 \\ 14 \\ 0 \\ 0 \\ 0 \end{bmatrix} \quad u = Ax + bu \quad (127a)$$

$$u = -(k_1 \ k_2 \ k_3 \ k_4) \begin{bmatrix} 1 & 0 & 0 & 0 & 0 & 0 \\ 0 & 1 & 0 & 0 & 0 & 0 \\ 0 & 0 & 0 & 0 & 1 & 0 \\ 1 & 0 & 0 & 0 & 0 & -15 \end{bmatrix} x. \quad (127b)$$

5.4.2. Dynamic Feedback of Pitch Rate

To check if the design specifications can be met using only pitch rate feedback, the system of Figure 5.20 was used with k_1 and k_4 both zero. Each nominal (emergency) eigenvalue region was mapped into the k_3, k_2 plane. The intersection of the four regions, $R_{nomq}(R_{emq})$, is shown in Figure 5.21. The nominal eigenvalue specifications can be met by choosing any gain set

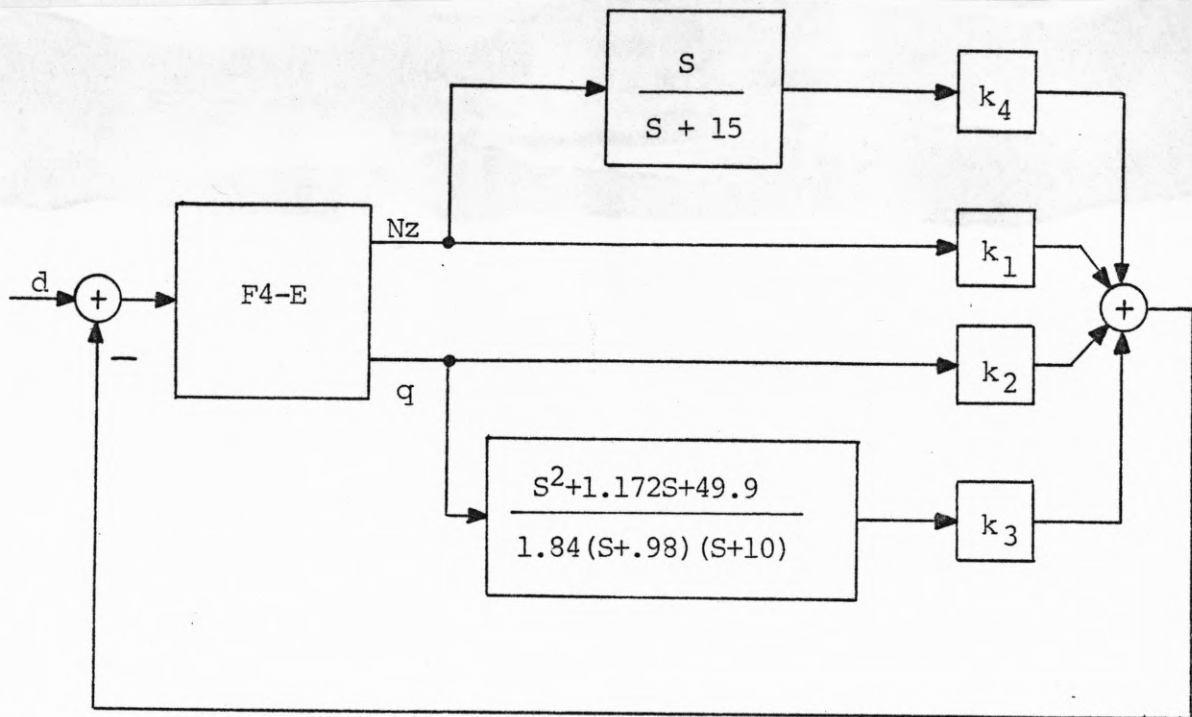


Figure 5.20. Structure of controller using dynamic output feedback.

from R_{nomq} . Similarly the emergency specifications can be met by use of any gains in R_{emq} .

Gyro failure now corresponds to a simultaneous reduction of k_2 and k_3 . For a system using m parallel gyros with identical feedback gains, the failure of f gyros reduces both k_2 and k_3 by a factor $(m-f)/m$. For $m=2$ and $f=1$, any gain in R_{21} of Figure 5.22 will meet the nominal specifications for the unfailed system and also meet the emergency specifications after failure of either gyro. Similarly for $m=3$, $f=1$ or 2 any gain in R_{32} will meet the nominal specifications without failure and still meet the emergency specifications after any two sensor failures. This is an especially nice result since reliability criteria often stipulate that the control system be capable of

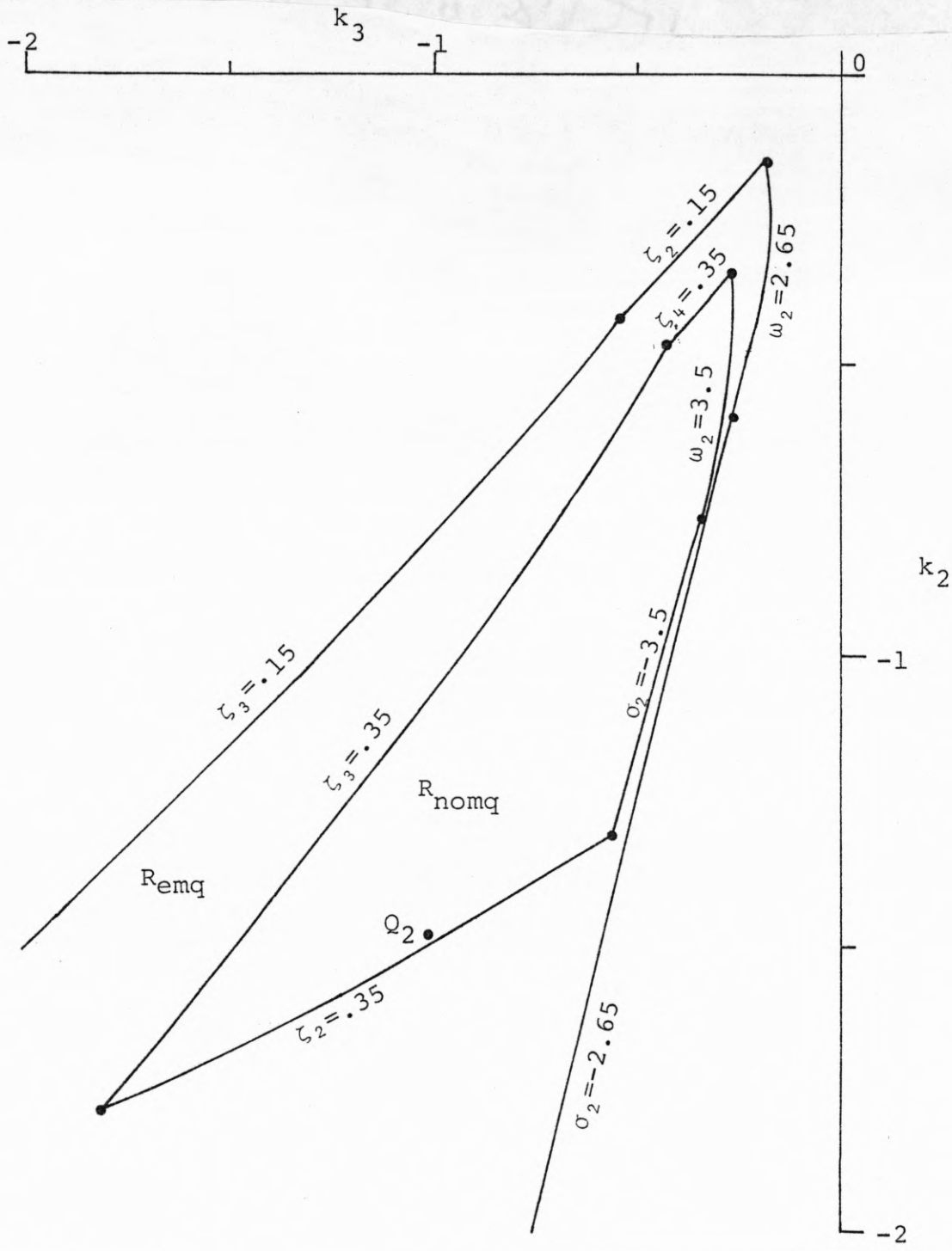


Figure 5.21. The regions R_{emq} and R_{nomq} .

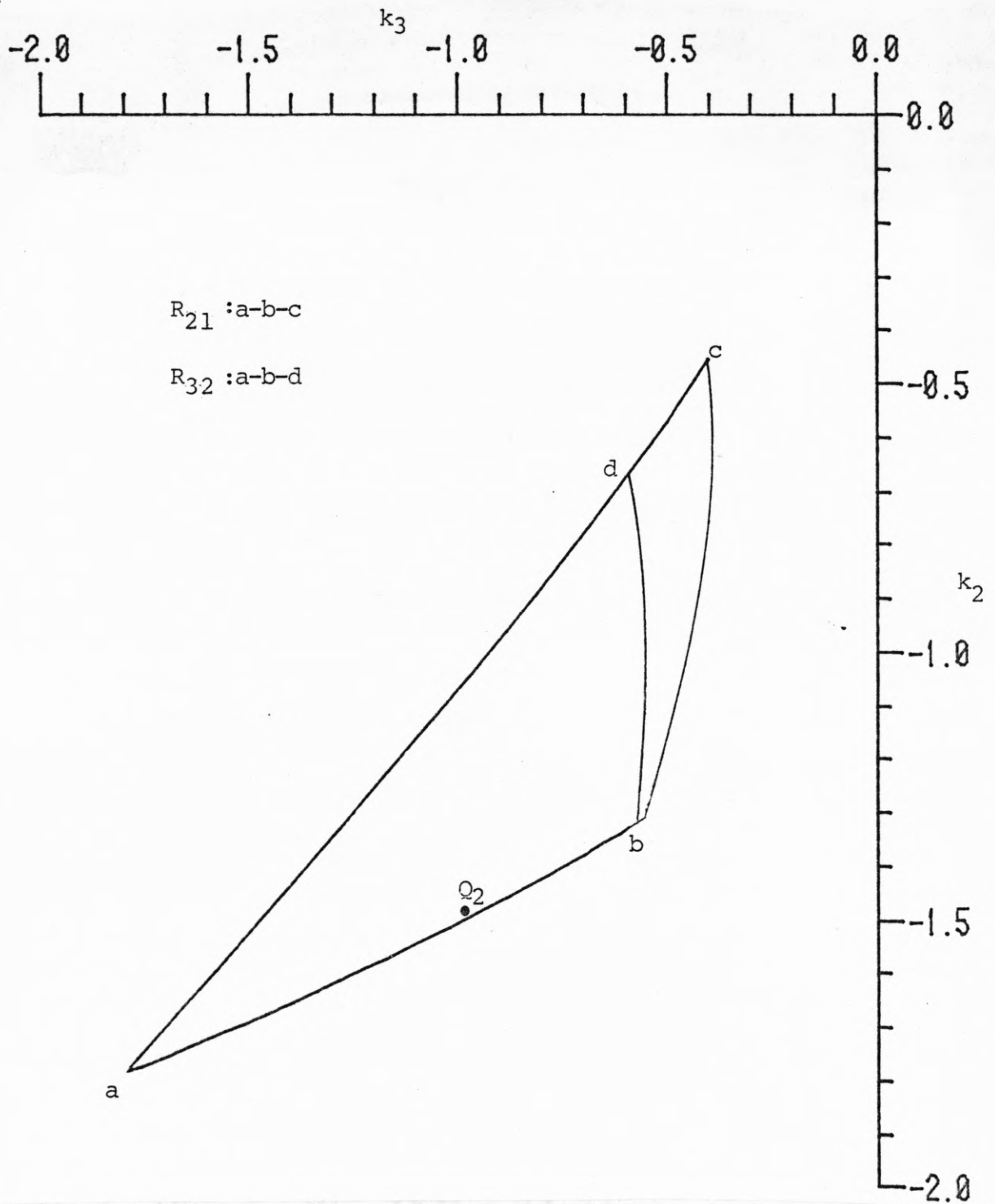


Figure 5.22. The regions R_{21} and R_{32} .

handling a failure of any two sensors. Specific eigenvalue locations and typical C_N^* responses are shown in the last section of this chapter.

5.4.3. Dynamic Feedback of Normal Acceleration

The system of Figure 5.19 was studied using the filter of equation (126). The nominal eigenvalue regions were mapped into the k_1, k_4 plane. There was no intersection of these regions. Thus, for the controller structure of Figure 5.20 the gyro is necessary. The intersection of the emergency regions R_{emNz} is shown in Figure 5.23. Any gain chosen from R_{emNz} will meet the emergency specifications at all flight conditions.

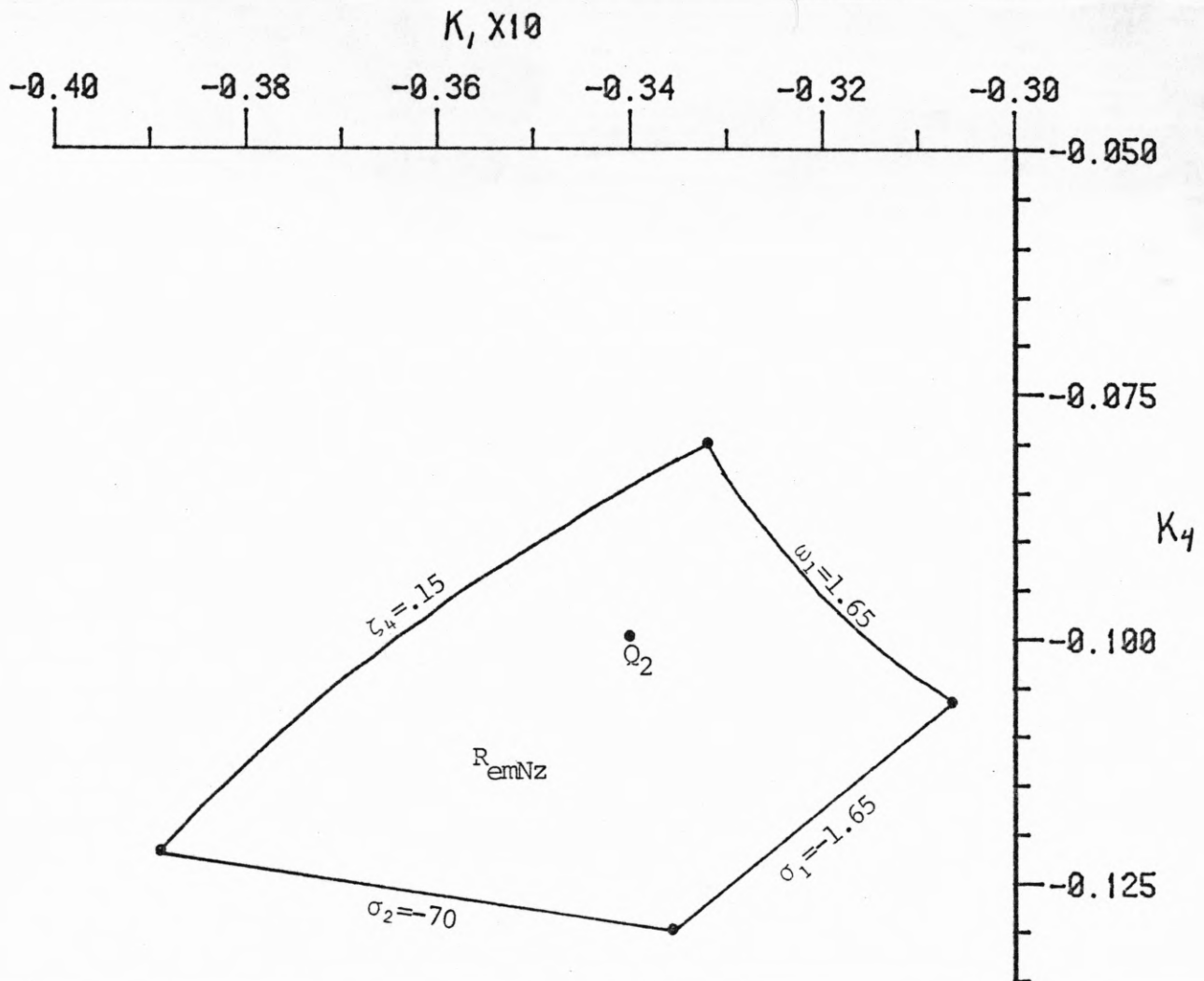


Figure 5.23. The region R_{emNz}

5.4.4. Dynamic Feedback of Both Outputs

Now the total system of Figure 5.20 will be considered and the complete regions in K-space will be four dimensional. First the system using a single gyro and a single accelerometer will be considered.

For the system to be robust with respect to either sensor failure, k_2 and k_3 should lie in the region R_{emq} of Figure 5.24 (partially shown in Figure 5.21), and k_1, k_4 should lie in the region R_{emNz} of Figure 5.23. Since graphical representations are limited to two dimensional subspaces of K-space, two of the four gains will have to be at least temporarily fixed. As k_1 and k_4 range throughout the region R_{emNz} the closed loop eigenvalues do not move much. It is therefore natural to select k_1 and k_4 as the gains to be fixed. They were fixed as

$$(k_1, k_4) = (-.034, -.1) \quad (128)$$

designated Q_2 in Figure 5.23. There are two free gains to be determined, k_2 and k_3 . The four dimensional problem has been reduced to looking in the k_3, k_2 plane for a solution.

As before, the nominal eigenvalue boundaries, Γ_{nomi} , are mapped into the k_3, k_2 plane using the algorithms of Chapter 4. A typical mapping is shown in Appendix II. Figure 5.23 shows the intersection of all four regions, labeled R_{nom} . For any k_2, k_3 chosen from R_{nom} of Figure 5.24 the nominal eigenvalue requirements will be met at all flight conditions. Since k_1, k_4 were chosen from R_{emNz} of Figure 5.23, the emergency requirements are met after gyro failure. If k_2, k_3 are also chosen from R_{emq} the system will also be robust with respect to accelerometer failure. All gains in the region R of Figure 5.24 meet the above requirements for k_1 and k_4 fixed as in equation (128).

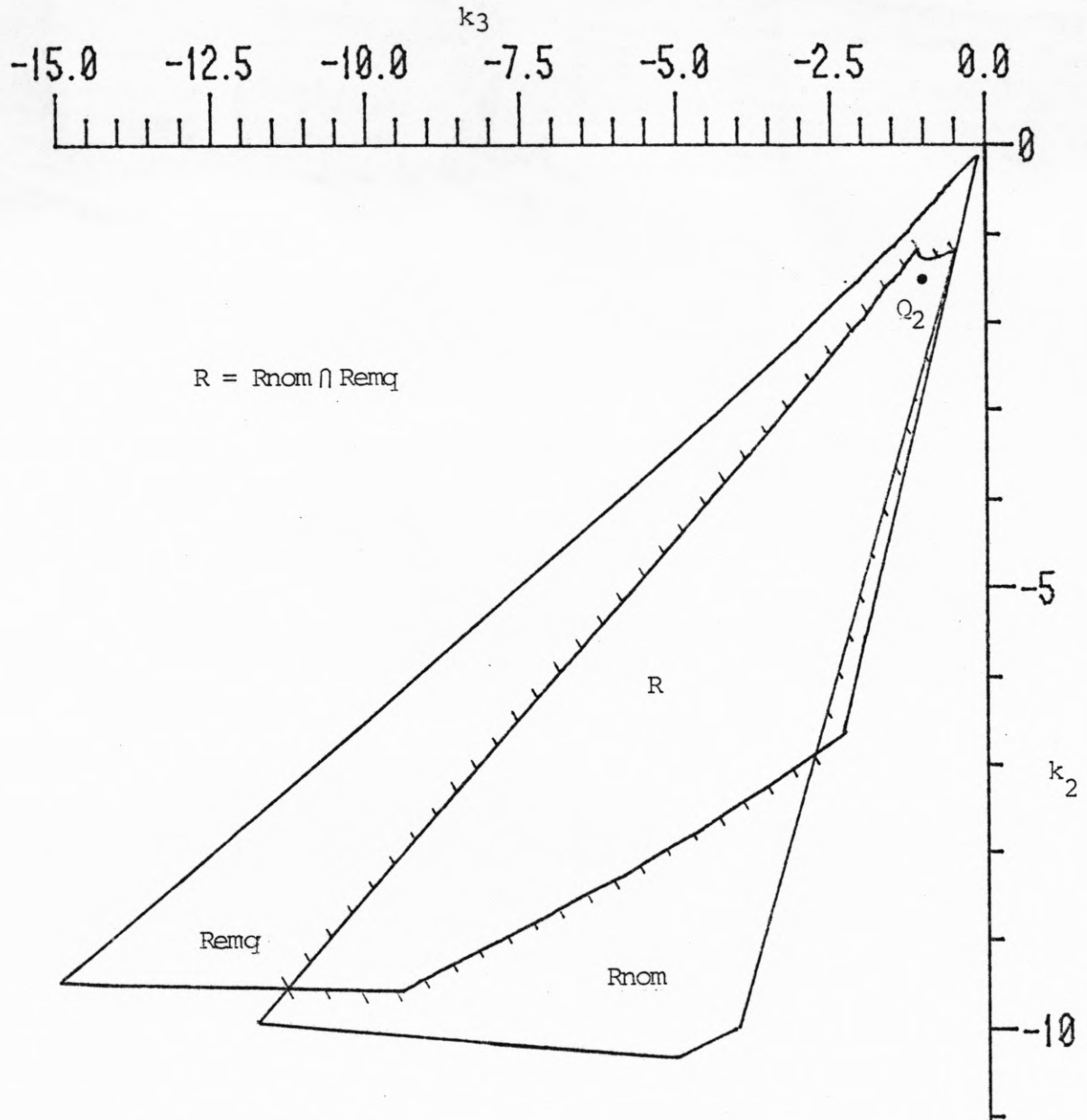


Figure 5.24. The regions R , R_{nom} , and R_{emq} .

5.4.5. Dynamic Feedback Design Summary

The eigenvalue requirements for the nominal and emergency conditions can be met with one accelerometer and one gyro, or with two gyros. With the assumed filter structure the gyro is necessary. Step responses were obtained for several robust gain combinations. The gains chosen were based on the parameter plane, tightening constraints and minimal control magnitude techniques discussed in subsection 5.3.2. The responses behaved as anticipated with the exception of some responses for flight condition 2. For this flight condition the pitch rate zero was the farthest from the "cancelling" pole in the Nz filter (see Table 5a). Figure 5.25 shows typical C_N^* responses at flight condition 2 using:

- 1) gains Q_1 from Chapter 4, $k_{Nz} = -.115$ $k_2 = -.8$,
- 2) gains Q_2 $k_1, k_2, k_3, k_4 = (-.034, -1.5, -1, -.1)$,
- 3) gains (0, -1.5, -1.0) (no accelerometer).

The filter pole at $-.98$ was exempted from the eigenvalue constraints under the assumption that it would have little effect on time response. As seen in Figure 5.25 the more acceleration feedback (and less use of \hat{Nz}), the better this assumption is. An accelerometer will therefore be included in the trial design point.

To ensure the system is robust with respect to any two sensor failures, two gyros will also be included. The gains chosen were those represented above by point Q_2 shown in Figures 5.5-5.8. The final configuration is shown in Figure 5.26. Figures 5. a,b show the response to pilot step commands for the unfailed system. The C_N^* responses are well within the required boundaries at all flight conditions. Table 5.5 lists the eigenvalue locations for the unfailed system and after all possible combinations of sensor

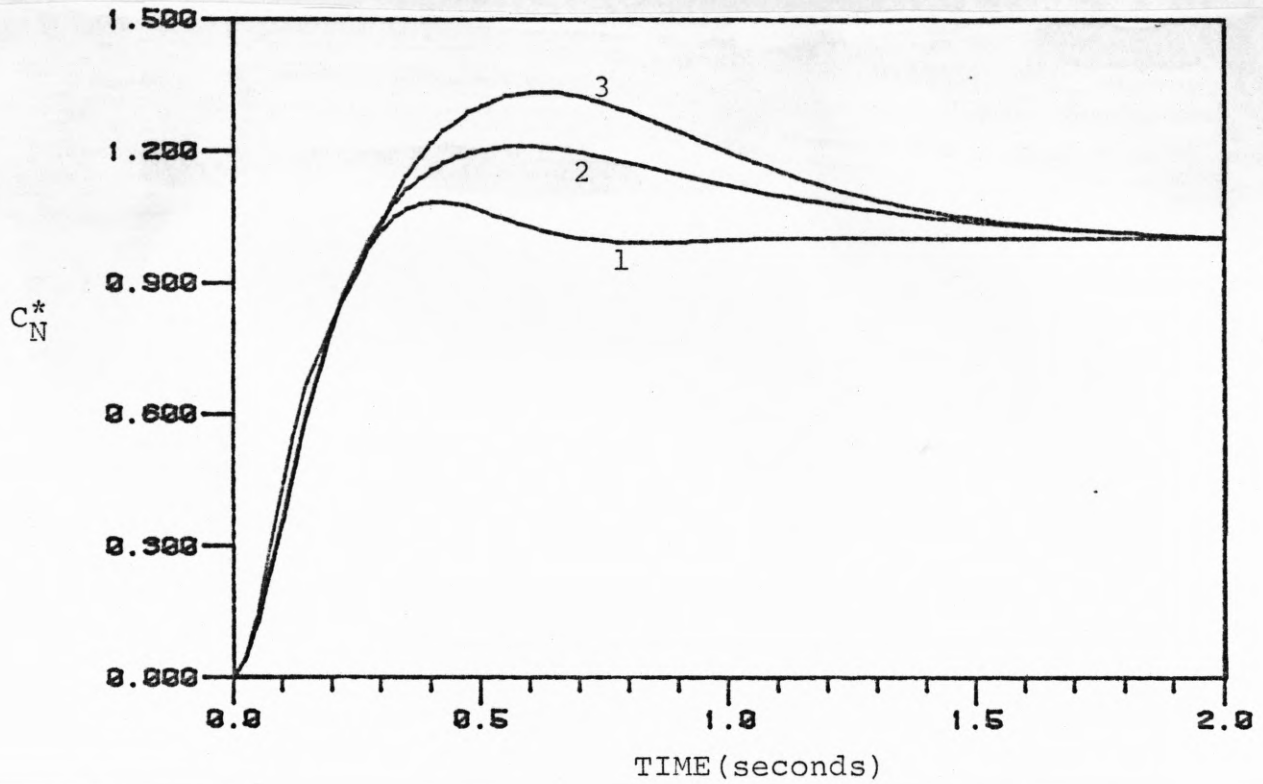


Figure 5.25. C_N^* responses for flight condition 2.

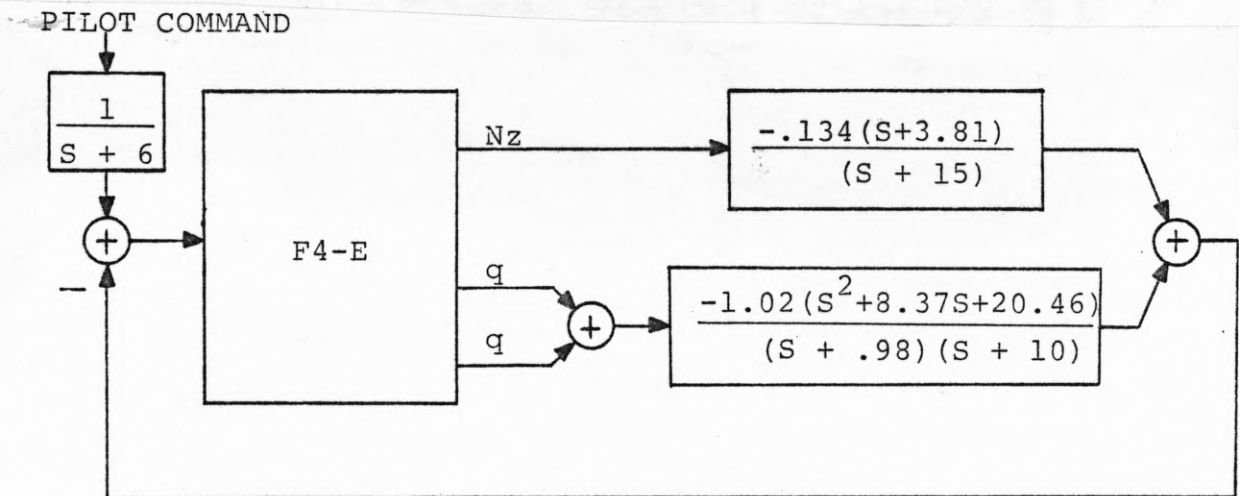


Figure 5.26. Final controller configuration.

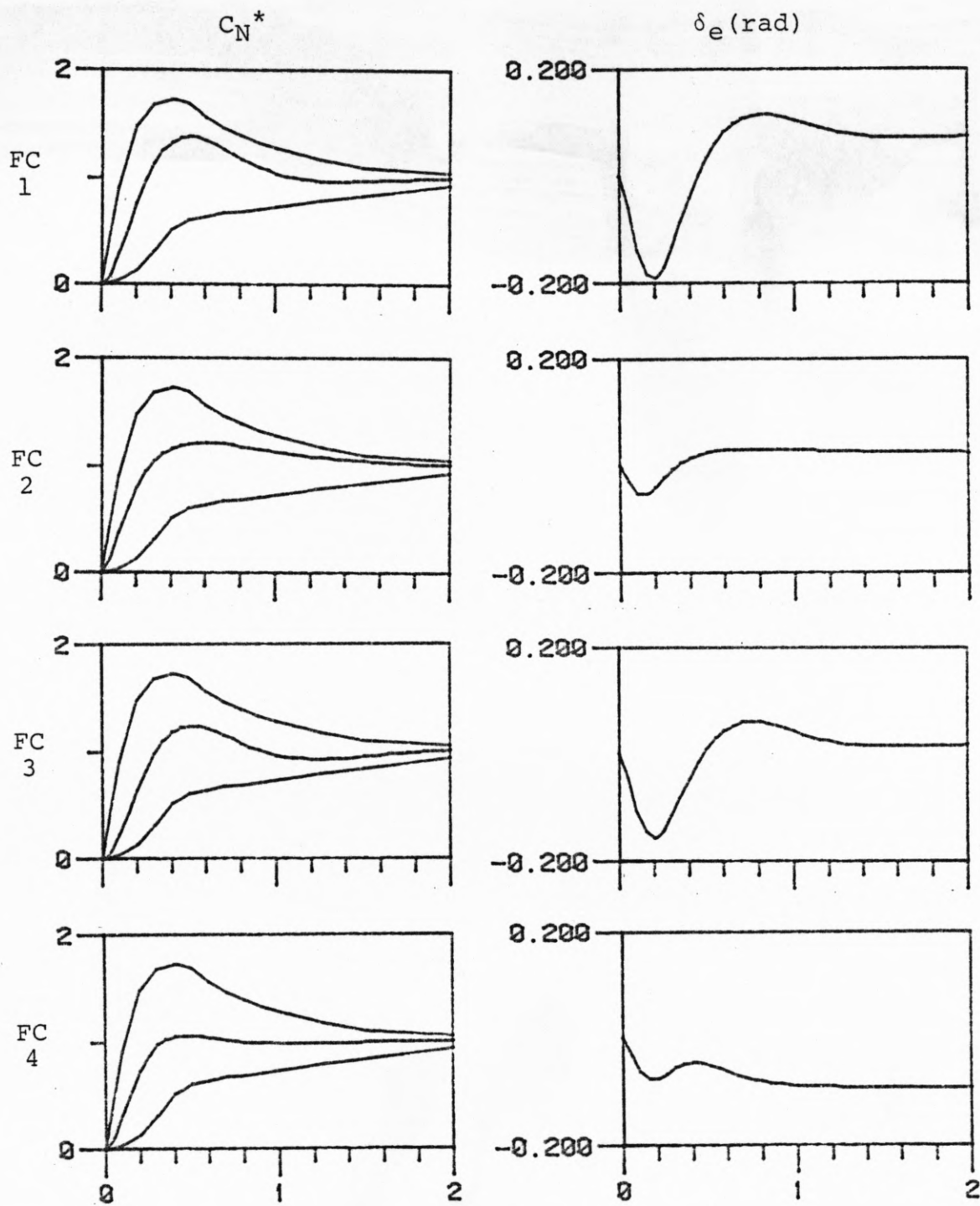


Figure 5.27a. C_N^* and δ_e responses for trial gains Q_2 .

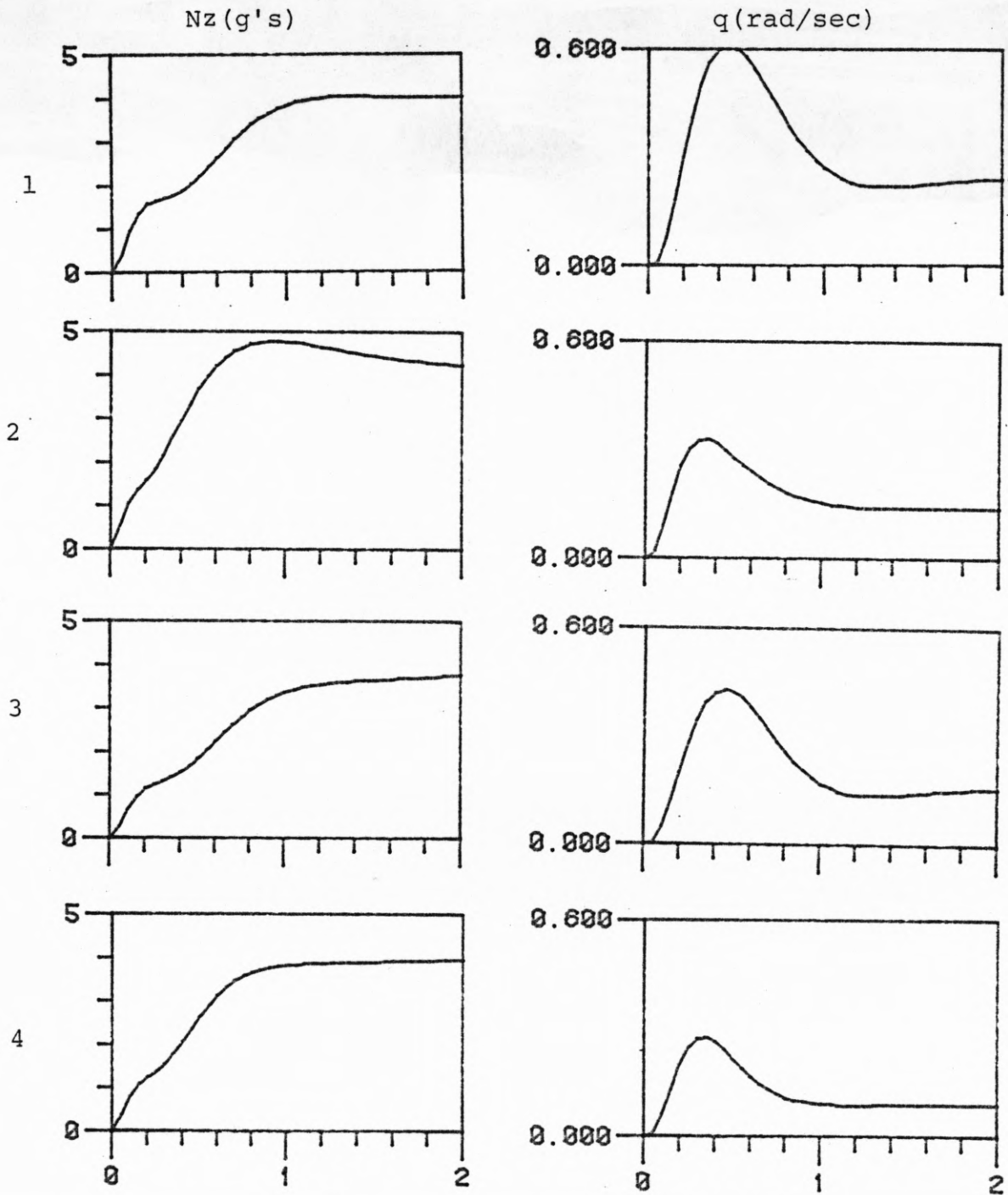


Figure 5.27b. N_z and q responses for trial gains Q_2 .

Table 5.5. Eigenvalues for System with Gains Q_2^*

Flight Condition	No Failures	All Sensors Failed	One Gyro Failed
1	-.89	1.23	-.89
	(.64, 4.85)	-.98	(.52, 4.29)
	(.78, 12.9)	-10.0	(.89, 9.88)
	-27.6	-14.0	-31.76
		-15.0	
2	-1.43	1.78	-1.35
	(.84, 5.66)	-.98	(.94, 6.28)
	(.66, 15.5)	-10.0	(.53, 10.3)
	-48.13	-14.0	-55.5
	-15.0		
3	-.67	.56	-.70
	(.61, 4.98)	-.98	(.49, 4.4)
	(.79, 12.3)	-10.0	(.9, 9.76)
	-26.5	-14.0	-30.1
	-15.0		
4	-.88	-.98	-.91
	(.77, 6.4)	(.20, 4.4)	(.91, 7.84)
	(.66, 13.2)	-10.0	(.45, 8.33)
	-37.1	-14.0	-42.5
	-15.0		

Table 5.5 (continued)

Flight Condition	Accel. Failed	Accel. and Gyro Failed	Two Gyros Failed
1	-.87	-.84	-.98
	(.65, 4.38)	(.59, 3.07)	(.80, 1.77)
	-15.0	-15.0	-5.78
	(.56, 18.1)	(.82, 13.7)	-10.0
			-35.33
2	-1.62	-1.81	-.98
	(.72, 4.62)	(.66, 3.83)	-3.54
	-15.0	-15.0	(.27, 6.73)
	(.35, 28.3)	(.59, 17.8)	-10.0
			-61.43
3	-.62	.59	-.98
	(.62, 4.46)	(.51, 3.23)	(.43, 2.34)
	-15.0	-15.0	-6.44
	(.60, 16.9)	(.85, 13.2)	-10.0
			-33.27
4	-.86	-.89	-.98
	(.68, 5.26)	(.53, 5.56)	(.16, 6.27)
	-15.0	-15.0	-5.35
	(.42, 22.3)	(.69, 14.4)	-10.0
			-46.98

*The notation (ζ, ω_n) refers to the damping and natural frequency of a complex pair of eigenvalues.

failure. All eigenvalues, of course, are in the required regions. Figures 5.28a,b,c show C_N^* responses for all possible sensor failures. In these figures the normalizing factor (Kc^* of equation (122)) was taken to be the value of C^* at 3 seconds, which is sufficiently close to the stationary value for the closed loop responses and finite for the unstable open loop responses.

5.5. Summary and Conclusions

A fixed gain controller has been designed for the short period mode of a F4-E aircraft which is destabilized by horizontal canards. The uncontrolled mode is unstable at all subsonic flight conditions and insufficiently damped in supersonic flight. Therefore, the control system is necessary at all flight conditions in order to achieve handling qualities as specified by the military requirements. The problem of sensor failures is usually solved by use of redundant sensors and failure detection. In this paper controller schemes not requiring failure detection were studied. The control system was designed using graphical techniques based on the K-space methods of Chapter 4. The main feature of this graphical design method is the ability to determine the effect of two controller parameters on the system eigenvalues. First the unfailed system using one gyro and one accelerometer was studied. This is a third order system with the two free parameters being the two feedback gains. The set of admissible gains was determined for which the nominal requirements are met at all flight conditions. No gains from this set are robust with respect to either sensor failure. If both sensors are paralleled by an identical sensor, the system can be made robust with respect to any single sensor failure, corresponding to a fifty percent gain reduction.

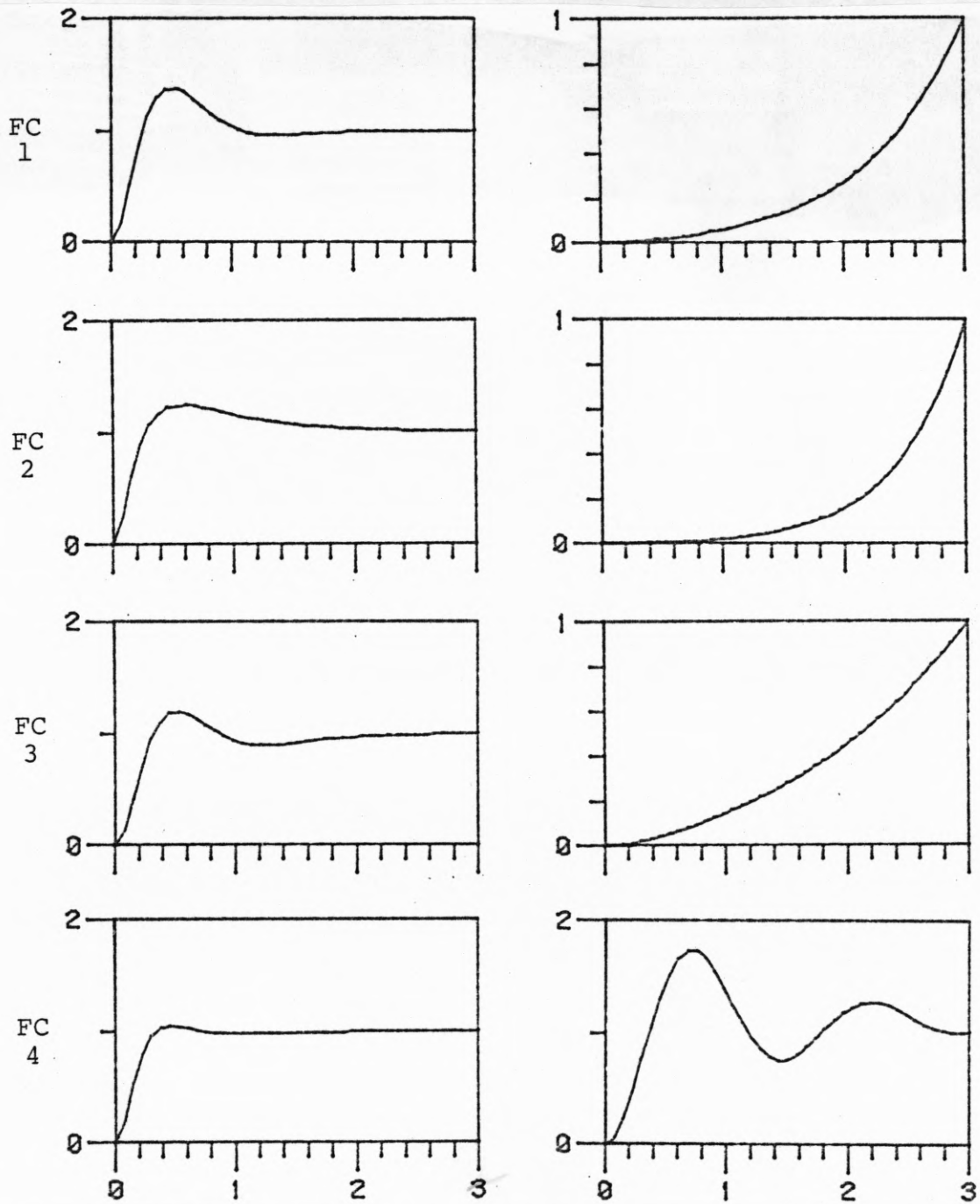


Figure 5.28a. C_N^* responses for the unfailed and open loop systems.

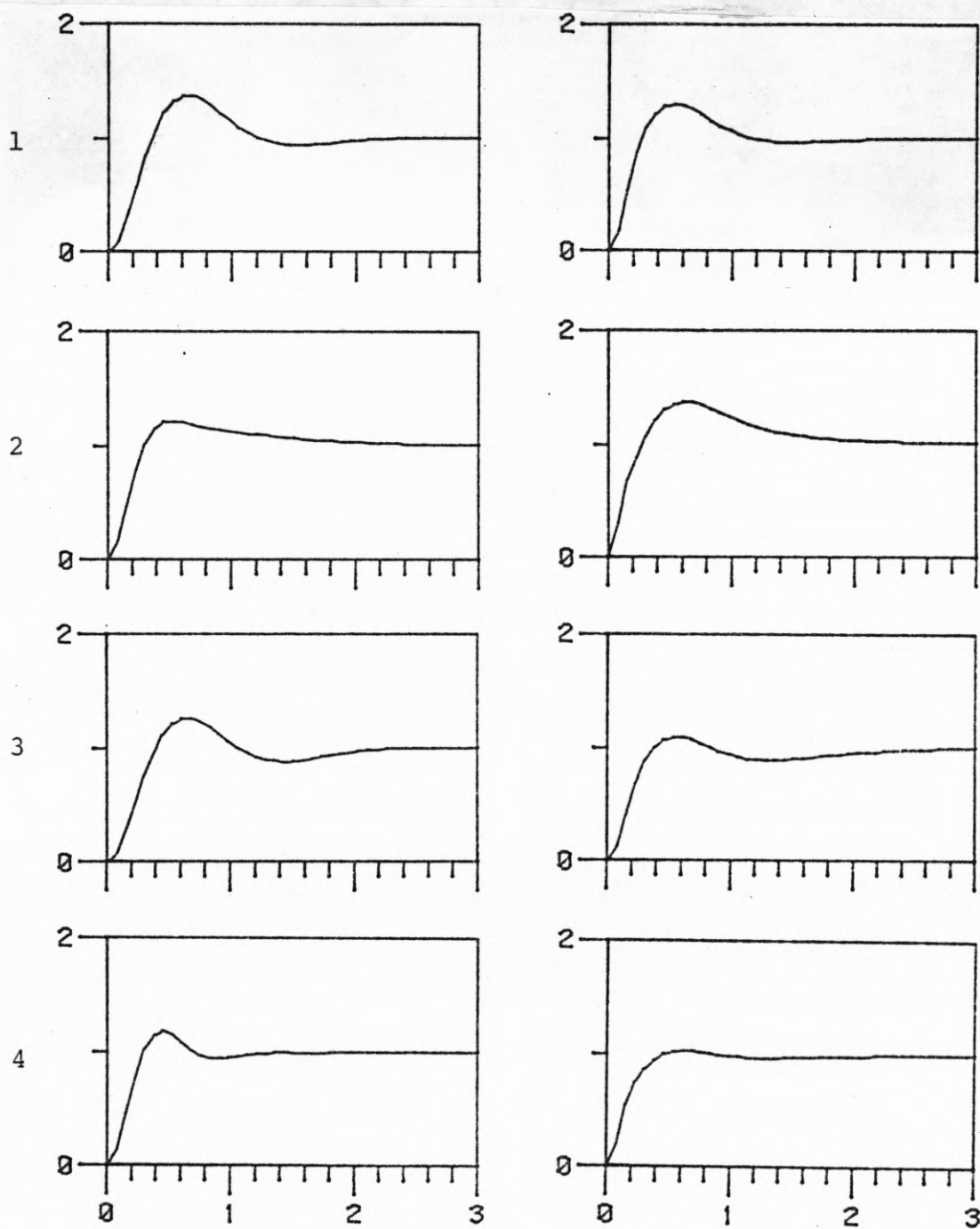


Figure 5.28b. C_N^* responses after failure of one sensor.

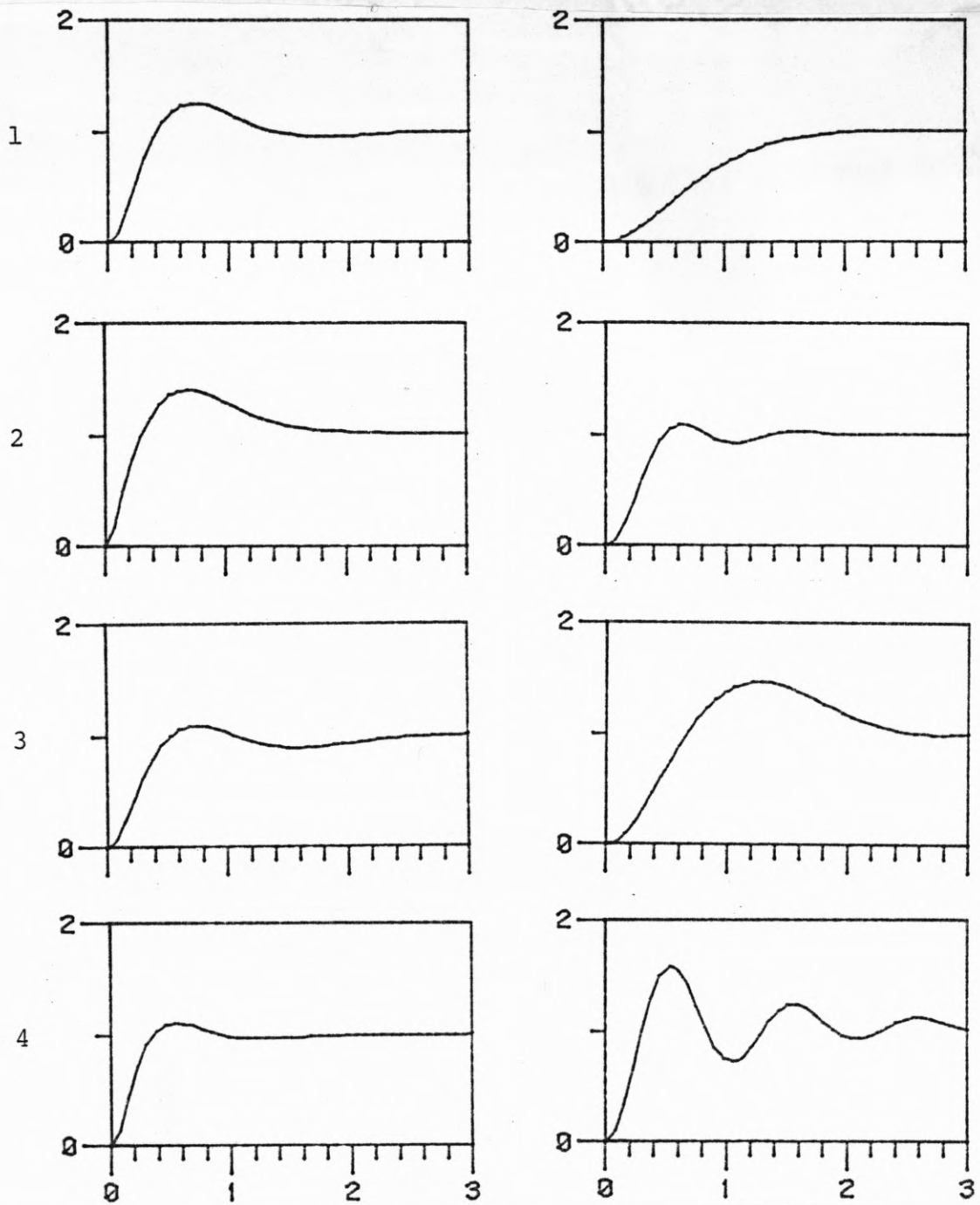


Figure 5.28c. C_N^* responses after failure of two sensors.

In order to reduce the number of sensors needed to three and to achieve robustness for double sensor failures, various dynamic feedback configurations were studied. In order to avoid the increased dimensionality of a general dynamic feedback configuration, preliminary studies were made to find good candidates for two filters, one for each input, such that after failure of either sensor there remain two independent variables for feedback. Using the most promising configuration, it turned out that without gyros only the emergency specifications could be met. The gains for the accelerometer and its filter were thus fixed to guarantee this property. In the plane of the two remaining gains for the gyro and its filter, the set of admissible solutions for both the nominal and emergency specifications was determined. A solution using two paralleled gyros and one accelerometer was found which met the nominal specifications with no failure or a failure of any single sensor, and met the emergency specifications after failure of any two sensors. These robustness properties pertain to all flight conditions.

Like all graphical methods this design technique is very intuitive for two dimensional problems, but not as well suited for higher dimensional problems, where the dimension here refers to the number of controller parameters being considered in a particular design step. To make the problem tractable, the designer has to break the problem into a series of two dimensional problems by fixing the additional parameters. While in this study the proper sequence was clear, for higher dimensional problems it will in general be more difficult. The multi-input and general dynamic feedback problems are particularly difficult because of the increased dimensionality. As seen from the results of this Chapter, however, \mathcal{K} -space techniques are useful tools in the design of control systems.

CHAPTER 6

AN OPTIMIZATION TECHNIQUE FOR ROBUST CONTROL SYSTEM DESIGN

6.1. Introduction

This chapter formulates an alternative design technique for the control of systems which are subject to large, structured perturbations. The problem formulation is the same as that of Chapter 4. It is assumed that a finite number of operating points can be used to accurately characterize the perturbations. Design objectives and constraints are modeled as constraints on the locations of the closed loop eigenvalues in the complex plane. The objective is to choose a fixed gain control system which satisfies the constraints on the pole locations.

The approach of this chapter is to use a quadratic cost functional to represent trade-offs between possible design points. The problem is reformulated as an optimization problem over the free parameters of the control system. This optimization is then solved using an augmented Lagrangian approach.

The outline of this chapter is as follows. In Section 6.2, a precise mathematical formulation of the problem is given. Section 6.3 discusses the nonlinear programming method which was used to solve the problem. Section 6.4 derives the gradients which are necessary to solve the problem. In Section 6.5, a second order numerical example is presented. The purpose of presenting this example is to discuss some of the problems involved in implementing this method. Finally, this approach to controller design is applied to the problem considered in Chapter 5 of designing a fixed gain controller for the linearized longitudinal flight dynamics of an F4 aircraft. The resulting design is compared to the corresponding design of Chapter 5.

6.2. The Problem and Its Reformulation

The purpose of this section is to present a precise mathematical formulation of the problem discussed in the Introduction of this thesis and then to reformulate the problem in a form that is computationally easier to work with. As mentioned in the previous section, this chapter deals with the problem of using output feedback to control a fixed structure system. The design problem is to choose the constant feedback gains which are best with respect to some cost function such that the closed loop system satisfies certain design specifications. It is assumed that these design specifications can be represented most naturally as regions in the complex plane where the eigenvalues of the closed loop system must be located. The system is also assumed to be linear time invariant.

The precise problem formulation is as follows:

$$\min_{k \in S} J = \frac{1}{2} E \left\{ \int_0^{\infty} [x^T(t) Q x(t) + u^T(t) R u(t)] dt \right\} \quad (129)$$

subject to

$$\dot{\underline{x}}(t) = A \underline{x}(t) + B \underline{u}(t); \quad \underline{x}(t_0) = \underline{x}_0 \quad (130)$$

$$E\{\underline{x}_0\} = 0; \quad E\{\underline{x}_0 \underline{x}_0^T\} = X_0$$

$$\underline{y}(t) = C \underline{x}(t) \quad (131)$$

$$\underline{u}(t) = -K \underline{y}(t) \quad (132)$$

$$g_i(\lambda) \leq 0 \quad i = 1, \dots, N \quad (133)$$

where $\underline{x}(t) \in \mathbb{R}^n$, $u(t) \in \mathbb{R}^m$, and $y(t) \in \mathbb{R}^p$. S is the space of permissible feedback gains. The expectation of the integral is used so that the cost, J , is independent of any particular initial state of the system, but depends instead on an average initial condition of all the possible initial states. Q and R are nonnegative definite constant matrices chosen so that given some predetermined criteria, by minimizing J , one is improving the closed loop behavior of the system. For example, if Q is the zero matrix and R is the identity, J represents the total energy used to control the system. By minimizing J , one is minimizing the total energy used. The functions, $g_i(\underline{\lambda})$, represent constraints on the location of the eigenvalues, $\underline{\lambda}$, of the closed loop system in the complex plane.

The problem (129)-(133) looks computationally difficult to solve; however, it can be reformulated as follows:

$$\min_{\underline{k} \in S} J = \frac{1}{2} \text{tr}\{M(\underline{k})P\} \quad (134)$$

subject to

$$g_i(\underline{\lambda}) \leq 0 \quad i = 1, \dots, N \quad (135)$$

where

$$S = \{\underline{k} / (A - B\underline{k}C) \text{ is asymptotically stable}\} \quad (136)$$

$$M(\underline{k}) = Q + C^T K^T R K C \quad (137)$$

$$\tilde{A}(\underline{k}) = A - B\underline{k}C \quad (138)$$

$$X_0 = E\{\underline{x}(0)\underline{x}^T(0)\} \quad (139)$$

$$\tilde{A}(\underline{k})P + P\tilde{A}^T(\underline{k}) = -X_0. \quad (140)$$

Here P is a constant positive definite matrix; \underline{k} is a vector comprised of the elements of the matrix K ; $\underline{x}(0)$ is the initial state of the system; and $\tilde{A}(\underline{k})$ is

the closed loop system for a given \underline{k} . Given this formulation, the cost J is easily found. To solve for J directly from (129), one would first have to calculate $\underline{x}(t)$ for each \underline{k} ; whereas to solve (134), one has to solve the Lyapunov equation (140) for each \underline{k} and then perform a few simple matrix operations. The derivation of (134)-(140) is a direct consequence of the results in [60].

Problem (134)-(140) is a mathematical representation of the problem (described in the introduction of this chapter) of choosing constant output feedback gains for a linear time invariant system subject to certain design criteria which are represented by a cost function and constraints on the locations of eigenvalues in the complex plane. The question of how to solve the problem (134)-(140) remains. Problem (134)-(140) is a nonlinear constrained minimization over a finite dimensional space. The next section will discuss methods of solving such a problem.

6.3. Nonlinear Programming Solution Procedure

There are several ways to solve a nonlinear problem of the form (134)-(140). As stated previously, the basic problem is

$$\min_{\underline{k} \in S} J(\underline{k}) \quad (141)$$

subject to

$$g_i(\underline{k}) \leq 0 \quad i = 1, \dots, N \quad (142)$$

where the exact form of the cost function is defined explicitly by equations (134), (139), and (140) in Section 6.2.

Two of the most common methods of solving a problem of this type are penalty function and Lagrange multiplier methods [61]. Each of these methods has certain problems (to be described below) which are inherent to the method. However, by using a

combination of both methods, these problems can be avoided and a better approximation to the solution for (141)-(142) can be obtained [62].

In its simplest form the Lagrange multiplier method solves the following problem [61]

$$\max \varphi(\underline{d}) \quad (143)$$

subject to

$$d_i \geq 0 \quad i = 1, \dots, N \quad (144)$$

where $\underline{d} \in \mathbb{R}^N$ and

$$\varphi(\underline{d}) = \min_{\underline{k} \in S} J(\underline{k}) + \sum_{i=1}^N d_i g_i(\underline{k}). \quad (145)$$

This problem is often easier to solve since the nonlinear constraints, $g_i(\underline{k})$, have been replaced by simple linear ones. The problem (143)-(144) is the dual problem of problem (141)-(142). The duality theorem states that as long as $\varphi(\underline{d}) > -\infty$ for some positive d_i 's and $J(\underline{k}) < \infty$ for some $\underline{k} \in S$, the solution to (143)-(144) is less than or equal to the solution to (141)-(142). When the solution to (143)-(144) is strictly less than the solution to (141)-(142), a duality gap exists [61]. For convex functions with convex constraints, this difficulty does not occur. The solution to (143)-(144) is also the solution for (141)-(142). However, for a general function, $J(\underline{k})$, a duality gap may exist so that the solution to (143)-(144) is a lower bound on the solution to (141)-(142), rather than the minimum [61].

On the other hand, exterior penalty functions solve the problem [15]:

$$\min_{\underline{k} \in S_1} J(\underline{k}) + cH(\underline{k}) \quad (146)$$

where c is some positive constant, S_1 is the region in \mathbb{R}^m where all the

constraints, (142), are satisfied, and $H(\underline{k})$ is a functional with these properties:

$$H(\underline{k}) \geq 0 \text{ for all } \underline{k} \in \mathbb{R}^m \quad (147)$$

$$H(\underline{k}) \text{ is continuous} \quad (148)$$

$$H(\underline{k}) = 0 \iff \underline{k} \in S_1. \quad (149)$$

As long as $\underline{k} \in S_1$, $H(\underline{k}) = 0$, so problems (141)-(142) and (146) are identical.

When \underline{k} is outside S_1 , the function $J(\underline{k}) + cH(\underline{k})$ is large. As c becomes large, the minimum of $J(\underline{k}) + cH(\underline{k})$ approaches S_1 . The most common penalty function is

$$H(\underline{k}) = \sum_{i=1}^N \max[0, g_i(\underline{k})]^2. \quad (150)$$

For this function, the value of $H(\underline{k})$ is the sum of the squares of the distances by which each constraint is violated, so the penalty term increases rapidly when the distance \underline{k} is outside S_1 . The advantage of this method is that problem (146) is an unconstrained minimization problem which is often easier to solve than problem (141)-(142). The disadvantage of this approach is that to obtain a good approximation to problem (141)-(142), c must become large. However, as c approaches infinity, the matrix of second partial derivatives of $J(\underline{k}) + cH(\underline{k})$ (the Hessian) becomes increasingly ill conditioned. Many algorithms for unconstrained minimization depend on either the Hessian or an approximation of the Hessian to find the minimum. If the Hessian is ill-conditioned, these algorithms will converge very slowly [61].

By combining penalty function methods with Lagrange multiplier methods, one can eliminate the duality gap and use a smaller value of c , thus

improving the conditioning of the Hessian at the solution [62]. Using the penalty function $H(\underline{k})$, in (150), consider the problem:

$$\min_{\underline{k} \in S} J(\underline{k}) + cH(\underline{k}) \quad (151)$$

subject to

$$g_i(\underline{k}) \leq 0 \quad i = 1, \dots, N. \quad (152)$$

Given the properties of $H(\underline{k})$, problem (151)-(152) is equivalent to (141)-(142).

The dual of problem (151)-(152) is

$$\max g_c(\underline{d}) \quad (153)$$

subject to

$$d_i \geq 0 \quad i = 1, \dots, N \quad (154)$$

where

$$g_c(\underline{d}) = \inf_{\underline{k} \in S} \{ J(\underline{k}) + cH(\underline{k}) + \sum_{i=1}^N d_i g_i(\underline{k}) \}. \quad (155)$$

Theorem 1: There exists a $c \in \mathbb{R}$ with $0 < c < \infty$ such that the solution to problem (153)-(154) is also the solution to problem (151)-(152).

Proof: See Bertsekas [63].

Theorem 1 implies there is no duality gap for problems (151)-(152) and (153)-(154). Moreover, since the value of c needed to solve this problem exactly is finite, the structure of the Hessian is more favorable for solving the problem.

Bertsekas [64] discusses a variation of problems (151)-(152) and (153)-(154) and suggests a very straightforward way to solve the maximization over \underline{d} . He suggests solving the problem

$$\max g_c(\underline{d}) \quad (156)$$

subject to

$$d_i \geq 0 \quad i = 1, \dots, N \quad (157)$$

where

$$g_c(\underline{d}, \underline{k}) = \inf_{\underline{k} \in S} \left\{ J(\underline{k}) + \frac{1}{2c'} \sum_{i=1}^N \{ \max[0, d_i + c'g_i(\underline{k})] \}^2 - d_i^2 \right\}. \quad (158)$$

For the case where the i th constraint is violated, the corresponding term in the summation is

$$d_i g_i(\underline{k}) + c'/2 g_i^2(\underline{k}) \quad (159)$$

which is identical to the corresponding term in (155) for $c = c'/2$ and $H(\underline{k})$ as defined in (150). For the case where the i th constraint is satisfied, but

$$d_i + c'g_i(\underline{k}) > 0 \quad (160)$$

equation (159) also applies; and, when

$$d_i + c'g_i(\underline{k}) < 0 \quad (161)$$

the corresponding term in the summation is

$$- \frac{1}{2c'} d_i^2. \quad (162)$$

Bertsekas has shown that the solution to (156)-(157) is equivalent to that of problem (141)-(147) for all values of c' greater than some lower bound \hat{c} (\hat{c} exists and is finite).

One can solve the problem (156)-(157) iteratively, viewing the iteration over \underline{d} as a fixed stepsize gradient problem [64]. The partial of $g_c(\underline{d}, \underline{k})$ with respect to d_i is

$$\frac{\partial g_c(\underline{d}, \underline{k})}{\partial d_i} = \max[-d_i/c', g_i(\underline{k})] \quad i = 1, \dots, N. \quad (163)$$

Hence the gradient of $g_c(\underline{d}, \underline{k})$ with respect to \underline{d} is the vector of these partials. The appropriate update of \underline{d}_{J+1} is

$$\underline{d}_{J+1} = \underline{d}_J + c' \nabla g_c(\underline{d}, \underline{k}). \quad (164)$$

For $J(\underline{k})$ and $g_i(\underline{k})$ convex, Bertsekas has shown that his method has demonstrated global convergence for a wide range of step sizes. The main advantages of using this method is that it combines the advantages of both penalty function and Lagrange multiplier methods and that the iterative method to solve the maximization over \underline{d} is very simple.

There remains the problem of solving the minimization over \underline{k} for a fixed \underline{d} . This problem can be solved using a variable metric algorithm [65]. At each iteration of the routine the user must supply the value of the function to be minimized and its gradient. From this information, the routine builds up an approximation to the inverse Hessian which improves as the routine gathers information from more points.

To solve for $g_c(\underline{d}, \underline{k})$ in (158) at each iteration, one must solve for $J(\underline{k})$ and $g_i(\underline{k})$, $i = 1, \dots, N$. For problem (134)-(140) from Section 2, $J(\underline{k})$ can be solved using (134) and (140). The constraints $g_i(\underline{\lambda}(\underline{k}))$ are chosen by the designer and thus are also readily available. The gradients are also needed at each iteration. Taking the partials of $g_c(\underline{d}, \underline{k})$ in (158) with respect to \underline{k} ,

$$\frac{\partial g_c(\underline{d}, \underline{k})}{\partial k_i} = \frac{\partial J(\underline{k})}{\partial k_i} + \max[0, d_i + c/g_i(\underline{k})] \frac{\partial g_i(\underline{k})}{\partial k_i}. \quad (165)$$

Thus to solve problem (155), the gradient of the constraints and of the cost with respect to \underline{k} must be provided. Section 6.4 discusses the computations required to solve for $\nabla_{\underline{k}} J(\underline{k})$ and $\nabla_{\underline{k}} g(\underline{k})$.

6.4. Cost and Constraint Gradient Calculations

As described in Section 3 our approach to the solution of problem (134)-(140) is to solve the equivalent problem (156)-(158) iteratively. To solve the minimization over \underline{k} , for a fixed \underline{d} , the gradient of $J(\underline{k})$ with respect to \underline{k} and the gradient of $g_i(\underline{\lambda}(\underline{k}))$ with respect to \underline{k} must be computed. Using linear operator theory, one can derive a fairly simple expression for the gradient of $J(\underline{k})$. Using eigenvalue sensitivity theory, one can derive an expression for the gradients of the constraints with respect to \underline{k} [66].

The gradient of $J(\underline{k})$ with respect to K is as follows:

Theorem 2:
$$\nabla_K J(\underline{k}) = (RKCP - B^T \Sigma P) C^T$$

where P and Σ are solutions of

$$\begin{aligned} \tilde{A}^T \Sigma + \Sigma \tilde{A} + M(\underline{k}) &= 0 \\ \tilde{A} P + P \tilde{A}^T + X_0 &= 0 \end{aligned} \tag{166}$$

and \tilde{A} and $M(\underline{k})$ are defined in (138) and (137) respectively.

Proof: Follows directly from [60].

$\nabla_{\underline{k}} J(\underline{k})$ is found by rearranging $\nabla_K J(\underline{k})$ (\underline{k} is a vector of the elements of the matrix K).

To compute the gradient of the constraints with respect to \underline{k} , one must compute the gradient of the eigenvalues with respect to \underline{k} . After finding the latter, one can use the rules of implicit differentiation to find the former. Consider equation (167).

$$\underline{w}^T (\tilde{A} - \lambda I) \underline{v} = 0 \tag{167}$$

where \underline{w}^T is the left eigenvector of \tilde{A} and \underline{v} is the right eigenvector corresponding to eigenvalue λ . Since \underline{w}^T and \underline{v} are the eigenvectors of \tilde{A} , (167) is true. When the Fréchet differential of a function $F(\underline{k})$ exists, it is given by [67]:

$$\delta F(\underline{k}, \Delta \underline{k}) \triangleq \left. \frac{\partial}{\partial \varepsilon} F(\underline{k} + \varepsilon \Delta \underline{k}) \right|_{\varepsilon=0}. \quad (168)$$

The Fréchet differential (168) can also be written in terms of an inner product as

$$\delta F(\underline{k}, \Delta \underline{k}) \triangleq \langle \nabla F(\underline{k}), \Delta \underline{k} \rangle \quad (169)$$

where

$$\langle \nabla F(\underline{k}), \Delta \underline{k} \rangle = \text{tr}\{\nabla F^T(\underline{k}) \Delta \underline{k}\}. \quad (170)$$

Take the Fréchet differential of both sides of (167)

$$\delta \underline{w}^T (\tilde{A} - \lambda I) \underline{v} + \underline{w}^T (\tilde{A} - \lambda I) \delta \underline{v} + \underline{w}^T (\delta \tilde{A} - \delta \lambda I) \underline{v} = 0. \quad (171)$$

Again since \underline{w}^T and \underline{v} are eigenvectors, the first two terms are identically zero, thus

$$\underline{w}^T \delta \lambda \underline{v} = \underline{w}^T \delta \tilde{A} \underline{v}. \quad (172)$$

Since $\delta \lambda$ is a scalar,

$$\delta \lambda \underline{w}^T \underline{v} = \underline{w}^T \delta \tilde{A} \underline{v}. \quad (173)$$

Since $\underline{w}^T \underline{v}$ is also scalar

$$\delta \lambda = \frac{\underline{w}^T \delta \tilde{A} \underline{v}}{\underline{w}^T \underline{v}}. \quad (174)$$

Notice, however, that if $\underline{w}^T \underline{v} = 0$, equation (174) will not hold. If $\underline{w}^T \underline{v} = 0$, then the left eigenvector, \underline{w}^T , is perpendicular to the right eigenvector, \underline{v} . This only happens when \tilde{A} has a Jordan block of dimension greater than one.

Continuing, from definition (138) and (169)

$$\begin{aligned} \delta \tilde{A}(\underline{K}, \Delta \underline{K}) &= \left. \frac{\partial}{\partial \varepsilon} \tilde{A}(\underline{K} + \varepsilon \Delta \underline{K}) \right|_{\varepsilon=0} \\ &= \left. \frac{\partial}{\partial \varepsilon} [A - B(\underline{K} + \varepsilon \Delta \underline{K})C] \right|_{\varepsilon=0} \\ &= -B \Delta \underline{K} C. \end{aligned} \quad (175)$$

Using definition (169)

$$\begin{aligned}\delta\lambda(K, \Delta K) &= \langle \nabla\lambda(K), \Delta K \rangle \\ &= \text{tr}\{\nabla\lambda^T(K)\Delta K\}.\end{aligned}\quad (176)$$

Substituting (175) and (176) in (174):

$$\begin{aligned}\text{tr}\{\nabla\lambda^T(K)\Delta K\} &= \frac{\underline{w}^T(-B\Delta K C)\underline{v}}{\underline{w}^T\underline{v}} \\ &= \text{tr}\left\{-\frac{\underline{w}^T(B\Delta K)C\underline{v}}{\underline{w}^T\underline{v}}\right\} \\ &= \text{tr}\left\{-\left[\frac{C\underline{v}\underline{w}^T B}{\underline{w}^T\underline{v}}\right]\Delta K\right\}.\end{aligned}\quad (177)$$

Since (177) must hold for an arbitrary ΔK ,

$$\nabla\lambda^T(K) = -\left[\frac{C\underline{v}\underline{w}^T B}{\underline{w}^T\underline{v}}\right]\quad (178)$$

or

$$\underline{\nabla}\lambda(K) = -\frac{B^T\underline{w}\underline{v}^T C^T}{\underline{w}^T\underline{v}}.\quad (179)$$

$\underline{\nabla}_k\lambda(\underline{k})$ is found by rearranging $\underline{\nabla}_K\lambda(K)$ (\underline{k} is a vector comprised of the elements of K).

Define λ_i in terms of two real variables, σ_i and ω_i .

$$\lambda_i = \sigma_i + j\omega_i.\quad (180)$$

Then

$$\frac{\partial\sigma_i}{\partial k_i} = \text{Real}\left(\frac{\partial\lambda_i}{\partial k_i}\right)\quad (181)$$

$$\frac{\partial\omega_i}{\partial k_i} = \text{Imaginary}\left(\frac{\partial\lambda_i}{\partial k_i}\right).\quad (182)$$

The constraint functions $g_i(\lambda)$ from equation (135) are considered functions of the two real variables, σ and ω . For the purposes of problem (134)-(140) each constraint will be a function of only one eigenvalue. If all the

eigenvalues must lie inside a particular boundary, then n of the constraints will be the equation for the boundary (one for each eigenvalue). Given this situation,

$$\left(\frac{\partial g_i(\sigma_j, \omega_j)}{\partial \underline{k}} \right) = \left(\frac{\partial g_i(\sigma_j, \omega_j)}{\partial \sigma_j} \right) \left(\frac{\partial \sigma_j}{\partial \underline{k}} \right) + \left(\frac{\partial g_i(\sigma_j, \omega_j)}{\partial \omega_j} \right) \left(\frac{\partial \omega_j}{\partial \underline{k}} \right). \quad (183)$$

Since the regions in the complex plane are chosen by the designer, it will be assumed that the regions are chosen so that the partials with respect to σ and ω exist. For the same reason, the functions $g_i(\sigma, \omega)$ are known explicitly, and thus, so are the partials. Thus using equations (179)-(183), the gradient of the constraints with respect to the feedback gains, \underline{k} , can be calculated.

In summary, both the gradients of the constraints with respect to \underline{k} and the gradient of the cost $J(\underline{k})$, as well as the values of the constraints and the cost, can be calculated given a point \underline{k} . Using this information, one can find the solution to (134)-(140) by solving the equivalent problem (153)-(155) as described in Section 6.3. The next section will discuss some of the specific details and problems involved in implementing this method to solve the reformulated problem (134)-(140).

6.5. Second Order Example

The purpose of the numerical example of this section is to demonstrate how well the method developed in Section 6.2 to solve problem (129)-(134) works on a simple second order example. The problem is as follows:

$$\min_{\underline{k} \in S} J = \frac{1}{2} \int_0^{\infty} \mathbf{u}^T(t) \mathbf{u}(t) dt \quad (184)$$

subject to

$$\dot{\underline{x}}(t) = A\underline{x}(t) + B\underline{u}(t) \quad (185)$$

$$u(t) = -[k_1 \quad k_2]\underline{x}(t) \quad (186)$$

$$S = \{k/(A-Bk) \text{ is asymptotically stable}\} \quad (187)$$

$$A = \begin{bmatrix} -1 & 5 \\ -5 & -1 \end{bmatrix} \quad B = \begin{bmatrix} 0 \\ 1 \end{bmatrix} \quad (188)$$

$$g_i(\sigma, \omega) \leq 0 \quad i = 1, 4 \quad (189)$$

where σ and ω are the real and imaginary parts of the eigenvalues of the closed loop system. The constraints are (see Figure 6.1):

$$g_1(\sigma, \omega) = \omega - 2.6\sigma \quad (190)$$

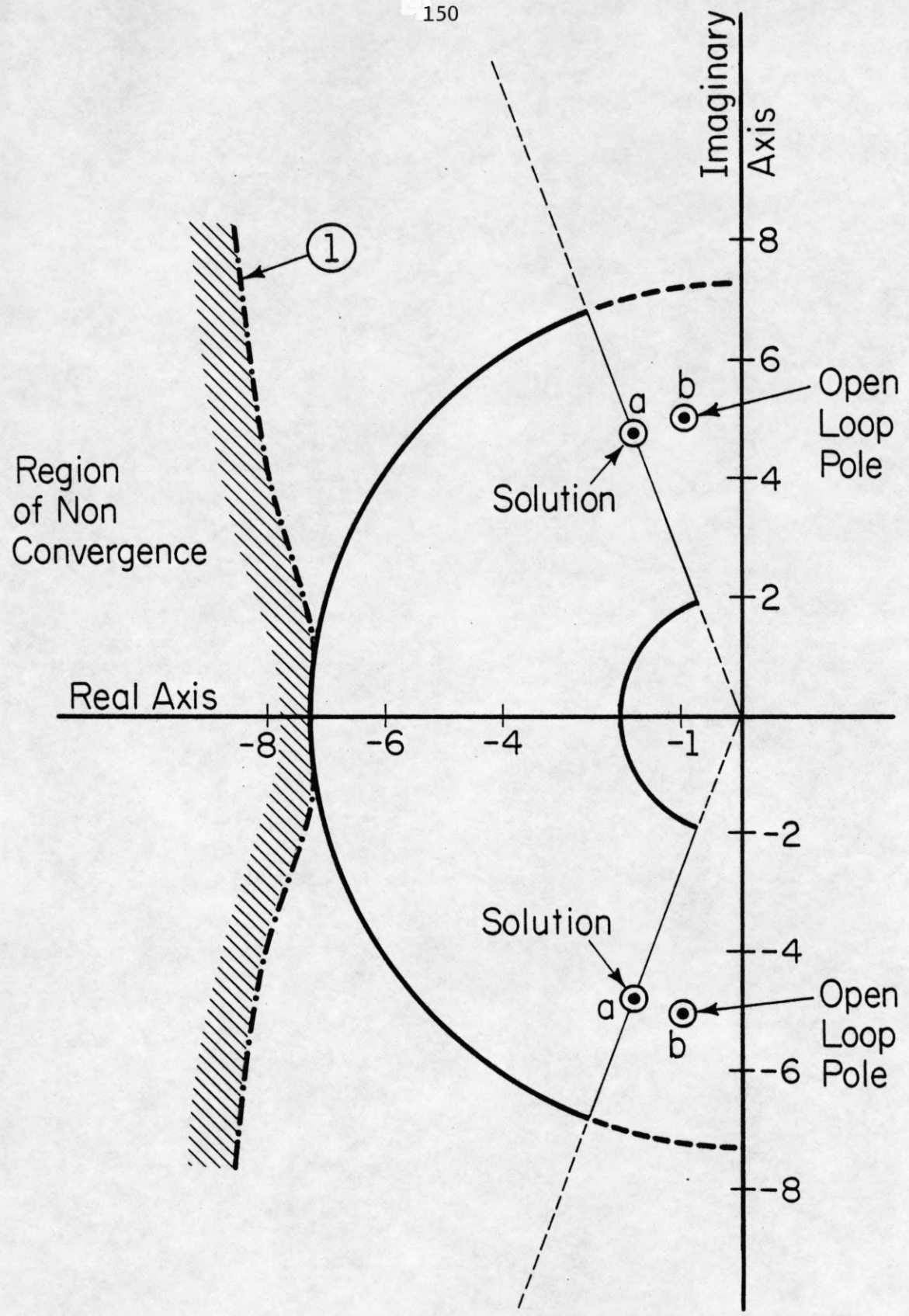
$$g_2(\sigma, \omega) = \omega + 2.6\sigma \quad (191)$$

$$g_3(\sigma, \omega) = 4.0804 - \sigma^2 - \omega^2 \quad (192)$$

$$g_4(\sigma, \omega) = \sigma^2 + \omega^2 - 53.1441. \quad (193)$$

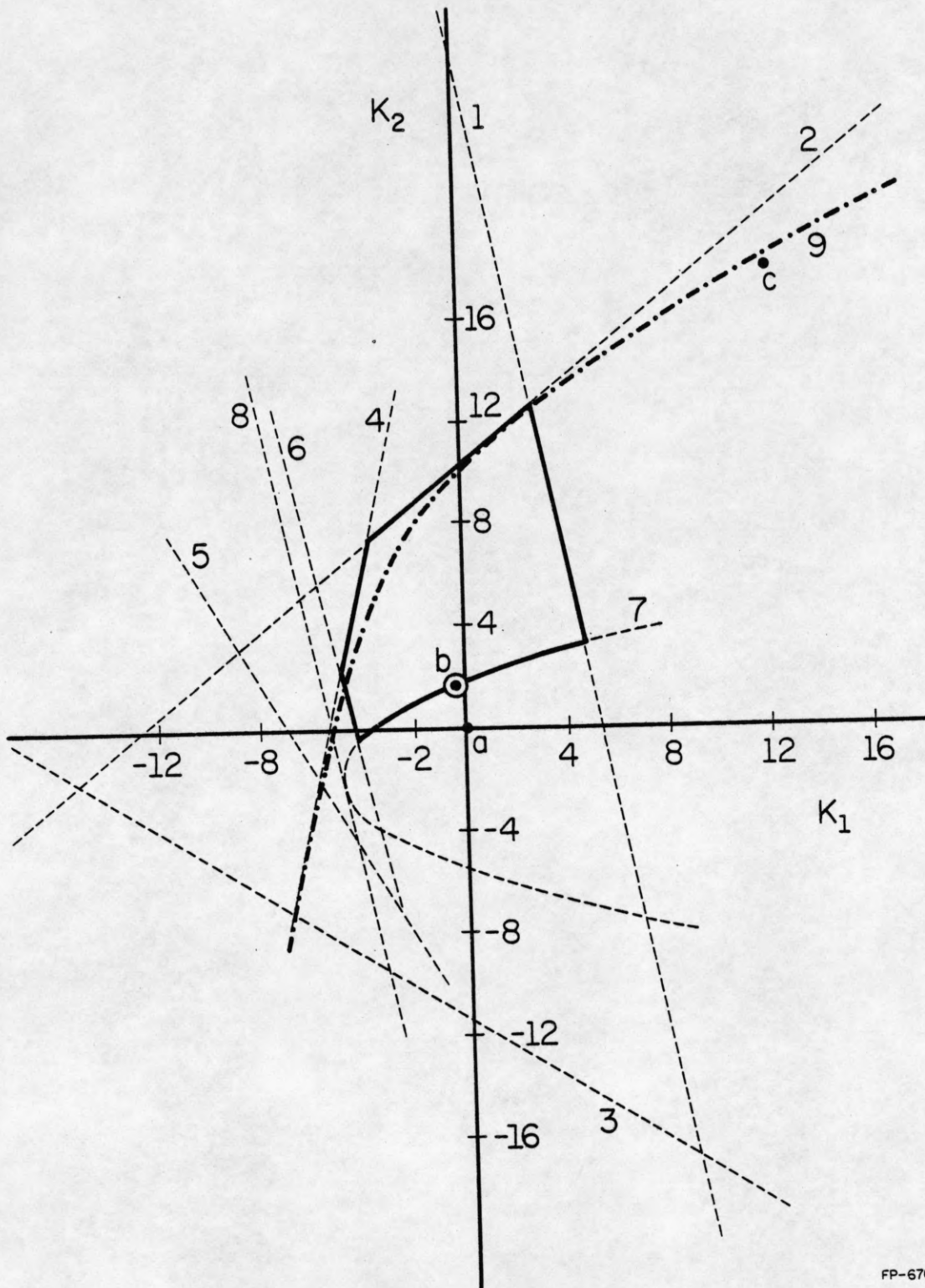
Each of these four equations must be satisfied for both eigenvalues so there are actually eight constraints.

Examining a second order system with a single input is particularly convenient for demonstrating the behavior of this algorithm. First, for a second order system one can derive explicit equations relating the feedback gains to the eigenvalues of the closed loop system. Second, equations mapping the boundaries in the complex plane to boundaries in k-space (the space of feedback gains) can be obtained using the mapping method described in Chapter 4. For this second order system and reasonable boundaries, like those given in (190)-(193), the boundaries in k-space are not too complex (Figure 6.2). Since the minimization is actually over \underline{k} in the k-plane, Figure 6.2 shows exactly what the constraints are in this space.



FP-6706

Figure 6.1. Second order example: constraint region in the complex plane.



FP-6707

Figure 6.2. Second order example: constraint region in the K-plane.

The closed loop characteristic equation for this system is

$$\lambda^2 + (2+k_2)\lambda + (26+5k_1+k_2) = 0. \quad (194)$$

Applying the quadratic formula to (194) yields

$$\lambda_{1,2} = -(1+.5k_2) \pm .5(k_2^2 - 20k_1 - 100)^{1/2}. \quad (195)$$

Taking the partials of λ_1 and λ_2 with respect to k_1 and k_2 ,

$$\frac{\partial \lambda_{1,2}}{\partial k_1} = \mp 10(k_2^2 - 20k_1 - 100)^{-1/2} \quad (196)$$

$$\frac{\partial \lambda_{1,2}}{\partial k_2} = -.5 \pm .5k_2(k_2^2 - 20k_1 - 100)^{-1/2}. \quad (197)$$

From (196) and (197), one can see that these partials have discontinuities precisely at the boundary where the closed loop system poles change from a complex pair to two real poles or vice versa. Not only are these partials discontinuous at this boundary, their magnitude approaches infinity as the poles approach this boundary. The equation of this boundary in k -space is

$$k_2^2 - 20k_1 - 100 = 0 \quad (198)$$

which corresponds to boundary 9 in Figure 6.2.

The other boundaries in Figure 6.2 correspond to the boundaries in the complex plane (Figure 6.1) as follows: the large circle (Figure 6.1) maps into the triangle formed by 1, 2, and 3 (Figure 6.2), the small circle maps into the triangle formed by 4, 5, and 6, the two lines into boundaries 7 and 8. The region enclosed by the solid line in Figure 6.2 is the region in the k -plane where all the constraints (190)–(193) are satisfied. The reason for choosing these boundaries in the complex plane is that such boundaries do occur in real problems (e.g., the aircraft example in the next section) as

constraints on the locations of closed loop system poles. A nice feature of using circles for boundaries in the complex plane is that for second order systems circles map into triangles in the k -plane. Hence some of the boundaries in the k -plane are straight lines (Chapter 4).

The problem (184)-(189) is to find the minimum energy control subject to the indicated constraints. Since system (185) is stable, the minimum energy control without constraints corresponds to zero gain. With the feedback gains set to zero, the poles of (185) are

$$\lambda_1, \lambda_2 = -1 \pm j5. \quad (199)$$

With the given constraints (Figure 6.1), the minimum energy feedback gains were found to be

$$k = [-.273 \quad +1.68] \quad (200)$$

which places the closed loop poles at

$$\lambda_1, \lambda_2 = -1.84 \pm j4.788. \quad (201)$$

This answer makes sense. From Figure 6.2, one can see that this point \underline{k} (points b) is approximately the point inside the constraint region closest to the origin. From Figure 6.1, one can see that the closed loop eigenvalues (points a) are about as close to the open loop eigenvalues (points b) as possible given the constraints. The algorithm converged to the minimum \underline{k} (200) for a wide range of initial guesses for \underline{k} . Initial guesses for \underline{k} which placed the closed loop poles outside the large circle and to the left of boundary 1 were the only ones for which the algorithm did not converge to the value of \underline{k} given in (200).

The region in the complex plane for which the algorithm did not converge corresponds to the area in the k -plane (Figure 6.2) to the right of

line 1 and just below curve 9. The fact that the algorithm could not converge from these points can be explained by the discontinuities in the partials of the eigenvalues with respect to \underline{k} mentioned in (196)-(198). Consider point c (Figure 6.2) as a typical point in this region. It corresponds to a complex pole pair outside the large circle in Figure 6.1. Line 1 in the k -plane represents the boundary for a complex pole pair crossing this circle; thus, the negative of the gradient in the k -plane for these points points towards line 1 and nearly perpendicular to it. Moving in this direction should reduce the cost function (158). However notice that from point c , for example, movement in this direction will lead to guesses for \underline{k} which fall above or on curve 9. A point on curve 9 corresponds to a double real root for which the partials of the eigenvalues with respect to \underline{k} are infinite. This will obviously cause problems. Notice also that for two real poles, the direction of decreasing cost is determined by boundary 2; whereas, for a complex pair, the direction of decreasing cost is determined by line 1. For all these points - points for which the routine would not converge to (200) - the minimization routine found points which approached boundary 9. However, the algorithm was not able to move across or along the boundary. In summary, the derivatives of the constraints with respect to the feedback gains are not continuous. This fact can lead to convergence problems. However, one can avoid these problems by choosing a better initial guess for \underline{k} (and lower values for c).

This example was also used to study the behavior of the algorithm with respect to changes in the constant c' in (158). As discussed in the section on nonlinear programming, for a very large value of c' , the minimi-

zation over \underline{k} converges to a solution which is close to the solution to the actual problem, in this case (184)-(189). For a smaller c' , each iteration over \underline{k} stops farther from the real solution than with a larger c' , but the iterations over \underline{d} lead more quickly to the true solution of the problem. For this problem, c' equal to 2000 seemed to work best. The minimization over \underline{k} led to a solution which was very close to the final solution of the algorithm. The iterations over \underline{d} merely served to bring the point a bit closer to the boundaries (within 10^{-7} , instead of 10^{-3}). This was true even for smaller values of c' , 20 and 200. The smaller values of c' led to more iterations over \underline{d} , but fewer over \underline{k} at each substep. For c' equal to 2, the first iteration over \underline{k} did converge to a solution which was different from the solution with c' equal to 2000. However the iterations over \underline{d} led to the same final solution as with c' equal to 2000. In terms of total function evaluations, c' equal to 2000 was the most efficient; moreover, the solutions for smaller values of c' were not significantly different from those with c' equal to 2000.

To summarize the results for this example, this algorithm works provided a good initial guess for \underline{k} and a reasonable value of c' are used. Provided these two conditions are satisfied, the minimum energy feedback gains for problem (184)-(189) are

$$k = [-.273 \quad +1.68]. \quad (202)$$

This gain places the closed loop system poles at

$$\lambda_1, \lambda_2 = -1.84 \pm j4.788. \quad (203)$$

The next two sections will present a more complex example and discuss some results for that example.

6.6. F-4E Example

The problem studied in this example is the same as that of Chapter 5. The system is a linearized model of the longitudinal motion of the F-4E Phantom. The model equations and design criteria are summarized here for clarity.

The system equations are:

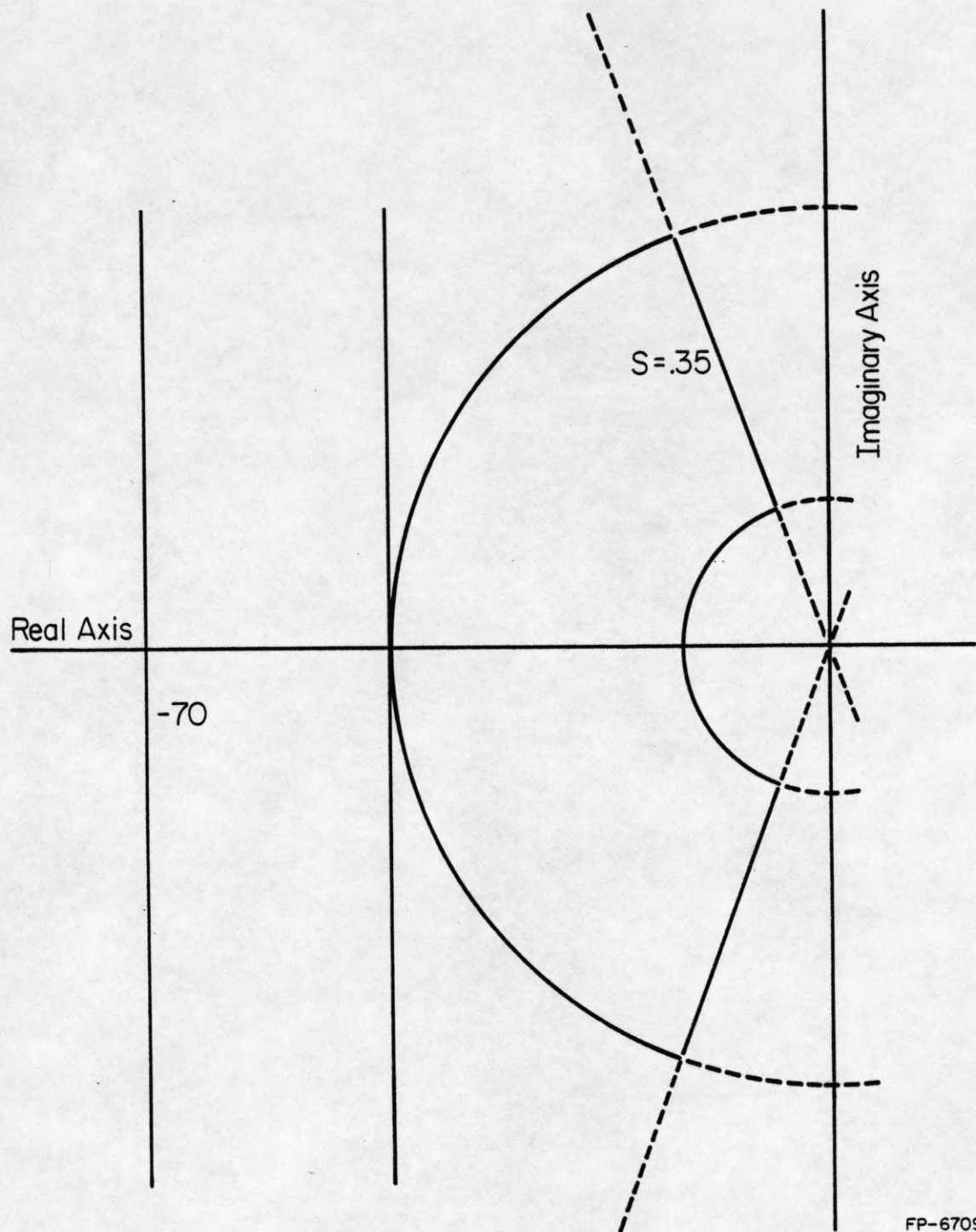
$$\frac{d}{dt} \begin{bmatrix} N_z \\ q \\ \delta_e \end{bmatrix} = \begin{bmatrix} a_{11} & a_{12} & a_{13} \\ a_{21} & a_{22} & a_{23} \\ 0 & 0 & -a \end{bmatrix} \begin{bmatrix} N_z \\ q \\ \delta_e \end{bmatrix} + \begin{bmatrix} b_1 \\ 0 \\ a \end{bmatrix} u \quad (204)$$

$$y(t) = \begin{bmatrix} 1 & 0 & 0 \\ 0 & 1 & 0 \\ 0 & 0 & 1 \end{bmatrix} \begin{bmatrix} N_z \\ q \\ \delta_e \end{bmatrix} \quad (205)$$

$$u(t) = -\underline{k}y(t). \quad (206)$$

The actuator bandwidth, a was assumed to be 14 rad/s. The values a_{ij} and b_1 are different for each flight condition and are given in Appendix I. The matrix \underline{k} is to be determined.

One design problem for this airplane was to choose \underline{k} such that the closed loop eigenvalues for each flight condition are in certain regions in the complex plane (Figure 6.3). Ideally one would like to find one set of gains which worked for all four flight conditions. The constraints on the short period eigenvalues are given by restrictions on the damping and the natural frequency of the short period mode. The characteristic equation for these eigenvalues is



FP-6709

Figure 6.3. Aircraft example: constraint region in the complex plane under normal operating conditions.

$$\lambda^2 + 2\xi_{sp}\omega_{sp}\lambda + \omega_{sp}^2 = 0 \quad (207)$$

where ξ_{sp} is the damping and ω_{sp} is the natural frequency. Under normal operating conditions (i.e., no sensor failures), ξ_{sp} and ω_{sp} are required to satisfy

$$.35 \leq \xi_{sp} \leq 1.3 \quad (208)$$

$$\omega_a \leq \omega_{sp} \leq \omega_b \quad (209)$$

where ω_a and ω_b depend on the flight condition (see Table 6.1). For the case when one of the sensors fail, ξ_{sp} and ω_{sp} must satisfy

$$.15 \leq \xi_{sp} \quad (210)$$

$$\omega_c \leq \omega_{sp} \quad (211)$$

where ω_c depends on the flight condition (Table 6.1). For the emergency situation, the actuator pole is also required to satisfy (210)-(211). For the nonemergency situation, the actuator pole (λ_a) is required to satisfy

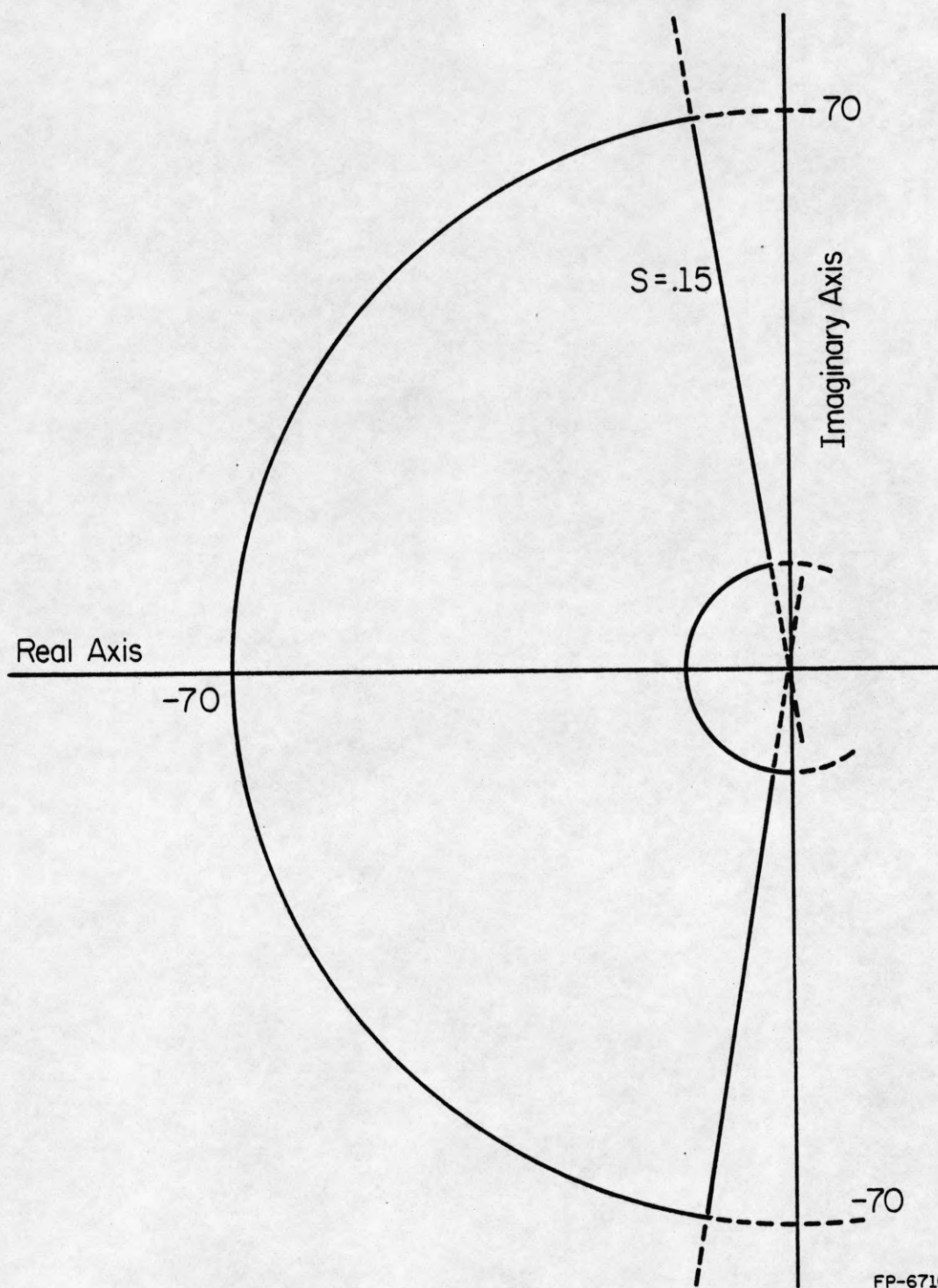
$$\omega_b < \lambda_a < 70 \text{ rad/s.} \quad (212)$$

These regions in the complex plane are shown in Figures 6.3 and 6.4.

For this chapter, an additional design criterion was added. The feedback gains were to be chosen such that the minimum total control energy is used given the constraints on the locations of the closed-loop poles described above. The appropriate cost function to minimize is

$$\min_{k \in S} J = \int_0^{\infty} u^T(t)u(t)dt \quad (213)$$

where S is the set of feedback gains for which the closed loop system (204)-(206) is asymptotically stable. Taken together with appropriate equations for the constraints in Figures 6.3 and 6.4, equations (204)-(206) and (213) repre-



FP-6710

Figure 6.4. Constraint region in the complex plane: emergency conditions.

sent a problem of the form (129)-(134) in Section 6.2. Thus the method of solution developed in the previous sections of this report can be applied. The results for this example are discussed in the next section.

Table 6.1. Frequency limits which determine boundaries in Figures 4 and 5

	Flight Condition #1	Flight Condition #2	Flight Condition #3	Flight Condition #4
ω_a (rad/s)	2.02	3.50	2.19	3.29
ω_b (rad/s)	7.23	12.6	7.86	11.8
ω_c (rad/s)	1.53	2.65	1.65	2.49

6.7. Results and Discussion for Airplane Example

The design problem for the F4-E airplane is to find one set of constant feedback gains for which the closed loop system poles are in the appropriate region in the complex plane for each one of the four flight conditions under normal operating conditions. After finding such a solution, the next problem is to look for a set of gains that satisfies the above criteria and also is robust with respect to sensor failures.

First, each flight condition was studied separately to see if a fixed gain controller could be found to satisfy the constraints under normal operating conditions. As mentioned in Section 6.5, a good initial guess for

the feedback gains is important for the algorithm to converge properly. Since the problem is to find the constrained minimum for J in (213), one sensible starting point is the set of gains which correspond to the unconstrained minimum of J . One can find these gains simply enough by solving a Riccati equation for each set of system matrices [68]. These gains were used, and gains for a fixed gain controller were found for each flight condition. The next step was to find one set of gains which would work for all four flight conditions.

Such a set of gains was found both for the case when all three states (204) were available and for the case when only the first two were available. Chapter 5 considered the latter case. Rather than looking for a particular set of gains, the procedure used was to map the constraints from the complex plane (Figure 6.3) into the space of feedback gains. The entire region of possible gains which satisfy the constraints (Figure 6.5) was found. Using the method described in this thesis, the minimum energy \underline{k} using only two gains was found to be (see Table 6.2)

$$\underline{k} = [-2.8281124 \times 10^{-2} \quad -2.0652172 \times 10^{-1}]. \quad (214)$$

This point is marked in Figure 6.5 and is near the boundary of the enclosed region found by Franklin, at the point approximately nearest the origin. Thus the results presented in this thesis are consistent with Franklin's. For the case with three feedback gains, the minimum energy \underline{k} was found to be (see Table 6.5)

$$\underline{k} = [-3.8498269 \times 10^{-2} \quad -2.7574095 \times 10^{-1} \quad 3.3295187 \times 10^{-1}] \quad (215)$$

An important measure of system performance is the C_N^* response discussed in Chapter 5. The C_N^* is a linear combination of the normal acceleration

Table 6.2. Minimum energy feedback gains: normal operating condition solution (2 gains)

$\underline{k} = [-2.8281124 \times 10^{-2} \quad -2.0652172 \times 10^{-1}]$	
Flight Condition #	Closed Loop Eigenvalues
1	-2.0483019, -2.0200008, -14.537826
2	-3.1624007 \pm j5.2143045, -18.493321
3	-1.589176 \pm j1.7992842, -14.547498
4	-2.1992634 \pm j5.8851873, -16.308839

Table 6.3. Minimum energy feedback gains: normal operating condition solution (3 gains)

$\underline{k} = [-3.8498269 \times 10^{-2} \quad -2.7574095 \times 10^{-1} \quad 3.3295187 \times 10^{-1}]$	
Flight Condition #	Closed Loop Eigenvalues
1	-2.0194637 \pm j3.3183791 $\times 10^{-9}$, -20.227559
2	-3.3792113 \pm j5.0261318, -25.502133
3	-1.5977817 \pm j1.7690526, -20.060981
4	-2.2968881 \pm j5.7580029, -22.569046

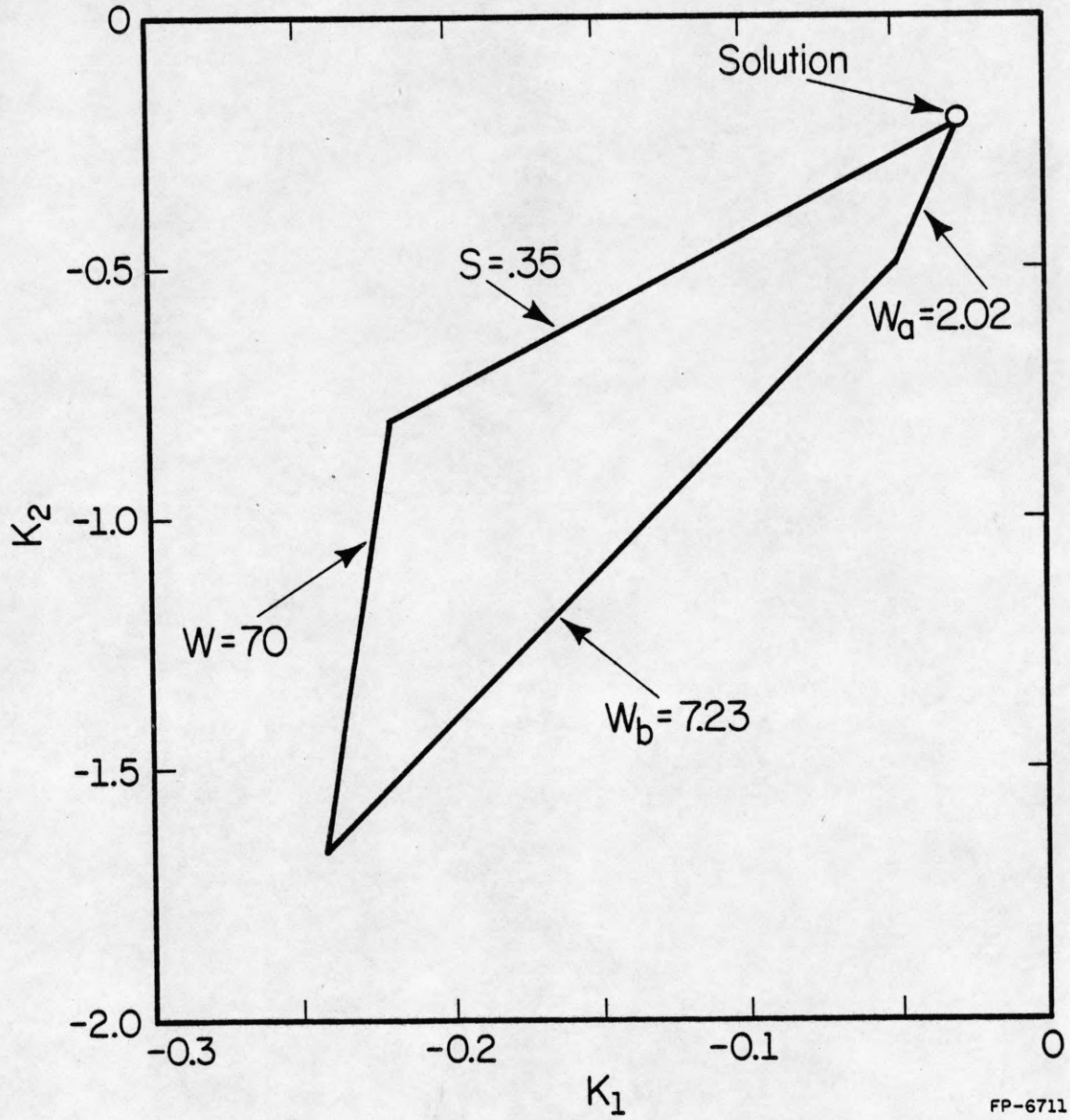


Figure 6.5. Region of possible gains which satisfy the constraints under normal operating conditions for all four flight conditions.

and the pitch rate of the plane, given by

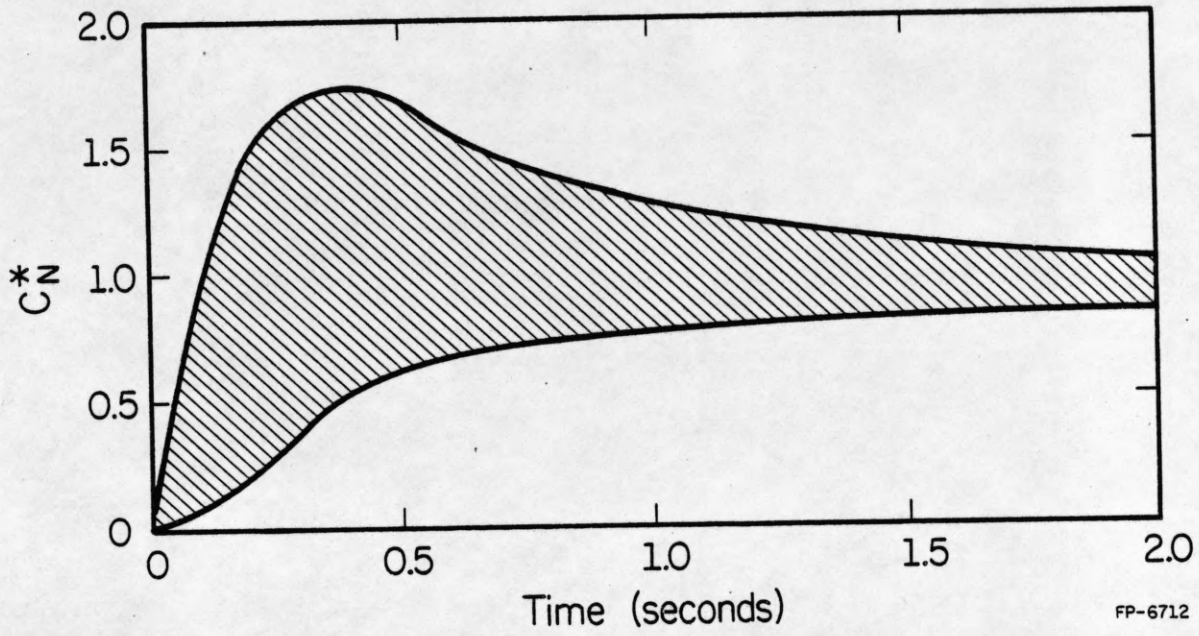
$$C_N^* = (N_z + 12.43q)/k_c^* \quad (216)$$

where k_c is the stationary value of C_N^* and is used for normalization. The C_N^* response to a step input should fall in the region shown in Figure 6.6. Figure 6.7 shows this response for each of the four flight conditions. The first column consists of the responses for the design presented in this section with \underline{k} as given in equation (215). Comparing these responses with Figure 6.6, one can see that they do lie within the required region. The second column contains the C_N^* responses for the following gain matrix

$$\underline{k} = [-.115 \quad -.8] \quad (217)$$

which is the design used in Chapter 5. These C_N^* time responses appear to be faster and to satisfy the requirement given by Figure 6.6 better than those presented in this section. This is not surprising; the gains (217) were chosen on the basis of the C_N^* criterion. The criterion used to choose the gains for this thesis was the minimization of the control energy. Thus, slower C_N^* responses should be expected.

More specifically, the design criterion used to choose the gains in equation (215) was the minimization of the control energy required to bring the system back to equilibrium from a disturbance. Figure 6.8 shows $u(t)$ for each of the four flight conditions (the first column contains the ones for this section; the second for those of Chapter 4). From these figures, one can see that the controls for this section are considerably smaller than the controls which result from Chapter 5. However, the system is stabilized faster (but at the expense of actuator control) for the gain (217).

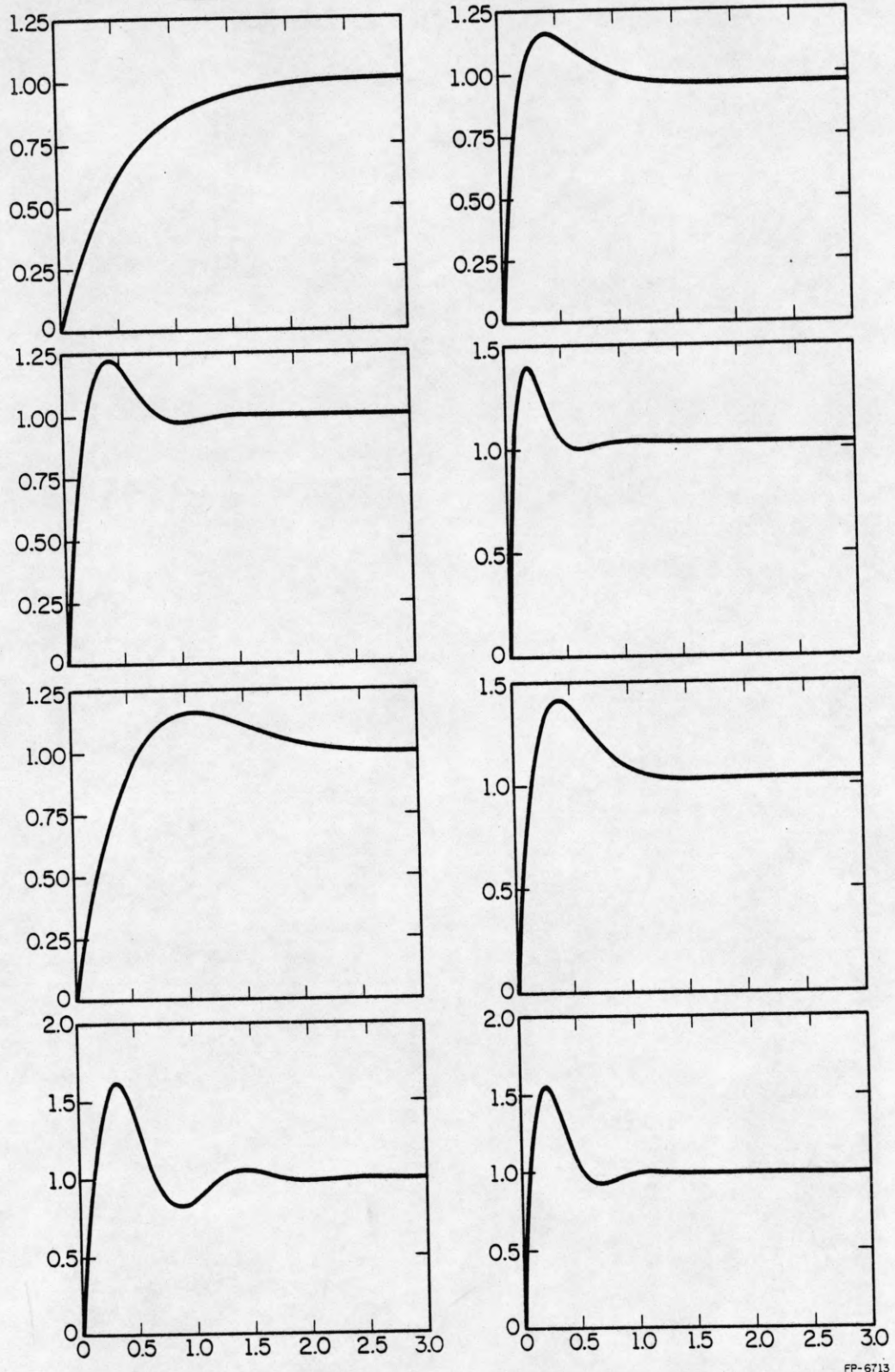


FP-6712

Figure 6.6. C_N^* response envelope.

Chapter 6

Chapter 5

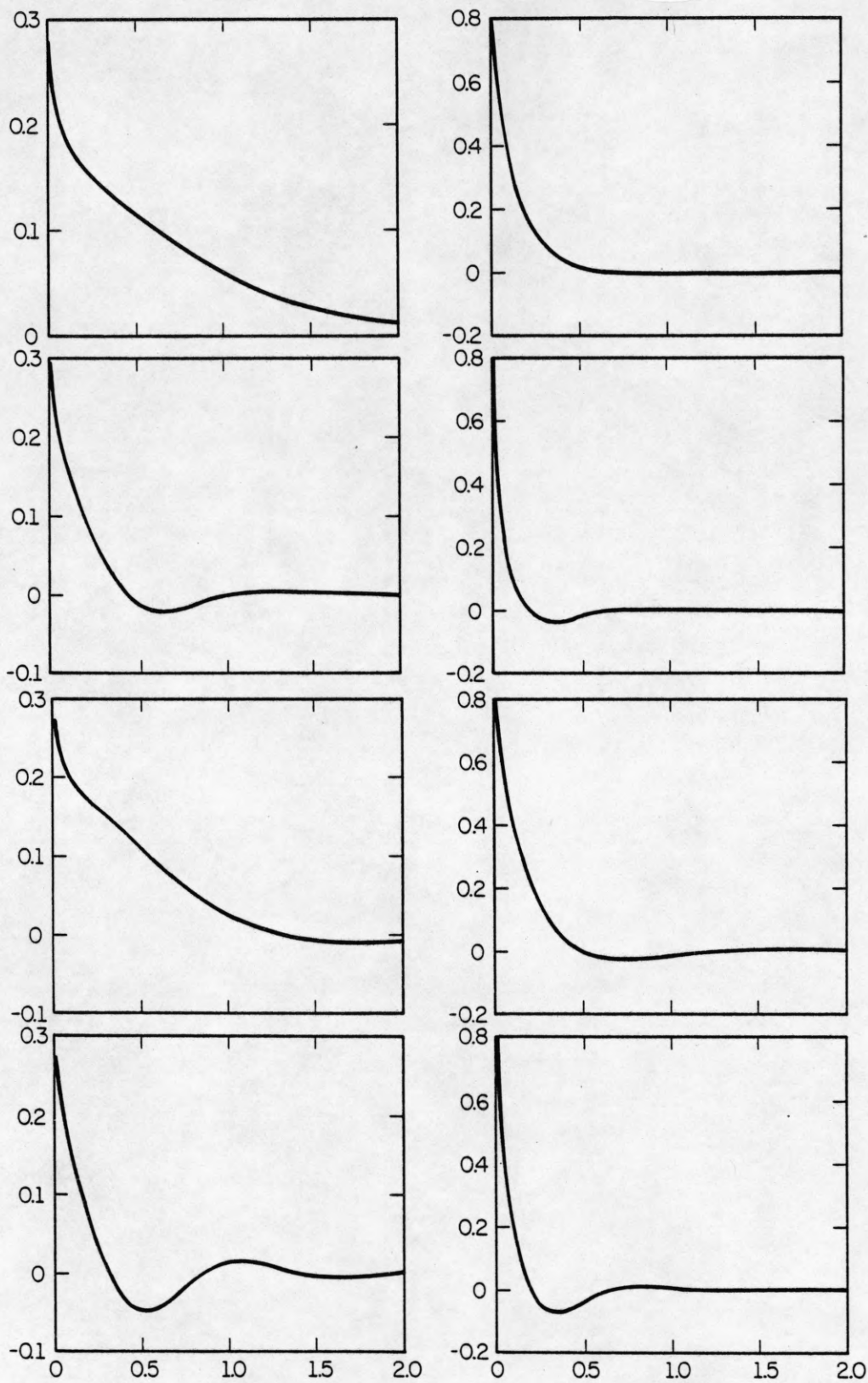


FP-6713

Figure 6.7. C_N^* responses of two designs.

Chapter 6

Chapter 5



FP-6714

Figure 6.8. Control inputs for two designs.

The feedback gains of Chapter 5 were chosen by looking at the time responses for several points and picking the best one. For this section, the gains (215) were chosen by using a cost function which represented the minimum energy control. By changing the cost function or the constraint boundaries in the complex plane, one could easily incorporate the C_N^* response criterion into the design. One could also choose the cost and the boundaries so that the solution would be a compromise between the minimum energy control and a fast response. Moreover, the results from this design indicate where trade-offs can be made and how to make them. In short, using a cost function to choose a set of feedback gains may provide more insight than trial and error alone.

Chapter 5 also mapped the emergency regions in the complex plane (Figure 6.4) into the gain space for the case with only two feedback gains. Unfortunately, the region for which all the constraints for both the normal and the emergency situations are satisfied does not intersect either axis in the gain space. For the problem with only the first two states available for feedback, this means no set of gains satisfying the constraints is robust with respect to the failure of either sensor.

In light of the results of Chapter 5, the problem of a robust controller was considered for the case with three feedback gains. For flight condition 4, a fixed gain using only the first two states was found which satisfied all the constraints and was robust with respect to either the first, the second, or both sensors failing. Adding the third gain set equal to zero, yields a set of three gains which is completely robust. However, this result is not surprising since the open loop poles for flight condition 4 already satisfy the emergency specifications. For

the other three flight conditions considered individually, no gains could be found which were robust with respect to the first sensor failing. Thus none could be found for all the flight conditions taken together. When considered individually, a set of gains which is robust with respect to the failure of the second sensor was found for each flight condition. A set of gains which is robust with respect to the second sensor failing was also found when the first three flight conditions were considered together (see Table 6.4). Unfortunately, when all four flight conditions were considered, no common solution which was robust with respect to the second sensor could be found. A solution which is robust with respect to the third sensor failing is just the solution given in Table 6.2 with a third gain equal to zero added. These results seem to indicate that a fixed gain controller is not adequate to satisfy the robustness requirements for this example.

While studying this example, some of the problems in implementing the algorithm for the second order example in Section 6.5 were also problems for this example. First, the gradient of the cost with respect to the feedback gains is discontinuous at a double real pole (see Section 6.4). For the minimum energy gains in Table 6.2, the eigenvalues of the first flight condition seem to be converging to a double real pole on the boundary of the constraints. Since the gradient is discontinuous at this point, it was necessary to try initial guesses for \underline{k} close to the apparent solution but on both sides of the discontinuity to be sure the algorithm was not hanging up there. The algorithm converged back to the double pole from both directions indicating that that point was indeed the solution. Also, an intelligent initial guess for \underline{k} was important in order to avoid being hung up at the

Table 6.4. Minimum energy feedback gains which are robust with respect to the failure of the second sensor (for the first 3 flight conditions only)

$\underline{k} = [-5.0138477 \times 10^{-2} \quad -4.0115944 \times 10^{-1} \quad 5.0676513 \times 10^{-1}]$		
Flight Condition #	Sensor #2	Closed Loop Eigenvalues
1	NF	-2.7084034, -2.0196952, -23.109953
	F	$-.72136579 \pm j1.3337152$, -26.395321
2	NF	$-4.0968046 \pm j5.1326$, -29.668796
	F	$-.77106637 \pm j5.0911232$, -36.320273
3	NF	$-1.8964697 \pm j1.7951444$, -22.887455
	F	$-.49872359 \pm j2.0622586$, -25.682948

NF: Sensor #2 has not failed

F: Sensor #2 has failed

double root boundaries away from the solution. In that case, a pole placement which places the poles on the opposite side of the double root boundary could be done. Using those gains as a new starting point might allow the algorithm to converge to the real solution.

Another observation was that the value chosen for c' in (158) affected the final solution returned by the algorithm. For large values of c' (200-2000), the algorithm converged quickly to the boundary of the constraint region, but had trouble moving along the boundary to the minimum with iterations over \underline{d} (156)-(157). As explained in Section 6.3, this is due to the ill conditioning of the Hessian for large values of c' . For smaller values of c' , the minimization over \underline{k} converged to a solution outside the boundary of the constraint region. The maximization over \underline{d} forced the solution to the boundary. For this particular example, choosing c' equal to a small number for the initial iteration over \underline{k} and then increasing it gradually for subsequent iterations to enforce the constraints more quickly seemed to work well. The results in this section are for c' equal to 1 for the initial iteration and doubled thereafter.

Summarizing the results of this section, the algorithm developed in this chapter was applied to the problem of designing a controller for the F4-E aircraft. A fixed gain controller was found which satisfied the design specifications under normal operating conditions. However, a fixed gain controller which was robust to either sensor failure was not possible. This example also served to re-emphasize some of the inherent problems with this design technique: the discontinuities of the gradient, the initial guess for \underline{k} , and the choice of c' .

6.8. Conclusion and Summary

This chapter has dealt with one method of solving the problem of designing a fixed gain controller for a linear time invariant system when some of the design criteria are represented as constraints on the location of the closed loop system eigenvalues in the complex plane and others are represented by a quadratic cost function which is to be minimized. First, the original problem (129)-(133) is reformulated to yield (134)-(140). In the form, the cost function is easier to calculate. Second, problem (134)-(140) is solved by an augmented Lagrangian method. The problem is a max-min problem. A variable metric method is used to solve the minimization over \underline{k} . A fixed step size method is used to solve the maximization over \underline{d} [64]. Third, expressions for the gradients needed to solve (153)-(155) are derived.

Two examples are studied: a simple second order numerical example and a model of the longitudinal motion of a F4-E plane. Both examples serve to point out several problems with implementing the solution of (153)-(155). First, there are discontinuities in the gradients for the case when a complex pair of system poles change to a real pair or vice versa. If the algorithm gets hung up at such a point, a new starting point on the other side of the boundary may help. Second, the value of c' in (155) must be chosen appropriately for a given problem. Too large a value of c' causes slow convergence of the algorithm. Too small a value yields a solution outside the boundary. The best approach seems to be to choose c' small for the first iteration and increase it thereafter. Finally, a good initial guess for \underline{k} is important in order for the algorithm to converge properly.

There are advantages to this design method. First, it has the ability to incorporate diverse design criteria such as minimum energy control, rate of change of input, constraints on the location of poles in the complex plane, etc. Second, multi-input, multi-output systems can be considered. Third, it has the ability to handle larger systems than some of the other methods used to solve this type of problem. Finally, it provides insight into the effects of the various design constraints. It can be used to determine which of the design specifications can be satisfied and which ones may be too stringent.

CHAPTER 7

SUMMARY AND FUTURE RESEARCH

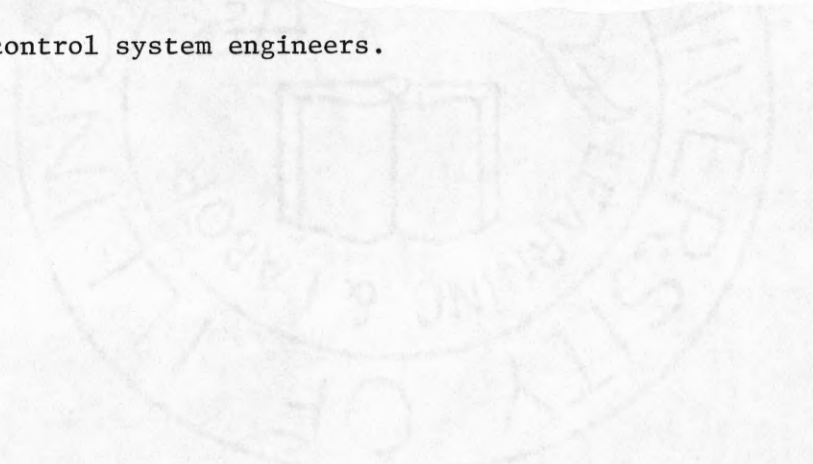
As Chapter 2 illustrates, the robust control problem statement encompasses a great variety of problems. However, the work can be classified into two general areas. The first models the plant perturbations as being largely unstructured. The design and analysis proceeds for the worst case situation and attempts to develop a posteriori bounds for the perturbation. As a result, the designs and bounds are often conservative. The second area assumes that the perturbations can be modeled a priori. The control system is then developed for the class of plants described by the perturbation model. This provides hope of designing less conservative (and likely more efficient) control systems. However, this problem appears to be more difficult and much less research has been conducted in this area.

The research presented in Chapters 4 through 6 of this report is directed at the second area described in the preceding paragraph. The parameter space design method of Chapter 4 provides great insight into the problem for the designer. Chapter 5 demonstrated that this method works well for single input, low order problems. The extension of this technique to higher order systems appears straightforward, with only technical problems to be overcome. The extension to multiple input systems will require more thought. One possible generalization is to use the multivariable pole placement equation [33] which exploits the characteristic polynomial matrix,

The optimization procedure of Chapter 6 also provides considerable insight for the designer. It also allows high order, multi-input systems to be considered. However, the computational procedure suffers from several

technical problems. The most serious of these problems are the extreme sensitivity of closed loop eigenvalues at double real roots and the requirement that an initial stabilizing guess be supplied. It is anticipated that additional computational experience with the algorithm and the designer's insight into the problem can alleviate these difficulties.

In conclusion, it should be emphasized that it is unlikely that a single technique can be developed which is able to handle all problems. It is necessary to have several design tools available and to use the method best suited to the problem at hand. A major purpose of this report is to present methods that will extend the domain of problems which can be handled by control system engineers.



APPENDIX I

AERODYNAMIC DATA

Table I.1 contains the values for a_i , c_j defined in equations (116). These data were obtained by transforming the aero data in [57] to be compatible with the state space representation of equations (116).

The data used in equations (117) are shown in Table I.2

Table I.1. Aero Data for Equations (3.2)

	M = .5	M = .85	M = .9	M = 1.5
	5000'	5000'	35000'	35000'
a_1	-.8532	-1.514	-.6314	-.8527
a_2	.9931	.9940	.9974	.9982
a_3	-.08756	-.1315	-.04332	-.04669
a_4	0	0	0	-.02274
a_5	4.641	11.25	1.488	-18.50
a_6	-.9876	-1.606	-.6680	-.8881
a_7	-10.25	-26.15	-8.104	-15.53
a_8	4.246	14.46	4.590	8.860
c_1	17.53	51.11	18.14	26.83
c_2	-.5152	-.8560	-.3576	-.4879
c_3	-5.078	-12.95	-4.018	-7.842
c_4	2.723	9.273	2.944	6.714

Table I.2. Aero Data for Equations (3.3)

	M = .5	M = .85	M = .9	M = 1.5
	5000'	5000'	35000'	35000'
a_{11}	- .9896	- 1.702	- .6607	- .5162
a_{12}	17.41	50.72	18.11	26.96
a_{13}	96.15	263.5	84.34	178.9
a_{21}	.2648	.2201	.08201	- .6896
a_{22}	- .8512	- 1.418	- .6587	- 1.225
a_{23}	-11.39	- 31.99	-10.81	- 30.38
b_1	-97.78	-272.2	-85.09	-175.6

APPENDIX II

A TYPICAL CONSTRAINT MAPPING

For flight condition 2 and the system of equations (127), the eigenvalue constraint regions shown in Figure II.1 will be mapped into K-space.

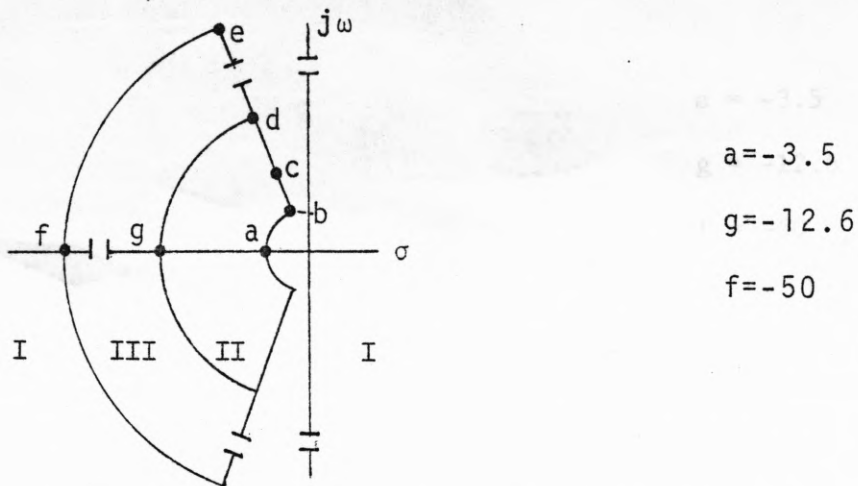


Figure II.1. Eigenvalue constraint region (not drawn to scale).

After k_1, k_4 were arbitrarily fixed at $(-.03, 0)$, these constraints were mapped into the regions shown in Figures II.2. Points $a'-g'$ of Figures II.2 are the images of points $a-g$ of Figure II.1, with points a', f', g' corresponding to double eigenvalues at a, f, g .

The boundaries partition K-space into regions which correspond to the number of eigenvalues in each region of Figure II.1, labeled I, II, III. The desired combination is:

- one eigenvalue in region I,
- two eigenvalues in region II,
- three eigenvalues in region III.

Table II.1 lists how the eigenvalues are distributed among regions I, II, III for gains in the regions labeled A-M in Figure II.3.

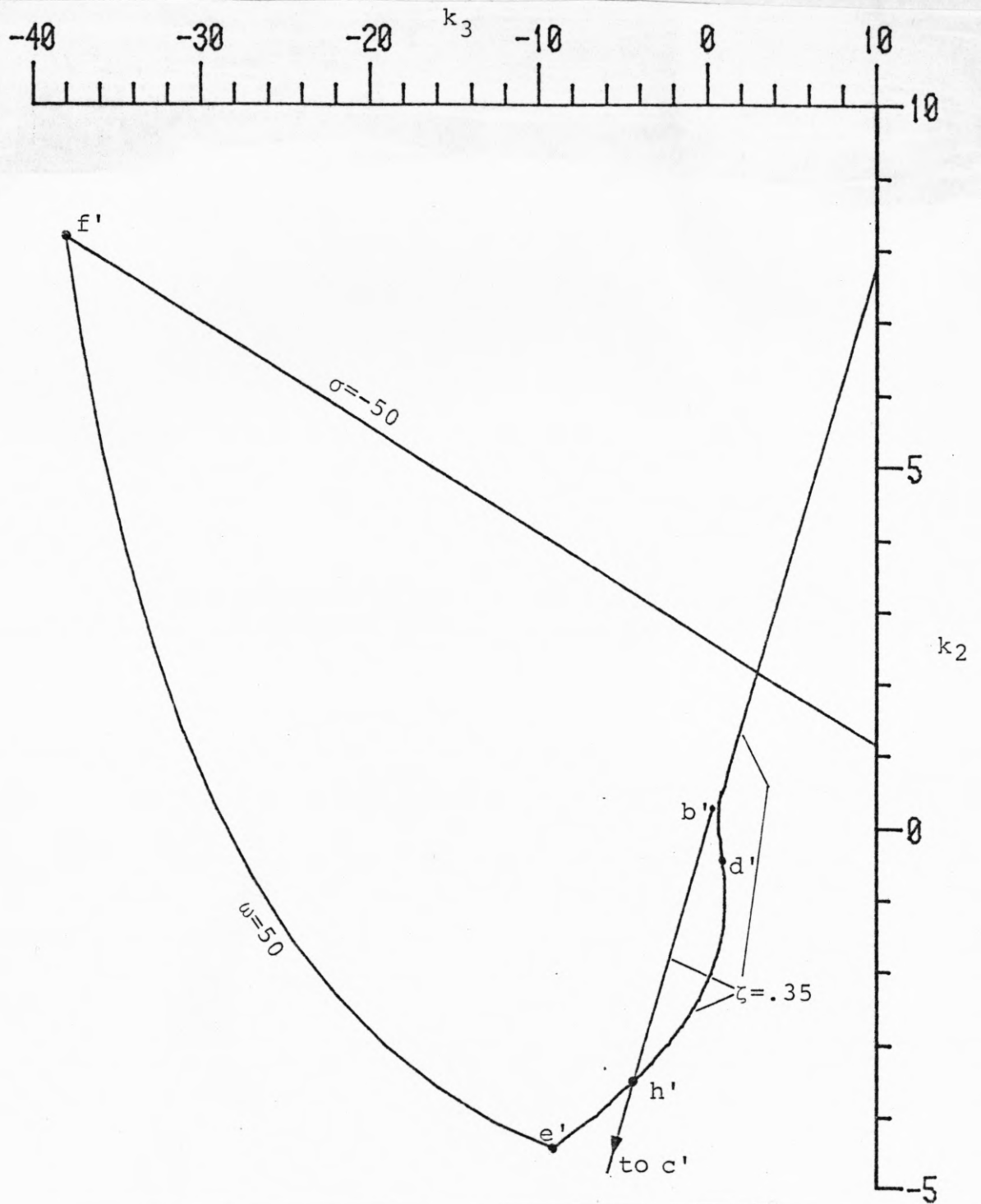


Figure II,2a. Boundaries in K-space,

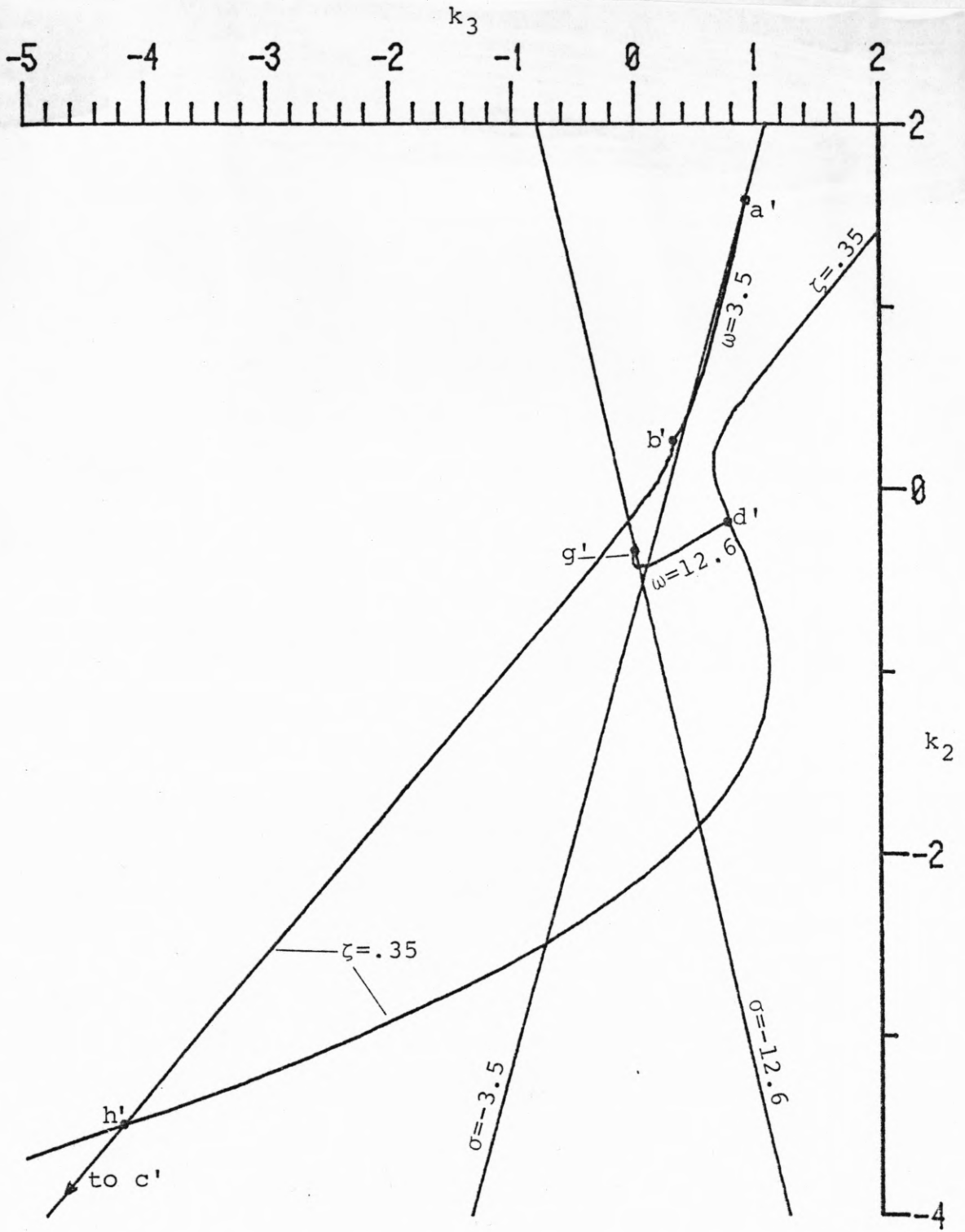


Figure II.2b. Boundaries in K -space (enlargement of A2.2a).

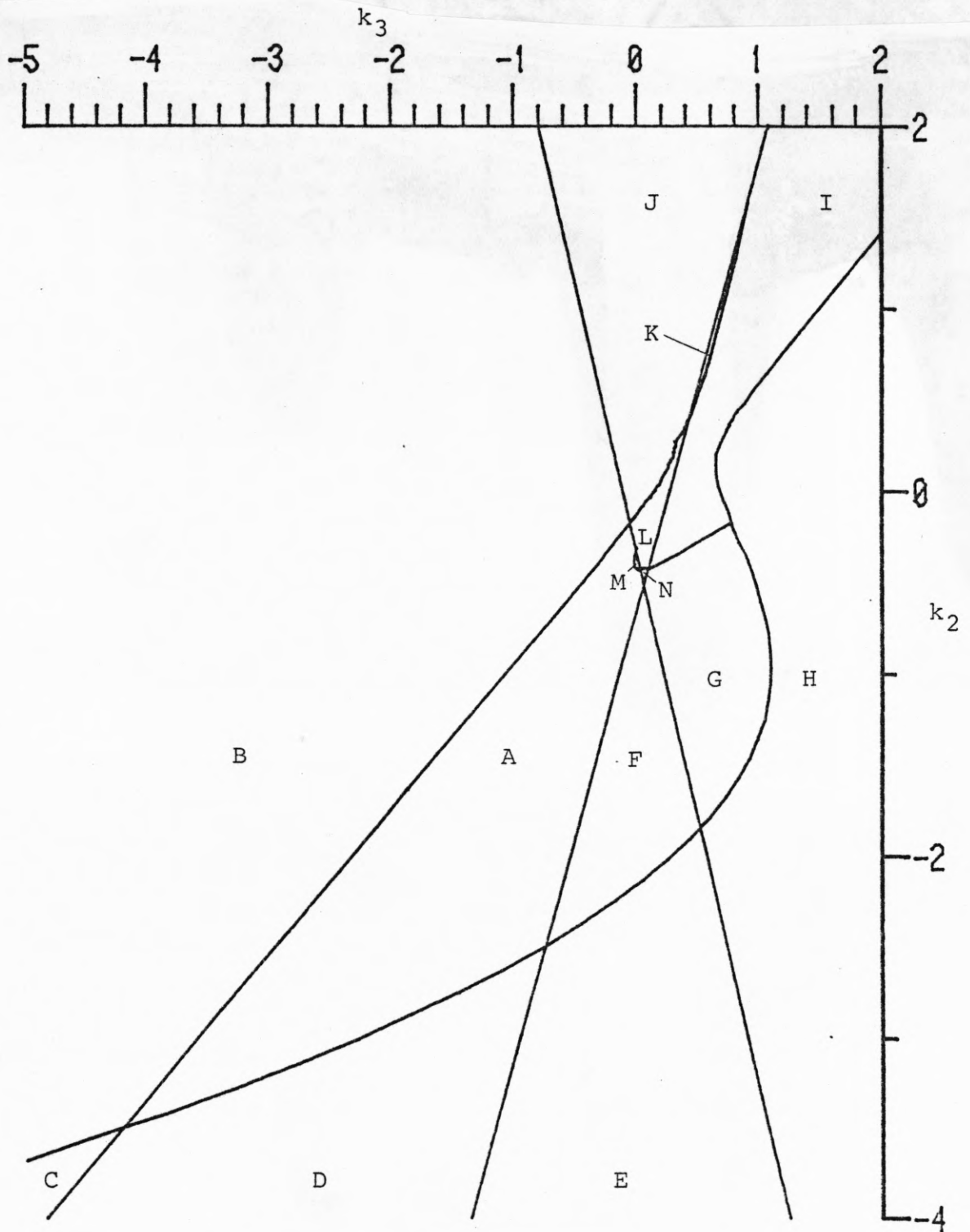


Figure II.3. Partitions of k_3, k_2 plane.

Table II.1. Distribution of Eigenvalues

Region	Number in I	Number in II	Number in III
A	1	2	3
B	3	0	3
C	5	0	1
D	3	2	1
E	4	1	1
F	2	1	3
G	2	2	2
H	4	2	0
I	2	2	2
J	3	1	2
K	4	0	2
L	1	3	2
M	1	4	1
N	1	1	4

REFERENCES

1. H. S. Black, "Stabilized Feedback Amplifiers," Bell Systems Technical Journal, 1934, pp. 1-18.
2. J. B. Cruz, Jr, (Ed.), "Effect of Feedback on Signal Distortion in Nonlinear Systems," Chapter 3 of Feedback Systems, McGraw-Hill, New York, 1972.
3. C. A. Desoer and Y. T. Wang, "Foundations of Feedback Theory for Nonlinear Dynamical Systems," IEEE Trans. on Circuits and Systems, 1979, to appear.
4. H. W. Bode, Network Analysis and Feedback Amplifier Design, D. Van Nostrand Company, Inc., Princeton, N.J., 1945.
5. J. B. Cruz, Jr. and W. R. Perkins, "A New Approach to the Sensitivity Problem in Multivariable Feedback System Design," IEEE Trans. on Automatic Control, 1964, pp. 216-223.
6. C. H. Hsu and C. T. Chen, "A Proof of the Stability of Multivariable Feedback Systems," Proc. IEEE, 1968, pp. 2061-2062.
7. A. G. J. MacFarlane, "Return Difference and Return-Ratio Matrices and Their Use in Analysis and Design of Multivariable Feedback Control Systems," Proc. IEE, 1970, pp. 2037-2049.
8. H. H. Rosenbrock, Computer-Aided Control System Design, Academic Press, London, 1974.
9. J. C. Doyle, "Robustness of Multiloop Linear Feedback Systems," Proc. 1978 IEEE Conf. on Decision and Control, San Diego, pp. 12-18.
10. A. J. Laub, "Computational Aspects of the Singular Value Decomposition and Some Applications," Proc. 16th Allerton Conf. on Communication, Control, and Computing, Univ. of Illinois, October 1978, pp. 432-442.
11. N. Sandell, "Robust Stability of Multivariable Feedback Systems," Proc. 16th Allerton Conf. on Communication, Control, and Computing, Univ. of Illinois, October 1978, pp. 471-479.
12. G. Stein and J. C. Doyle, "Singular Values and Feedback: Design Examples," Proc. 16th Allerton Conf. on Communication, Control, and Computing, October 1979, pp. 461-470.
13. M. Safonov, "Tight Bounds on the Response of Multivariable Systems with Component Uncertainty," Proc. 16th Allerton Conf. on Communication, Control, and Computing, October 1978, pp. 451-460.
14. R. E. Kalman, "When is a Linear Control System Optimal?" Trans. ASME (J. Basic Eng.), 1964, pp. 51-60.

15. B. D. O. Anderson and J. B. Moore, Linear Optimal Control, Prentice-Hall, Englewood Cliffs, N.J., 1971.
16. M. Safonov and M. Athans, "Gain and Phase Margin for Multiloop LQG Regulators," IEEE Trans. on Automatic Control, 1977, pp. 173-197.
17. O. J. M. Smith, Feedback Control Systems, McGraw-Hill, New York, 1958.
18. J. B. Doyle, "Guaranteed Margins for LQG Regulators," IEEE Trans. on Automatic Control, 1978, pp. 755-756.
19. J. C. Doyle and A. Stein, "Robustness with Observers," Proc. 1978 IEEE Conf. on Decision and Control, San Diego, pp. 1-6.
20. H. Kwakernaak, "Optimal Low Sensitivity Linear Feedback Systems," Automatica, 1969, p. 279.
21. Jacques Willems and H. van der Voorde, "The Return Difference for Discrete-Time Optimal Feedback Systems," Automatica, 1978, pp. 511-513.
22. C. A. Harvey and R. E. Pope, "Study of Synthesis Techniques for Insensitive Aircraft Control Systems," NASA Contractor Report CR-2803, April 1977.
23. C. A. Harvey and R. E. Pope, "Insensitive Control Technology Development," NASA Contractor Report 2947, February 1978.
24. A. Vinkler and L. Wood, "A Comparison of Several Techniques for Designing Controllers of Uncertain Dynamic Systems," Proc. 1978 IEEE Conf. on Decision and Control, San Diego, pp. 31-38.
25. D. M. Salmon, "Minimax Controller Design," IEEE Trans. on Automatic Control, 1968, pp. 369-373.
26. U. Ly and R. H. Cannon, "A Direct Method for Designing Robust Optimal Control Systems," Proc. AIAA Guidance and Control Conf., Palo Alto, Calif., August 1978, pp. 440-448.
27. A. Vinkler and L. J. Wood, "Guaranteed Cost Control of Linear Systems with Uncertain Parameters--Application to Remotely Piloted Vehicle Flight Control Systems," Proc. AIAA Guidance and Control Conf., Palo Alto, Calif., August 1978, pp. 226-239.
28. D. L. Kleinman and P. K. Rao, "An Information Matrix Approach for Aircraft Parameter Insensitive Control," Proc. 1977 IEEE Conf. on Decision and Control, New Orleans, La., pp. 316-325.
29. K. K. D. Young, P. Kokotovic, and V. Utkin, "A Singular Perturbation Analysis of High-Gain Feedback Systems," IEEE Trans. on Automatic Control, 1977, pp. 931-938.

30. V. Utkin, "Variable Structure Systems with Sliding Modes," IEEE Trans. on Automatic Control, 1977, pp. 212-222.
31. K. K. D. Young, "Design of Variable Structure Model Following Control Systems," IEEE Trans. on Automatic Control, 1978, pp. 1079-1085.
32. E. J. Davison, "The Robust Decentralized Control of a General Servo-mechanism Problem," IEEE Trans. on Automatic Control, 1976, pp. 14-24.
33. J. Ackermann, Abtastregelung, Springer, Berlin, 1972.
34. J. Ackermann, "Parameter Space Design of Robust Control Systems," preliminary version, Proc. of the JACC, Denver, Colo., June 1979.
35. N. Franklin and J. Ackermann, "Robust Flight Control--A Design Example," in preparation.
36. A. T. Fam and J. S. Meditch, "A Canonical Parameter Space for Linear Systems Design," IEEE Trans. on Automatic Control, 1978, pp. 454-458.
37. A. Schy, "Nonlinear Programming in Design of Control Systems with Specified Handling Qualities," Proc. 1972 IEEE Conf. on Decision and Control, New Orleans, La.
38. A. Schy, W. M. Adams, and K. A. Johnson, "Computer Aided Design of Control Systems to Meet Many Requirements," AGARD Conf. Proc. on Advances in Control Systems, Nr. 137, Gailo, Norway, 1973, pp. 6.1-6.7.
39. F. D. Hauser, "A Nonlinear Programming Algorithm for Automated Design and Optimization of Flexible Space Vehicle Autopilots," AIAA Guidance and Control Conf., Key Biscayne, Fla., 1973.
40. J. S. Karmarkar, "A Regulator Design by Mathematical Programming Methods," Proc. of the JACC, 1973, pp. 699-710.
41. A. Kanarachos, "Computer Aided Design of Control Loops by Parameter Optimization Methods," (in German), Regelungstechnik, 1978, pp. 220-226.
42. A. Kreisselmeier and R. Steinhauser, "Insensitive Control for Large Parameter Variations for a Stabilizer for the F-4C Aircraft," to appear as DFVLR-Forschungsbericht.
43. A. Kreisselmeier and R. Steinhauser, "Systematic Control Design by Optimizing a Vector Performance Index," Proc. IFAC Symp. on Computer-Aided Design of Control Systems, Zurich, Switzerland, August 1979.
44. J. J. Belletrutti and A. G. J. MacFarlane, "Characteristic Loci Techniques in Multivariable Control System Design," Proc. IEE, 1971, pp. 1291-1297.
45. D. H. Owens, "Integrity of Multivariable First-Order-Type Systems," Int. J. of Control, 1976, pp. 827-835.

46. O. A. Solheim, "Some Integrity Problems in Optimal Control Systems," AGARD Conf. Proc. on Advances in Control Systems, Nr. 137, Geilo, Norway, 1973, pp. 4.4-4.10.
47. P. K. Wong, A. Stein, and M. Athans, "Structural Reliability and Robustness Properties of Optimal Linear-Quadratic Multivariable Regulators," Proc. 7th IFAC Congress, Helsinki, Finland, 1978, pp. 1797-1805.
48. A. Kreisselmeier, "Considerations on the Robustness of Control Systems," European Space Agency, Technical translation ESA-TT-453, May 1978, (translation of DFVLR-IB-552-77/19).
49. D. D. Siljak, Nonlinear Systems, The Parameter Analysis and Design, J. Wiley, New York, 1969, Chaps. 1 and 2.
50. J. Rissanen, "Control System Synthesis by Analogue and Computer Based on the Generalized Linear Feedback Concept," Intl. Seminar of Analog Computation Applied to the Study of Chemical Processes, Brussels, Presses Academiques Europeennes, Nov. 1960.
51. E. J. Davison, "On Pole Assignment in Linear Systems with Incomplete State Feedback," IEEE Trans. on Automatic Control, Vol. AC-15, 1970, pp. 348-351.
52. M. Marden, Geometry of Polynomials, American Mathematical Society, Providence, R.I., 1966.
53. H. R. Sirisena and S. S. Choi, "Pole Placement in Prescribed Regions of the Complex Plane Using Output Feedback," IEEE Trans. on Automatic Control, Vol. AC-20, 1975, pp. 810-812.
54. S. N. Franklin, "Design of a Robust Flight Control System," M.S. thesis University of Illinois, Urbana, 1979.
55. J. Ackermann, "On the Synthesis of Linear Control Systems with Specified Characteristics," Automatica, Vol. 13, 1977, pp. 89-94.
56. V. M. Popov, "Invariant Description of Linear Time-Invariant Controllable Systems," SIAM J. Control, Vol. 10, 1972, pp. 252-264.
57. R. L. Berger, J. R. Hess, and D. C. Anderson, "Compatibility of Maneuver Load Control and Relaxed Static Stability Applied to Military Aircraft," AFFDL-TR-73-33, April 1973.
58. "Flying Qualities of Piloted Airplanes," MIL-F-8785B (ASG), August 7, 1969.
59. D. McRuer, I. Ashkenas, and D. Graham, Aircraft Dynamics and Automatic Control, Princeton University Press, Princeton, N.J., 1973.
60. D. P. Looze and N. R. Sandell, Jr., "Gradient Calculations for Linear Quadratic Fixed Structure Control Problems," IEEE Trans. on Automatic Control, Vol. AC-25, No. 2, April 1980.

61. D. G. Luenberger, Introduction to Linear and Nonlinear Programming, Addison-Wesley, Reading, Mass., 1973.
62. M. R. Hestenes, "Multiplier and Gradient Methods," J. Optimization Theory and Applications, Vol. 4, No. 5, 1969.
63. D. P. Bertsekas, "Combined Primal-Dual and Penalty Methods for Constrained Minimization," SIAM J. Control, Vol. 13, No. 3, May 1975.
64. D. P. Bertsekas, "On the Method of Multipliers for Convex Programming," IEEE Trans. on Automatic Control, Vol. AC-20, No. 3, June 1975.
65. J. E. Dennis and H. H. W. Mei, "An Unconstrained Optimization Algorithm which Uses Function and Gradient Values," Technical Report TR 75-246, Dept. of Computer Science, Cornell University, Ithaca, N.Y., June 1975.
66. J. B. Mankin, A Study of Control System Sensitivity, Management Information Services, Detroit, Mich., 1972.
67. D. G. Luenberger, Optimization by Vector Space Methods, Wiley, New York, 1969.
68. H. Kwakernaak and R. Sivan, Linear Optimal Control Systems, Wiley-Interscience, New York, 1972.